UNIVERSIDADE FEDERAL DO CEARÁ

CENTRO DE TECNOLOGIA

DEPARTAMENTO DE ENGENHARIA QUÍMICA

PROGRAMA DE PÓS-GRADUAÇÃO EM ENGENHARIA QUÍMICA

EDILSON PIMENTEL DRUMOND FILHO

AN ADAPTIVE IMPLICIT COMPOSITIONAL RESERVOIR APPROACH USING 2D/3D UNSTRUCTURED GRIDS

FORTALEZA

2017

EDILSON PIMENTEL DRUMOND FILHO

AN ADAPTIVE IMPLICIT COMPOSITIONAL RESERVOIR APPROACH USING 2D/3D UNSTRUCTURED GRIDS

Dissertação apresentada ao Curso de do Programa de Pós-Graduação em Engenharia Química do Centro de Tecnologia da Universidade Federal do Ceará, como requisito parcial à obtenção do título de mestre em Engenharia Química. Área de Concentração: Engenharia Química

Orientador: Prof. Dr. Francisco Marcondes

FORTALEZA

2017

Dados Internacionais de Catalogação na Publicação
Universidade Federal do Ceará
Biblioteca Universitária
Gerada automaticamente pelo módulo Catalog, mediante os dados fornecidos pelo(a) autor(a)

D858a Drumond, Edilson.
An Adaptive Implicit Compositional Reservoir Approach Using 2D/3D Unstructured Grids / Edilson Drumond. – 2017.
104 f. : il. color.

Dissertação (mestrado) – Universidade Federal do Ceará, Centro de Tecnologia, Programa de Pós-Graduação em Engenharia Química, Fortaleza, 2017.
Orientação: Prof. Dr. Francisco Marcondes.

1. reservoir simulation . 2. Adaptive Implicit Method. 3. formulations . 4. EbFVM. I. Título.
CDD 660

EDILSON PIMENTEL DRUMOND FILHO

AN ADAPTIVE IMPLICIT COMPOSITIONAL RESERVOIR APPROACH USING 2D/3D UNSTRUCTURED GRIDS

Thesis presented to the Graduate Program in Chemical Engineering of the Federal University of Ceará as a partial requirement for obtaining the Master's degree in Chemical Engineering. Concentration Area: Chemical Processes.

Approved in: August 11th, 2017

COMITEE MEMBERS

Prof. Dr. Francisco Marcondes (Orientador)
Federal University of Ceará (UFC)

Prof. Dr. Luis Glauber Rodrigues
Federal University of Ceará (UFC)

Prof. Dr. Sebastião Mardônio Pereira de Lucena
Federal University of Ceará (UFC)

Dr. Luiz Otávio Schmall dos Santos
Petrobrás

To my mother and the memory of my father.

ACKNOWLEDGEMENTS

Primarily, I must express my undying gratitude to my mother, Terezinha Bandeira, for the constant support and confidence in my competence, as well as for the countless lessons she taught me during the years. I also have to recognize and thank Edilson Pimentel Drumond, my father for always putting our family first. I am proud to carry his name and his teachings.

A lot of gratitude also has to be directed at my fiancée, Raíssa Azevedo. Even through the hardships, she has been my safe heaven. I am extremely thankful for the affection and patience I demanded from you. To my brothers, Rômulo and Felipe, I own many thanks for the times they, unwillingly, made me realize what was really important. I still need to show my great friend, Victor, how much I value our conversations and how they provided a relief in the worst moments.

I thank my supervisor, Prof. Francisco Marcondes, for supporting me through this research and long before. His example has taught me to continuously strive to achieve more and become a better professional. To my colleagues during these years, my sincere thanks. All of them helped me to along the way, even if they are not aware. I avoid to mention everyone by name, fearing anyone might accidentally be left out.

I would also like to acknowledge PETROBRAS S/A for the financial support for this research. I extend my thanks to the Center for Petroleum and Geosystems Engineering at The University of Texas at Austin for allowing us to use the UTCOMP simulator. Specially, I thank Prof. Kamy Sepehnoori for the guidance during the brief time I spent under his supervision.

RESUMO

Um dos principais aspectos da simulação composicional de reservatórios são os algoritmos, ou formulações, utilizadas para a solução das equações de fluxo. A pesquisa na literatura mostra o desenvolvimento de diversos métodos nas últimas décadas, sempre focados na melhoria de precisão dos resultados e de performance. A escolha das variáveis primárias e o nível de implicitude são dois meios fundamentais pelos quais tais formulações diferenciam-se. Modelos Implicit Pressure, Explicit Composition tratam uma única variável implícita, reduzindo o tempo de computação por passo de tempo, tornando-se, simultaneamente, mais vulnerável à instabilidade numérica. Em contraposição, os modelos Fully Implicit avaliam todas as variavéis primárias acopladas na matrix Jacobiana, de forma a alcançar grande estabilidade numérica. O tamanho dos sistemas lineares, no entanto, é muito maior, requerendo maior esforço computacional por passo de tempo. É desenvolvido uma metodologia que incorporar as duas formulações para produzir um método adaptativo com diferentes níveis de implicitude ao longo das simulações. Isso é possível identificando as fontes de instabilidade no reservatório e avaliando-as em um procedimento dinâmico. Dois critérios de seleção são aplicados para estabelecer a correta quantidade de variáveis implícitas por volume da malha e para conduzir as devidas trocas de formulação. Adicionalmente, o Adaptive Implicit Method (AIM) é combinaddo com a técnica EbFVM para malhas não estruturadas, possibilitando o uso para reservatórios com geometrias complexas. A precisão do AIM é comparada com os métodos IMPEC e Fully Implicit para vários casos de estudo em termos de curvas de produção de óleo e gás, e através dos tempos de computação para comparação de desempenho.

Palavras-chave: simulação de reservatório, Adaptive Implicit Method, formulaçoes, EbFVM

ABSTRACT

One of the main aspects of compositional reservoir simulation concerns the algorithms, or formulations, to solve flow equations. A literature survey shows that several approaches have been developed in the last decades, always aiming increasing the accuracy of results and run performances. The choice of primary variables and applied implicitness level are two of the fundamental ways in which these methods differentiate themselves. Implicit Pressure, Explicit Composition models treat a single variable implicit, reducing the run time for each time step while becoming more vulnerable to numerical instabilities. On the other hand, Fully Implicit schemes evaluate all primary variables coupled within the Jacobian matrix, which confers great stability, but produces much larger linear systems and are, therefore, more expensive per time step. Herein, we develop a model that incorporates both formulations to produce an adaptive method with variable level of implicitness throughout the simulation. This is achieved by identifying the sources of instabilities in a reservoir and setting them implicit in a dynamic procedure. Two switching criteria are applied into establishing the correct amount of implicit unknowns for each grid volume and performing the required shifts. Additionally, this Adaptive Implicit Method (AIM) is combined with the EbFVM scheme for unstructured meshes, enabling the handling of more complex reservoir geometries. The accuracy of the Adaptive Implicit Method is compared with both IMPEC and Fully Implicit formulations for several case studies in terms of oil and gas production rate curves, while the CPU run times are applied into verifying performance.

Keywords: reservoir simulation, Adaptive Implicit Method, formulations, EbFVM

LIST OF FIGURES

LIST OF TABLES

LIST OF SYMBOLS

a	Equation of state parameter
A	Area
b	Equation of state parameter
C_f	Rock compressibility
D	Depth
f_{ij}	Fugacity
F	Gibbs phase rule degrees of freedom
F_i	CFL function
g	Gravity
G^T	Total Gibbs free energy
k_{rj}	Phase relative permeability
$\overrightarrow{\overrightarrow{K}}$	Formation absolute permeability tensor
$\overrightarrow{\overrightarrow{K}}_j$	Effective permeability tensor
L_j	Phase mole fraction
MW_i	Molar mass
n_p	Number of fluid phases
n_c	Number of hydrocarbon components
N_i	Number of moles
$\tilde{N}_i$	Shape function
P	Pressure
P_c	Capillary pressure
q_i	Component molar flow rate
Q_j	Phase volumetric flow rate
R	Universal gas constant
S_j	Phase saturation
T	Temperature

T_{ij}	Transmissibility
$\vec{u}_j$	Phase velocity
V_p	Pore volume
V_t	Total fluid volume
WI	Well index
x_{ij}	Component phase molar fraction
Z	Compressibility factor
ρ_j	Phase mass density
ξ_j	Phase molar density
μ_j	Phase viscosity
$\overline{\mu}_{ij}$	Chemical potential
λ_j	Phase mobility
ϕ	Porosity
Φ_j	Phase hydraulic potential
ν	Molar volume
ω	Acentric factor

CONTENTS

1 INTRODUCTION

This introductory chapter aims to present a general view of reservoir engineering and the related numerical simulation. Afterwards, the main objectives and importance of the work are presented, and a brief summary of the chapters is described.

1.1 Reservoir Simulation

The importance of the oil and gas industry is a commonly known fact. Its final products are applied in large scale on an enormous variety of fields, which explains the size of this market. For instance, in 2016, the Brazilian production went up to 2.144 million barrels per day (ECONOMIA, 2017). In the US, an average of 12.704 millions barrels per day were produced in 2015 (STATISTA, 2017). An expected consequence of theses number is the impact on global markets. For decades, the economy has been profoundly affected by the result of political events on oil prices.

Given this scenario, it is no surprise that oil production has attracted the attention of companies and research groups in a continuous effort to improve efficiency and reduce risks. Evaluating the entire petroleum chain, extracting oil is likely the most uncertainty prone step. The advent of computational simulators produced a huge impact on this field, since these tools enabled a much faster increase on effectiveness in a few decades than observed before. Reservoir simulation has become a key instrument for companies evaluating new and old prospects, as well as academic researches studying new production processes.

Most reservoir simulators currently available have reached a good level of accuracy and ability to handle several recovery processes, from the most traditional ones to the most recent developed propositions. Then, a large amount of effort has been directed into efficiency. Simulating real field applications demands large amounts of processing power and storage capacity, leading to large computation times. The present work means to tackle this issue on a simulator already equipped with several formulations. Our approach consists in combining two of these algorithms into a new method for a performance improvement requiring few changes on the simulator framework.

1.2 Research Objectives

The first goal of this work is to implement and verify the advantages of an Adaptive Implicit Method (AIM) when compared with other methods. The new model is born from the combination of the ACS *et al.* (1985) Implicit Pressure, Explicit Composition and the FERNANDES (2014) formulations. These are also the techniques against which the comparison is performed.

Achieving this objective requires the evaluation of production curves accuracy and performance in terms of CPU time. Several two and three-dimensional case studies, mainly gas flooding problems, are applied in multiple reservoir geometries. We should note the different fluids produce very distinct problems concerning the phase behavior, giving a chance to see how the scheme performs.

Another major aspect considered is the role of switching criterion for the AIM. A weak shifting algorithm can effectively undermine any performance improvement and produce instabilities. Therefore, a complementary objective of the present study is to implement two already reportedly used criteria. All comparisons are done for both approaches in order to understand their behavior in various situations.

Finally, we aim at combining the AIM with Element-based Finite Volume Method unstructured grids. This represents the chief scientific contribution of the research, since there are not many studies concerning the association of these methodologies. All these points combined can produce a new, faster and reliable formulation.

1.3 Chapters Overview

Chapter 2 provides an analysis on the state of art in reservoir simulation. The focus lies first on numerical formulations, the different approaches and increasing complexity. In sequence, an evaluation of the adaptive methods is presented. Finally, griding techniques are reviewed aiming specifically unstructured meshes.

Following, Chapter 3 shows the mathematical model behind the implemented formulation. The chapter sections investigate the material balances (flow equations), constraint relations and phase behavior description for a compositional scheme.

In Chapter 4, the implemented Adaptive Implicit Method is presented in detail. The basic formulation aspects are described, such as the Jacobian matrix handling, as well as the

THOMAS; THURNAL (1982) and COATS (2001) switching criteria.

The results and discussion are shown in Chapter 5. Accuracy and performance analysis are performed for several 2D and 3D cases studies in different reservoir geometries. The proposed model is compared with the previously validated IMPEC and FI models.

2 LITERATURE REVIEW

This chapter is dedicated to review the main aspects discussed in this work as an effort to verify contributions to the state of art on reservoir simulation. Three sections explore each specific matter: the development of numerical formulations; the advent and evolution of the Adaptive Implicit approach; and griding techniques, with special focus on unstructured meshes.

2.1 Numerical Formulations

Petroleum reservoir simulation is a relatively recent area of study. The theoretical basis behind multiphase flow in porous media was known for quite some time. However, the model's complexity, composed of several equations and unknowns, made its application prohibitive. Before the second half of the 20th century, most models were extremely simple and based on analytic solutions for overall material balances or one-dimensional problems (COATS, 1982). These were far from reproducing actual field applications and limited to very specific analysis. For instance, one of the first applied techniques was proposed by Buckley e Leverett (1942). Their analytical model described incompressible and immiscible flow up to two phases. The advent of computers and their rapid advancement allowed for the development of more sophisticated numerical methods which led to a surge on the amount of works published in the matter (COATS, 1982). These simulators, developed around the 1960's, also presented some limitations. Most methods focused on two-phase and three-phase black oil problems, as well as recovery methods associated to depletion or pressure maintenance. Most field applications were actually well described by theses models, posing no serious issues.

The scenario dramatically changed in the next decade. The 1973 Oil Crisis was the first of a series of politically motivated embargoes that caused a fast rise of oil prices on the international market (GUARDIAN, 2011), which in turn allowed for the widespread implementation of enhanced oil recovery (EOR) processes. More complex simulators were developed in order to describe phenomenons such as miscible flow, chemical injection and CO_2 injection, as well as handle more elaborate equilibrium calculations. Kazemi *et al.* (1978) was one of the first to propose a compositional formulation for three-dimensional reservoir with up to three fluid phases, while still evaluating phase equilibrium calculations through correlations. As a consequence, phase related properties calculation generated relevant convergence issues.

Fussel e Fussel (1979) applied the Redlich e Kwong (1949) equation of state (EOS)

into their simulator , and showed how it improves the convergence rates. From this point on, most models proposed in the literature also will lay hand of advantages of using EOS. However, before we proceed further, there should be a deeper investigation on the concept of formulation in order to better differentiate the studies mentioned in this work. Describing flow in porous medium requires the evaluation of several variables, specially if we are dealing with multiphase and multicomponent fluids. Computing all these unknowns in an iterative procedure leads to a huge computational effort, therefore many algorithms, or formulations, have been proposed to optimize performance and guarantee stability. It is important to note not all properties must be computed in order to define a system, as expressed by the Gibb's phase rule:

$$F = n + 2 - n_p \tag{2.1}$$

The above expression calculates the minimum amount of intensive properties required to describe a thermodynamic state (F), also called degrees of freedom, as a function of both the number of phases (n_p) and components (n) in equilibrium. Once these unknowns are evaluated, all remaining properties are computed afterwards. It is important to highlight applying this expression assumes the local equilibrium condition, meaning every point in the reservoir must be in phase equilibrium. Additionally, adjustments are required for the reservoir production specific case. First, the methodology developed in this work, in accordance with several studies in the literature, is isothermal, meaning one less intensive property to be determined. Following, another usual procedure applied here is to remove water from the flash calculations. This requires two modifications on Eq. (2.1): replacing n for the number of hydrocarbon components (n_c), and n_p for $n_p - 1$. Finally, the evaluation of phase flow demands the calculation of phase saturations, adding another $n_p - 1$ degrees of freedom, since the saturation constraint can be used to compute the remaining saturation.

$$\sum_{j=1}^{n_p} S_j = 1 \tag{2.2}$$

All theses changes implemented make Eq. (2.1) assume the form:

$$F = n_c + 1 \tag{2.3}$$

Equation (2.3) represents the amount of primary variables in a reservoir simulators. As already mentioned, this set of unknowns is enough to portray a thermodynamic state. The

remainder of properties, called secondary variables, are all computed as a functions of them. Additionally, the extensive state is defined if we include a single more degree of freedom, like, for instance, a hydrocarbon component amount of moles. The definition of primary and secondary variables is relevant mainly because all reservoir simulations models apply them into their scope. For instance, Fussel e Fussel (1979) applies a dynamic primary variables selection. Apart from pressure, the remaining state defining unknowns are chose according to the predominant phase in each grid block. Should more gas phase moles be present in a given control volume, the amount of oil phase moles per pore volume and $n_c - 1$ oil phase compositions are selected. The procedure is analogous for oil phase predominant volumes. From these variables, only the pressure is treated implicit, yielding an Implicit Pressure/ Explicit Composition (IMPEC) model.

The first Fully Implicit model for compositional simulation was proposed by Coats (1980). The Redlich e Kwong (1949) EOS is used to describe phase behavior. Additionally, the author chooses to account for capillary, gravity and viscous forces. Only physical dispersion is neglected. As the name suggests, this approach means to treat all primary variables implicit. Initially, each Jacobian matrix entry has a $2n_c + 4$ size, accounting for oil and gas phases molar fractions, all saturations and pressure. A Gaussian elimination decouples the secondary unknowns from the linear system, yielding $n_c + 1$ sized entries. We should note the remaining primary variables are dependent on the amount of phases present in each grid block. For the case the two hydrocarbon phases exist, the gas phase pressure, both saturations and $n_c - 2$ gas compositions are chosen. If only the gas phase is encountered, the pressure, saturation and $n_c - 1$ compositions for the gas phase are the primary unknowns. The choice is analogous for volumes containing only the oil phase. The author reports stable runs even for thermodynamic conditions close to the critical point, while noting significant numerical dispersion. The FI method, as largely reported in the literature, served as the counterpoint for the IMPES, since it guarantees great stability at the cost of larger Jacobian matrix. This concept is further developed later on this chapter.

Nghiem *et al.* (1981) developed an IMPEC model based on Kazemi *et al.* (1978). Two main differences can be highlighted First, the authors inserted the Peng e Robinson (1976) EOS into the model, mitigating convergence issues. Second, weighting factors are used on the flow equations in order to obtain the pressure expression. This change is performed to guarantee the linear system is symmetric and diagonal dominant. The model was compared with experimental data for CO_2 displacement showing great agreement. However, the authors were

not able to attain quadratic convergence. Young e Stephenson (1983) also proposed changes to IMPEC model. The authors modified the Jacobian matrix structure from Fussel e Fussel (1979), reordering equations in an effort to improve efficiency and facilitate the insertion of new fluid properties correlations. As for the primary variables, there is no dependence on the number of existing phases. The chosen parameters are pressure, gas phase amount of moles per pore volume, and $n_c - 1$ gas phase compositions.

A new IMPEC approach was shown by Acs *et al.* (1985). A volume constraint is the basis for the pressure equation. This feature itself is not innovative. Both Kazemi *et al.* (1978) and Nghiem *et al.* (1981) used this notion. The difference, however, lies in the procedure. Starting from the assumption the total fluid volume must equal the pore volume, both terms are expanded by a Taylor series truncated in the first order term. The equation generated from this development is unique for it is completely decoupled from phase behavior calculations and its discretized version is linear. This produces an important consequence. Since no non-linearities exist, there is no need for an Newton iterative procedure. Another significant change is on the primary variables. The authors argue phase saturations, as volumetric ratios, are not usual thermodynamic parameters. Instead, pressure and the n_c component masses are selected. It should be noted, however, the method presents two rather undesirable features. First, obtaining the pressure equation requires computing total fluid volume derivatives, a complex task not describe in Acs *et al.* (1985). Following, the truncation on the first order term demands a volumetric error term to be placed into the equation. This addition, however described as a means to maintain the volumetric error stable and allow large time steps, not always produces the desired effect (WONG *et al.*, 1990).

Chien *et al.* (1985) designed a variation from the Coats (1980) model. The parameters are decoupled from the linear system in the same manner. However, the authors opted for a different set of primary variables. Pressure, $n_c(n_p - 1)$ phase equilibrium ratios, water and $n_c - 1$ hydrocarbon components overall molar fraction are selected. This group yields $n_c(n_p - 1)$ extra variables than required by Eq. (2.3). The pivotal unknowns, as named by the authors, are removed from the matrix. Finally, only pressure and the overall molar fractions are solved implicit.

The dichotomy between IMPEC and FI models was then broken by Watts (1986). The author noted the shortcoming in both approach and proposed a new model with an intermediate level of implicitness. Basically, the pressure is still solved implicit as in Acs *et al.* (1985).

Following the $n_p - 1$ phase saturations are also implicitly computed. This requires an evaluation of phase velocities between the two steps, meaning more n_p implicit parameters. Goods results are reported while highlighting the method presents inherit inconsistencies generated from the phase velocities evaluation and the molar fractions treatment. The author does not discusses this matter beyond mention, and notes no relevant errors were observed.

Later, Quandalle e Savary (1989) addressed these matters. They verified two main sources for the already mentioned inconsistencies. One of them is related to the relative permeabilities and capillary pressures. When solving the pressure linear system, these properties are treated explicit. Nevertheless, computing saturations demands an implicit evaluation of the same parameters. The second issue is observed by the fact $n_c + 1$ flow equations are able to provide a solution for $n_c + 2$ unknowns. As a consequence, the gas phase saturation is evaluated in two different ways: a secondary variable obtained as a result of the flash calculations and, at the same time, an input parameter for calculating the implicit relative permeabilities and capillary pressures. The authors define extra $n_c - 2$ compositional parameters for the flow equations. A set of primary variables is built by these new unknowns, the oil phase pressure, gas and water phases saturations. Further, the relative permeabilities and capillary pressures are submitted to an implicit approximation in the event of computing the interblock flow terms in the pressure equation.

Almost simultaneously, two works offered new insights into the volume-based models, such as Acs *et al.* (1985). The first one, Wong *et al.* (1987), presented the total fluid volume derivatives calculations. The authors also reported these methods, even without requiring Newton iterations, did not present meaningful advantages in terms of accuracy and performance when compared with other IMPEC models. Wong *et al.* (1990) went further and addressed the specifics on this matter. Two types of formulations were delineated. The first one was the Newton-Raphson models (NR), composed of approaches with non-linear pressure equations and therefore requiring an iterative procedure within each time step. Some examples of this kind are the works of Fussel e Fussel (1979), Coats (1980) and Young e Stephenson (1983). The Volume Balance (VB) techniques were their opposite in this specific matter. Their principal example was Acs *et al.* (1985), also followed by Kazemi *et al.* (1978), Nghiem *et al.* (1981) and even Watts (1986). The analysis highlights the VB models main feature does not necessarily produces better performances, for evaluating the volume derivatives adds significant computation time to the simulation. Beyond that, the volumetric error treatment, as mentioned earlier, sometimes

leads to smaller maximum time steps, also effecting run CPU times. The authors also found many similarities between the two sets of formulations, such as in the Jacobian matrix. This is also verified in the computed derivatives. While VB methods obtain it through direct analytic calculations, the same values appear as a consequence of the Gaussian elimination in NR techniques.

Watts *et al.* (1991) proposed a Fully Implicit variation of Acs *et al.* (1985) for thermal simulation. The authors argue this approach was necessary to handle thermal recovery processes, once the level of implicitness of Acs *et al.* (1985) and Watts (1986) was not enough to handle the high flow rates near wells and the strong coupling between energy and flow equations. Comparison with commercial packages revealed competitive results. Also on modified models, Branco e Rodriguez (1996) presented an approach with a implicitness degree between FI formulations and Watts (1986). Within an iterative step, compositions are fixed and all unknowns but pressure and $n_p - 1$ phase saturations are decoupled from the Jacobian matrix, yielding $n_p \text{x} n_p$ sized entries. Only after the implicit parameters are computed, the evaluation of compositions and remaining properties is performed.

Wang *et al.* (1997) aimed reducing the non-linearities in the fugacity equation and, therefore, improve convergence. This was done by choosing pressure, n_c amount of hydrocarbon component moles and the n_c equilibrium ratio logarithms on their FI formulation. It should be noted, however, the $ln(K)$ parameters are removed from the linear system through factorization and solved only afterwards.

Later on, some authors conducted extensive comparative studies on some of the previous mentioned methods. Santos (2013) implemented the Coats (1980), Branco e Rodriguez (1996), and Wang *et al.* (1997) models and compared their performances. The author reports the Coats (1980) model is generally faster than the others. Additionally, an IMPEC version of Branco e Rodriguez (1996) was developed. Fernandes (2014) compared several techniques applied on unstructured grids. Three new methods are also shown. The first one is a Fully Implicit version of the Acs *et al.* (1985) model. The other two are variations of the Watts (1986) work. One of them regards the application of the Buckley-Leverett form for computing phase velocities in the saturation linear system solution. The other one defines an iterative procedure for the implicit variables. After saturations are calculated, a new step begins by recomputing pressure with updated relative permeabilities and capillary pressures. On convergence, all primary variables use the same phase velocity values.

2.2 Adaptive Implicit Methods

For several years, most simulators applied implicit pressure, explicit saturation (IMPES) models or its variations, mainly because those were the only techniques capable of handling field scale problems due to limited computational resources. Fully Implicit models were limited to a few theoretical case studies. The memory and computational effort required for this approach made the application on more complex problems prohibitive. At the same time, explicit techniques imposed severe restrictions to time step size, specially for some specific regions of the reservoir like well surroundings, as in coning studies (COLLINS *et al.*, 1992)), and saturation fronts.

Thomas e Thurnal (1983) and Thomas e Thurnal (1983)) set up the first black oil Adaptive Implicit Method, which will also be referred as TT from now on, by acknowledging there is no need to treat the entire simulation domain FI. At any given time step during a run, some regions of the reservoir present potential sources of instability IMPEC methods are not able to handle. The authors argue only these areas need the maximum level of implicitness. This way only a certain amount of variables really need to be calculated into the linear system, reducing the computational effort required and allowing large time steps. Each primary unknown was computed implicit if its total variation over the previous time step exceeded a previously defined threshold. This stability test is based on Peaceman (1977) with some extrapolation. The authors note these property variation limit values do not hold any theoretical basis and each simulation should be submitted to preliminary trial runs in order to achieve optimal thresholds.

Another variation, the Inexact Adaptive Newton (IAN) method, was presented by Bertiger e Kelsey (1985), where the off-diagonal Jacobian matrix coefficients relating to the explicit unknowns are only removed. This yields a linear system closer to the Fully Implicit models, which, as argued by the authors, can produce more stable runs in comparison with AIM. However, this approach is non-conservative in essence, causing a new possibly source of instability. Tan (1988) addresses this issue by reintroducing the residual errors as source terms in the respective equations in the next time step, reporting successful limitation the material errors.

Forsyth e Sammon (1986) were the first critics of the threshold switching algorithm. They argued implicit grid blocks could observe large throughputs not accompanied by significant saturation changes, rendering the backward switching (implicit to explicit) unreliable. The proposed alternative was to set, at the event of a well opening, its neighboring blocks implicit, while the remainder of the domain turns explicit. From this point, only forward switches (explicit

to implicit) are allowed until another well becomes operational and the procedures starts again. The authors reported stable runs and optimized CPU times in comparison with a FI model. Another major modification concerned the evaluation of explicit unknowns. As proposed by Thomas e Thurnal (1982), at each Newtonian iterative step, the explicit variables are updated following the primary unknowns evaluation. This new approach first obtained the Newton-Raphson iterative procedure convergence for the implicit unknowns. Only then, all explicit properties were computed. Russel (1989) compared both methodologies, noting the AIM label would better suit the latter, while TT actually provided a shortcut to the FI solution. We should emphasize there is not an overall consensus about this matter.

Later, alternatives to the threshold switching criterion were the subject of many works. Forsyth (1989) argued the original approach aimed to bound the model solution, which does not necessarily guarantees stability. The author then proposed another threshold to preserve monotonicity, which in term would lead to stable runs. Fung *et al.* (1989) developed an entirely different numerical test for black oil simulations aiming to improve the AIM stability. The principle was to predict whether numerical errors would increase in the next time step for each grid volume, and then set implicit all primary variables in these blocks. The backward switching, from implicit to explicit, followed an analogous procedure, and would leave only pressure inside the Jacobian matrix, as in an IMPEC model. Similar results to the original threshold criterion were found while avoiding the trial and error procedure. This procedure was, however, too cumbersome to be applied in the entire grid. Therefore, only the blocks in the IMPES/FI interface were tested every few time steps. At the same time, Grabenstetter *et al.* (1991) noted the numerical criterion was develop to identify whether the entire domain was unstable. In turn, Fung *et al.* (1989) simplify the method for single volumes stability check without profound discussion on its merit.

Russel (1989) proposed the first Courant-Friedrichs-Lewis (CFL) condition based switching criterion for black oil simulation. The model allows each primary unknown to be switched independently of the other, observing the interval between IMPEC and FI methods. The author also argues AIM simulations bounded by the CFL criterion reduces numerical dispersion in comparison with FI, therefore producing more accurate solutions. Grabenstetter *et al.* (1991) then presented a CFL based switching technique for compositional models. The author states the test is not exactly rigorous, noting, for instance, the effect of non-hyperbolic variables on the stability of the explicit unknowns is not properly accounted for. Still, the reported results show no

relevant instability. It should be noted both Russel (1989) and Grabenstetter *et al.* (1991) methods are advantageous in face of Fung *et al.* (1989) approach, for most required derivatives are already computed on a simulator, greatly reducing the computational effort. The Grabenstetter *et al.* (1991) formulation was studied by Collins et al. (1992), outperforming both IMPEC and FI formulations. We should note Collins *et al.* (1992) decouples the flash calculations from the primary equations, similar to Forsyth e Sammon (1986).

The CFL condition was also the subject of Young e Russel (1993). The authors proposed a more robust mixed switching criterion. A CFL based criterion is written in such a way to account for the influence of all downstream neighbors for any given block, and supported by a complementary threshold. This addition is rendered necessary once the CFL criterion itself does not guarantee stability in problems where strong nonlinearities occur. This set up, the authors point, allows for the CFL limit to exceed the unity. Good results are reported in comparison with Fully Implicit models. However, it is highlighted the comparative performance with IMPES does not show significant enhancements. Meanwhile, the AIM approach was also evaluated for thermal simulators by Farkas e Valko (1994). The authors observed that coupling mass and energy constraint equations could impose even stricter time step size limitations. Hence, a direct IMPES formulation, derived from the Acs *et al.* (1985) method, is proposed as the basis for a adaptive technique.

Later, Coats (2001) introduced a CFL function able to compute IMPES models largest time step size and act as switching criterion for AIM. The method is, at first, very similar to the one proposed by Young e Russel (1993), however some differences must be highlighted. First, the Coats (2001) criterion does not allow any implicitness level between Fully Implicit and IMPEC. In contrast, the Young e Russel (1993) logic allows any configuration between these two extremes. Second, the new model is added of a new CFL function designed specifically to handle the effects of explicitly treating compositions. No threshold over properties is computed. The author, however, notes the lack of theoretical basis of the new expression when both oil and gas phases are mobile. The author also reports non-oscillatory stable runs when CFL=1. Higher values for the criterion also generated stable runs in specific situations. Coats (2003) advances further showing several cases may require stricter limitation, while coarse meshes may be able to support values up to CFL=2. Moncorge e Tchelepi (1995) applied a similar analysis for their TAIM (Thermal Adaptive Implicit Method). Their approach, also based on von Neumann error growth analysis, reduces to the one presented by Coats (2001) for isothermal systems. The

main difference lies on an exclusive CFL function for temperature, which in turn means three implicitness degrees are possible.

The Coats (2001) stability test is used in Cao e Aziz (2002) for their new technique, the IMPSAT based adaptive implicit model (IMPSAT-AIM). The authors argue the IMPSAT can outperform both IMPEC and FI, given its intermediate level of implicitness. Hence, the new adaptive approach admits a third evaluation for any given volume, yielding a combination of FI, IMPES and IMPSAT formulations. The reported results indicate the new model can consistently outperform the traditional AIM.

2.3 Griding

In order to implement all numerical formulations discussed in the previous sections it is necessary the spacial discretization of the model equations. This procedure, which allows problems to be evaluated at a discreet number of points, needs to be performed in a way to reduce simulation errors. We should also note all methods can respond well to different discretization, once their derivations are relatively grid independent. Still, for many decades all reservoir numerical calculations were based on orthogonal Cartesian grids. Spatial derivatives are usually described on the orthogonal system, which in turn makes it only "natural" to follow the same approach in a simulator (WADSLEY, 1980). However, as observed by Fung *et al.* (1992), the application of Finite-Volume Methods (FVM) in conjunction with Cartesian grids produces a series of issues when attempting to describe complex geometries and discontinuities, which are almost unanimously present in real field simulations. Furthermore, Pedrosa e Aziz (1986) noted this type of mesh cannot satisfactorily represent near well flow.

The first alternative largely applied on reservoir simulators were the Boundary Fitted (BF) meshes, also known as Corner Point (CP) grids. Their assessment is actually similar to the Cartesian discretization. These are still structured orthogonal meshes. However, the BF approach dictates the grid has to fit the domain boundaries, hence its name. Their application on reservoir engineering dates the work of Sheldon e Dougherty (1961) on front-tracking simulation for open pattern displacements. Hirasaki e O'Dell (1970) applied this method for simulations on reservoir with changing dip and thickness, and stated the new approach presents a much more accurate portrait of the geometry, leading to lower numerical errors. Similar results are reported by Wadsley (1980).

Orthogonal boundary fitted grids were still limited to a certain level of distortion

before also occurring on relevant numerical errors, causing accuracy issues. Leventhal *et al.* (1985) was able to avoid this problem adjusting the grid lines tangent to match the streamlines on a single phase flow solution. A Non-Orthogonal BF (NOBF) technique, a presented by Chu (1971), proved to better address such cases. Nevertheless, this approach would only gain notoriety after the study conducted by Thompson *et al.* (1974). Maliska e Raithby (1984) applied the NOBF to fluid problems on varying cross-sectional ducts for two and three-dimensional grids. The authors report the mesh layout greatly influences the linear system shape, defining the number of points on the pressure equation. Later, the same approach was applied by Cunha *et al.* (1994) for two-phase (water + oil) black oil simulations with 2D meshes. The results show NOBF can mitigate grid orientation effects. Maliska *et al.* (1994) presented similar results for black oil three-dimensional problems. Later, Maliska *et al.* (1997) combined the NOBF with a black oil Fully Implicit approach using pressure and mass fractions as primary unknowns. A well model is also proposed to address non-orthogonality. Edwards (1998) adopted another approach, by retaining the same linear system bandwidth as in Cartesian grid discretization, and inserting the cross-flux terms into the residual term. The author argues the method provides more accurate results in comparison with orthogonal alternatives, while better handling full tensors. Marcondes *et al.* (2005) expanded Maliska *et al.* (1997) for FI compositional simulation. Good agreement was found for three-dimensional water flooding problems, while mesh orientation effects were not reported. The authors also evaluated the Boundary Fitted method in conjunction with parallel computing, obtaining good speedups for a relative large number of processors. Regarding cross-flow terms, Marcondes *et al.* (2008) showed their absence in the linear system can produce relevant discrepancies even for meshes with small distortion levels.

The boundary fit approach was not, however, the answer for the desire to represent reservoirs and its particularities with ever growing precision. Unstructured grids, are in essence capable of handling any geometry, also allowing boundary conditions to be easily evaluated in any circumstance, what does not necessarily occur for NOBF meshes (HEINEMANN *et al.*, 1989). This flexibility was exclusive to the Finite Element Method (FEM), not widely applied on reservoir simulation due to its non-conservative nature. Baliga e Patankar (1980) were able to address this issue combining FEM and FVM into a conservative, flexible technique named Control Volume Finite Element Method (CVFEM). This name, Maliska (2004) notes, produces the false impression of a FEM based on the FVM. In reality, the CVFEM is a Finite Volume Method added of the element concept and all the advantages it brings. Maliska (2004) then

proposed the name Element-based Finite Volume Method (EbFVM). This nomenclature has been increasingly adopted since then. In the present work, the author will also apply the EbFVM label.

Unstructured grids in reservoir simulation first appeared on Heinemann e Brand (1988), closely followed by Heinemann *et al.* (1989). The presented method generates the Perpendicular Bisection (PEBI) grids. This approach requires the grid to be constructed in a way all interfaces between two neighboring control volumes must be perpendicular to the line segment composed by the center of these volumes. The consequence is only two points are taken into account when evaluating fluxes though any given interface.

Rozon (1989) was the first to apply unstructured EbFVM meshes into reservoir simulation. Its work was limited to single phase flow problems using meshes composed only of quadrilateral elements. The author compares the method with an analytic solution, reporting a good agreement. Forsyth (1990) used the EbFVM grids on local grid refinement. Consistent computational time was observed for both FI and AIM. Fung *et al.* (1992) went further, applying the EbFVM for multiphase flow problems in meshes of triangle elements. The results show the unstructured discretization outperforms Cartesian grids while allowing for local grid refinement without occurring on numerical errors. Darwish e Moukalled (2003) investigated Total Volume Diminishing (TVD) interpolations functions, originally developed for Cartesian meshes, in conjunction with unstructured grids. An extended analysis on this matter was performed by Fernandes *et al.* (2003). The authors adapted the work of Darwish e Moukalled (2003) on TVD schemes, implementing the MINMOD (ROE, 1986) and Koren (KOREN, 1993) flux limiters. Other interpolation functions are applied on unstructured grids by Fernandes *et al.* (2003): the Mass Weighted Upwind scheme (MAW) (Masson *et al.* (1994); Saabas e Baliga (1994a); Saabas e Baliga (1994b)), the Hurtado *et al.* (2007) modified MAW, and a Streamline based Upwind method (Swaminathan e Voller (1992a); Swaminathan e Voller (1992b)).

Still on EbFVM meshes, Cordazzo (2006) conducted an analysis of two-phase (oil and water) flow for meshes composed of triangular and quadrilateral elements. The author also combined this approach with a multigrid method. Many of the conclusions draw to local grid refinement and performance show accordance with other mentioned works. The author also highlights the severe reduction of grid orientation in comparison with structured models. Marcondes e Sepehrnoori (2010) studied EbFVM meshes on two-dimensional heterogeneous and anisotropic reservoirs in a Fully Implicit compositional simulator. The authors applied triangle

and quadrilateral element meshes, noting a good agreement with the Cartesian discretization while requiring a much smaller amount of grid blocks. Marcondes *et al.* (2013) expanded the previous work for three-dimensional grids with hexahedron, tetrahedron, prism and pyramid elements. Fernandes (2014) compared IMPEC, FI and Implicit Pressure and Saturations (IMPSAT) formulations using unstructured and Cartesian grids. Thermal recovery processes were investigated by Marcondes *et al.* (2015) also on a FI compositional simulator. Later, Araujo *et al.* (2016) performed an analysis similar to Marcondes *et al.* (2013) for an IMPEC simulator. The present study relies on these works to use EbFVM grids for quadrilateral and triangular elements 2D grids, as well as 3D meshes of hexahedron, tetrahedron, prism and pyramid elements.

3 PHYSICAL MODEL

As mentioned earlier, reservoirs are porous media in which various hydrocarbon components are unevenly distributed over several fluid phases. The most usually observed phases are water, oil, gas. Modeling such systems requires the evaluation of material balances, phase behavior and constraint equations. The last two set of expressions arise from the necessity to properly describe multiple fluid phases and the mass transfer between then.

The physical model applied in this work is built on a series of assumptions listed below:

1. Isothermal system.
2. Slightly compressible porous medium.
3. No-flow reservoir boundaries.
4. Flow is described by the multiphase Darcy's law.
5. Physical dispersion is neglected.
6. Local phase equilibrium.
7. No chemical reactions occur.
8. The mass transfer between the water and hydrocarbon phases is neglected.
9. There are a maximum of two hydrocarbon phases in equilibrium.

All of these simplification hypothesis are widely used on academic and commercial simulators. Even so, we must discuss some of the listed items. First, the implications of the two last assumptions are investigated. Both of them relate to the amount of phases in thermodynamic equilibrium. For several applications, such hypothesis would not cause any concern. However, the results for the proposed formulation are obtained using gas flooding case studies. Additionally, these problems are characterized by CO_2 rich injection fluids. Such conditions, combined with the right thermodynamic state, may favor mass transfer between water and hydrocarbon phases, as well as the appearance of an extra hydrocarbon phase. Also, the physical dispersion influence might not be negligible for highly miscible phases. Nevertheless, we choose to maintain these simplifications in order to avoid the additional numerical complexity which their evaluation would produce. At the same time, the applied case studies have been severely tested with various formulations, constituting effective means of validating the work.

The following subsections present and develop the concepts behind the equations mentioned above.

3.1 Material Balance Equations

Compositional models imply several hydrocarbon components (or pseudo-components) which may be present in several phases. This way, the material balance equation for each of the hydrocarbon components are described as in Chang (1990). After neglecting the physical dispersion term, they are given by

$$\frac{\partial}{\partial t}\left(\phi \sum_{j=2}^{n_p} \xi_j S_j x_{ij}\right) + \vec{\nabla} \cdot \left(\sum_{j=2}^{n_p} \xi_j x_{ij} \vec{u}_j\right) + \frac{\dot{q}_i}{V_b} = 0, \quad i = 1, ..., n_c \tag{3.1}$$

where ϕ stands for the medium porosity, ξ_j denotes the phase molar density, S_j is the phase saturation, x_{ij} is the $i-th$ component molar fraction in the $j-th$ phase, $\vec{u}_j$ denotes the phase velocity vector, q_i is the $i-th$ component source/sink term and V_b is the bulk volume. This equation is also written in similar fashion for water:

$$\frac{\partial}{\partial t}(\phi \xi_w S_w) + \vec{\nabla} \cdot (\xi_w \vec{u}_w) + \frac{\dot{q}_w}{V_b} = 0 \tag{3.2}$$

where the w subscript denotes all the above mentioned properties are evaluated for the water phase. The first term on both balance equations represents the number of component moles variation with respect to time. This can be shown defining the total amount of moles for the $i-th$ hydrocarbon component, as well as for water.

$$N_i = V_b \phi \sum_{j=2}^{n_p} \xi_j S_j x_{ij}, \quad i = 1, ..., n_c \tag{3.3}$$

$$N_w = V_b \phi \xi_w S_w \tag{3.4}$$

Replacing Eqs. (3.3) and (3.4) respectively into Eqs. (3.1) and (3.2) yields the modified material balances equations after some manipulation.

$$\frac{1}{V_b}\frac{\partial N_i}{\partial t} + \vec{\nabla} \cdot \left(\sum_{j=2}^{n_p} \xi_j x_{ij} \vec{u}_j\right) + \frac{\dot{q}_i}{V_b} = 0, \quad i = 1, ..., n_c \tag{3.5}$$

$$\frac{1}{V_b}\frac{\partial N_w}{\partial t} + \vec{\nabla} \cdot (\xi_w \vec{u}_w) + \frac{\dot{q}_w}{V_b} = 0 \tag{3.6}$$

Equations (3.5) and (3.6) require the evaluation of $\vec{u}_j$. From assumption (4.), the phase velocities are computed by the Darcy's law for multiphase flow, written as

$$\vec{u}_j = -\frac{1}{\mu_j} \overrightarrow{\overrightarrow{K}}_j \cdot \vec{\nabla} \Phi_j, \quad j = 1, ..., n_p \tag{3.7}$$

where μ_j is the phase viscosity, Φ_j denotes the phase hydraulic potential, and $\overrightarrow{\overrightarrow{K}}_j$ is the effective permeability tensor. The last two parameters are described by the following expressions:

$$\Phi_j = P_j - \rho_j g D, \quad j = 1, ..., n_p \tag{3.8}$$

$$\overrightarrow{\overrightarrow{K}}_j = k_{rj} \overrightarrow{\overrightarrow{K}}, \quad j = 1, ..., n_p \tag{3.9}$$

In Eqs. (3.8) and (3.9) P_j is the phase pressure, ρ_j denotes the phase mass density, g is the gravity acceleration and D stands for the depth (positive in the downward direction), k_{rj} is the $j-th$ phase relative permeability with respect to the reference phase, and $\overrightarrow{\overrightarrow{K}}$ denotes the formation absolute permeability tensor. Computing the phase pressures requires the evaluation of the capillary pressure relations. From a reference phase, set as the oil in UTCOMP, the capillary pressure relations with the remaining phases are computed.

$$P_j = P_r + P_{cjr}, \quad j = 1, ..., n_p \tag{3.10}$$

where P_{cjr} stands for the capillary pressure between the $j-th$ and the reference phase. These material balances yield the first $n_c + 1$ primary equations. Previously, it was noted the system definition in intensive terms demands one more equation. The remaining expression is presented in the next section for it derives from a physical constraint condition.

3.2 Constraint Equations

The material balances shown require some physical constraints. It is important to notice these restrictions arise from the very definitions of some properties, such as phase saturations and molar fractions, as follows:

$$\sum_{j=1}^{n_p} S_j = 1 \tag{3.11}$$

$$\sum_{i=1}^{n_c} x_{ij} = 1, \quad j = 1, ..., n_p \tag{3.12}$$

Equation (3.11) can also be interpreted as a volume constraint. As such, it is possible to rewrite this expression in terms of pore volume and total fluid volume. This analysis leads to

the pressure equation as described by Acs *et al.* (1985). Its development start with Eq. (3.13) below:

$$V_t\left(P,\vec{N}\right) = V_p\left(P\right) \tag{3.13}$$

This equation basically states the total fluid volume V_t needs to be precisely the same as the pore volume V_p. It also assumes the left hand side of the equation to be a function of both pressure and the total amount of moles of each component $\vec{N} = (N_1, ..., N_{n_c}, N_{n_c+1})$. As for the right hand side, the pore volume is taken solely as a pressure function. Deriving both sides of the equation with respect to time, and applying the chain rule yields the following expression:

$$\left(\frac{\partial V_t}{\partial P}\right)_{N_i}\frac{\partial P}{\partial t} + \sum_{i=1}^{n_c+1}\left[\left(\frac{\partial V_t}{\partial N_i}\right)_{P,N_{k(k\neq i)}}\frac{\partial N_i}{\partial t}\right] = \frac{\partial V_p}{\partial P}\frac{\partial P}{\partial t} \tag{3.14}$$

Before we advance further, it is convenient to develop the left hand side of Eq. (3.14) defining the partial molar volume, $\overline{V}_{ti}$, as described in Eq. (3.15).

$$\overline{V}_{ti} = \left(\frac{\partial V_t}{\partial N_i}\right)_{P,N_{k(k\neq i)}} \tag{3.15}$$

Another important step on obtaining the pressure equation is to specify the pore volume as a pressure function. This can be achieved defining V_p:

$$V_p = \phi V_b \tag{3.16}$$

In Eq. (3.16), the bulk volume is, for the purposes of this work, a constant and porosity, from assumption (2.), is a function of pressure described as

$$\phi = \phi^0\left[1 + C_f\left(P - P^0\right)\right] \tag{3.17}$$

where C_f is the rock compressibility, and ϕ^0 is the formation porosity at a P^0 reference pressure. Inserting Eqs. (3.15), (3.16) and (3.17) into Eq. (3.14) and rearranging the terms leads to

$$\left[\phi^0 C_f - \frac{1}{V_b}\left(\frac{\partial V_t}{\partial P}\right)_{N_i}\right]\frac{\partial P}{\partial t} = \frac{1}{V_b}\sum_{i=1}^{n_c+1}\left(\overline{V}_{ti}\frac{\partial N_i}{\partial t}\right) \tag{3.18}$$

Finally, the N_i derivatives with respect to time can be obtained from Eqs. (3.5) and (3.6) simply by rearranging the equations. Once replaced into Eq. (3.18), the final pressure equation takes the form

$$\begin{aligned}\left[\phi^0 C_f - \frac{1}{V_b}\left(\frac{\partial V_t}{\partial P}\right)_{N_i}\right]\frac{\partial P}{\partial t} + \overline{V}_{tw}\vec{\nabla}\cdot\left(\xi_w\vec{u}_w\right) + \\ \sum_{i=1}^{n_c}\overline{V}_{ti}\sum_{j=2}^{n_p}\vec{\nabla}\cdot\left(\xi_j x_{ij}\vec{u}_j\right) + \sum_{i=1}^{n_c+1}\overline{V}_{ti}\frac{q_i}{V_b} = 0\end{aligned} \tag{3.19}$$

Equation (3.19) completes the set of primary equations. The complete model, however, still requires phase behavior and physical properties evaluation, both of which are explored in the next sections.

3.3 Thermodynamic Equations

Handling multi-phase systems requires the evaluation of phase equilibrium and thermodynamic states in order to compute several physical properties. The next sub-sections develop how these issues are tackled in the simulator.

3.3.1 Phase Equilibrium

At a given state (fixed temperature and pressure), the phase equilibrium is achieved when the total Gibbs free energy G^T, described in Eq. (3.20), reaches a minimum.

$$G^T = \sum_{j=2}^{n_p} \sum_{i=1}^{n_c} n_{ij} \overline{\mu}_{ij} \tag{3.20}$$

where n_{ij} and $\overline{\mu}_{ij}$ are respectively the amount of moles and the chemical potential of component i in phase j. The latter can be defined as follows:

$$\overline{\mu}_{ij} = \overline{\mu}_{ij}^0 + RT \ln \frac{f_{ij}}{f_{ij}{}^0}, i = 1, ..., n_c, \quad j = 2, ..., n_p \tag{3.21}$$

In Eq. (3.21) the superscript 0 means properties are evaluated at a reference state, and f_{ij} denotes the $i-th$ component fugacity in phase j. This expression is simplified setting the chemical potential at the reference state as zero and fugacity as unity.

$$\overline{\mu}_{ij} = RT \ln f_{ij}, i = 1, ..., n_c, \quad j = 2, ..., n_p \tag{3.22}$$

Replacing Eq. (3.22) into Eq. (3.20) and deriving the latter with respect to n_{ij} yields the total Gibbs free energy minimization condition as presented below:

$$\ln f_{ij} = \ln f_{ir}, \quad i = 1, ..., n_c, \quad j = 2, ..., n_p (j \neq r) \tag{3.23}$$

where the r subscript indicates the reference phase for comparison, set as the oil on UTCOMP. Regardless of the reference phase, Eq. (3.23) states the fugacity of any given component must be the same in every phase if phase equilibrium is to be achieved.

3.3.2 Phase Behavior

Once equilibrium between the hydrocarbon fluid phases is established, phase related properties need to be computed. Even though UTCOMP models phase behavior through various equations of state, only the Peng e Robinson (1976) EOS (PREOS), as implemented by Perschke (1988), is taken into account on the course of this study.

$$P = \frac{RT}{v-b} - \frac{a}{v(v+b)+b(v-b)} \tag{3.24}$$

where parameters a and b are computed for pure substance as shown below:

$$a = \Omega_a \frac{\alpha (RT_c)^2}{P_c} \tag{3.25}$$

$$b = \Omega_b \frac{RT_c}{P_c} \tag{3.26}$$

The subscript c in Eqs. (3.25) and (3.26) denotes temperature and pressure are evaluated at the critical point, and R is the universal gas constant. The Ω_a and Ω_b parameters are constant, and α is a function of the component and temperature. All three terms are presented as follows:

$$\Omega_a = 0.45724; \quad \Omega_b = 0.0778 \tag{3.27}$$

$$\alpha = \left\{ 1 + m \left[1 - \left(\frac{T}{T_c} \right)^{0.5} \right] \right\}^2 \tag{3.28}$$

where m is computed as

$$m = \begin{cases} 0.37464 + 1.54226\omega - 0.26992\omega^2, & for \quad \omega \leq 0.49 \\ 0.379642 + 1.48503\omega - 0.164423\omega^2 + 0.016666\omega^3, & for \quad \omega > 0.49 \end{cases} \tag{3.29}$$

In Eq. (3.29), ω denotes the acentric factor.

Equation (3.24) describes a simple one-component, two-phase system. For multi-phase/multicomponent problems, the PREOS assumes the following form:

$$P = \frac{RT}{v_j - b_j} - \frac{a_j}{v_j \left(v_j + b_j\right) + b_j \left(v_j - b_j\right)} \tag{3.30}$$

The a and b parameters are now phase related and obtained applying the mixing rule, yielding the results below:

$$a_j = \sum_{i=1}^{n_c} \sum_{k=1}^{n_c} x_{ij} x_{kj} a_{ik}, \quad j = 2, ..., n_p \tag{3.31}$$

$$b_j = \sum_{i=1}^{n_c} x_{ij} b_i, \quad j = 2, ..., n_p \tag{3.32}$$

where a_{ik} is computed as

$$a_{ik} = (1 - \kappa_{ik}) (a_i a_k)^{0.5} \tag{3.33}$$

Equation (3.33) basically allows for the binary iteration coefficients κ_{ik} influence to be accounted for on the phase behavior. The PREOS can also be described in terms of compressibility factor Z. This way, Eq. (3.30) admits the following form:

$$Z_j^3 - \left(1 - B_j\right) Z_j^2 + \left(A_j - 3B_j^2 - 2B_j\right) Z_j - \left(A_j B_j - B_j^2 - B_j^3\right) = 0 \tag{3.34}$$

where the parameters A_j and B_j are calculated as

$$A_j = \frac{a_j P}{(RT)^2} \tag{3.35}$$

$$B_j = \frac{b_j P}{RT} \tag{3.36}$$

It is important to note all above mentioned equations are solved regarding P as the oil phase pressure. Additionally, the solution of Eq. (3.34) can produce more than one real compressibility factor value. In this case, the real Z_j value providing the lower Gibbs free energy is chosen for each phase.

The phase modeling presented in this section works generally as tool to obtain a series of quantities necessary to evaluate the transport equations, such as phase and overall molar fractions, and hydrocarbon phase amounts. This procedure is usually called flash calculation. A profound analysis on this matter, as well as others, such as phase appearance and disappearance, is not on the scope of the present work and will not be discussed. Chang (1990) and Perschke (1988) provide more detailed insights on UTCOMP phase modeling.

3.4 Physical Properties

In this section we present the equations applied to the fluid properties evaluation. These parameters are mainly modeled through EOS or correlations. Listed below are models for molar and mass densities, phase saturation, relative permeability, capillary pressure and viscosity.

3.4.1 Molar and Mass Densities

For the hydrocarbon phases, molar density is computed from the EOS compressibility factor:

$$\xi_j = \frac{P}{Z_j RT}, \quad j = 2, ..., n_p \tag{3.37}$$

The water phase is assumed slightly compressible, therefore a simple pressure function as follows:

$$\xi_w = \xi_w^0 \left[1 + C_w \left(P - P^0\right)\right] \tag{3.38}$$

where ξ_w^0 is the water molar density at the P^0 reference pressure, and C_w is the water compressibility. As for the mass densities, the expression for hydrocarbon phases goes as below.

$$\rho_j = \xi_j \sum_{i=1}^{n_c} x_{ij} MW_i \tag{3.39}$$

In Eq. (3.39), MW_i is the $i-th$ component molar mass. Analogously, the water mass density is computed as

$$\rho_w = \xi_w MW_w \tag{3.40}$$

3.4.2 Saturation

For hydrocarbon and water phases the saturations are respectively given by:

$$S_j = (1 - S_w) \frac{L_j/\xi_j}{\sum_{m=2}^{n_p} L_m/\xi_m}, \quad j = 2, ..., n_p - 1 \tag{3.41}$$

$$S_w = \frac{N_w \nu_w}{V_p} \tag{3.42}$$

where L_j stands for the phase mole fractions and ν_w is the water phase molar volume.

3.4.3 Relative Permeability

The UTCOMP has various relative permeability models implemented. For this work, only the modified Stone II approach (STONE, 1973) is taken into account. For a two-phase flow, the expressions are shown below:

$$k_{rw} = k_{rw}^0 \left(\frac{S_w - S_{wr}}{1 - S_{wr} - S_{or}} \right)^{e_w} \tag{3.43}$$

$$k_{ro} = k_{ro}^0 \left(\frac{S_o - S_{or}}{1 - S_{wr} - S_{or}} \right)^{e_o} \tag{3.44}$$

where k_{rw} is the end-point permeability, S_r denotes the residual saturation and e is a model parameter.

A three-phase system version the model takes the form:

$$k_{rw} = k_{rw}^0 \left(\frac{S_w - S_{wr}}{1 - S_{wr} - S_{orw}} \right)^{e_w} \tag{3.45}$$

$$k_{rg} = k_{rg}^0 \left(\frac{S_g - S_{gr}}{1 - S_{gr} - S_{wr} - S_{org}} \right)^{e_g} \tag{3.46}$$

$$k_{ro} = k_{row}^0 \left[\left(\frac{k_{row}}{k_{row}^0} + k_{rw} \right) \left(\frac{k_{rog}}{k_{row}^0} + k_{rg} \right) - (k_{rw} + k_{rg}) \right] \tag{3.47}$$

where k_{row}^0 denotes the end-point relative permeability for oil in water, S_{orw} and S_{org} are the residual oil saturations in water and gas, respectively. Additionally, the relative permeabilities of oil in water and gas are described as follows:

$$k_{row} = k_{row}^0 \left(\frac{1 - S_w - S_{orw}}{1 - S_{wr} - S_{orw}} \right)^{e_{ow}} \tag{3.48}$$

$$k_{rog} = k_{rog}^0 \left(\frac{1 - S_g - S_{wr} - S_{org}}{1 - S_{wr} - S_{gr} - S_{org}} \right)^{e_{og}} \tag{3.49}$$

The terms on Eqs. (3.48) and (3.49) are analogous to the ones previously described. Lastly, on a four-phase flow both k_{rw} and k_{rg} are computed as in Eqs. (3.45) and (3.46). For the oil and second hydrocarbon liquid (l) phases, the following expressions apply:

$$k_{ro} = k_{row}^0 \frac{S_o}{S_o + S_l} \left[\left(\frac{k_{row}}{k_{row}^0} + k_{rw} \right) \left(\frac{k_{rog}}{k_{row}^0} + k_{rg} \right) - (k_{rw} + k_{rg}) \right] \tag{3.50}$$

$$k_{rl} = k_{row}^0 \frac{S_l}{S_o + S_l} \left[\left(\frac{k_{row}}{k_{row}^0} + k_{rw} \right) \left(\frac{k_{rog}}{k_{row}^0} + k_{rg} \right) - (k_{rw} + k_{rg}) \right] \tag{3.51}$$

3.4.4 Capillary Pressure

Leverett (1941) describes the capillary pressures as a function of interfacial tension, permeability, porosity and saturations. For the three-phase flow problem, the model assumes the form:

$$P_{cwo} = -C_{pc}\sigma_{wo}\sqrt{\frac{\phi}{k_y}}\left(1-\overline{S}_w\right)^{E_{pc}} \tag{3.52}$$

$$P_{cog} = -C_{pc}\sigma_{og}\sqrt{\frac{\phi}{k_y}}\left(\frac{\overline{S}_w}{\overline{S}_o+\overline{S}_g}\right)^{E_{pc}} \tag{3.53}$$

where C_{pc} and E_{pc} are parameters evaluated through experimental data matching, and σ values denote the interfacial tension of the water and gas phases with respect to the oil phase. Additionally, the $\overline{S}$ parameters are the normalized phase saturations. For the purposes of this work, these properties are computed following the relative permeability Corey model (COREY, 1986), also implemented in UTCOMP. Their expressions follow:

$$\overline{S}_w = \frac{S_w - S_{wr}}{1-S_{wr}-S_{orw}-S_{gr}} \tag{3.54}$$

$$\overline{S}_o = \frac{S_o - S_{or}}{1-S_{wr}-S_{orw}-S_{gr}} \tag{3.55}$$

$$\overline{S}_g = \frac{S_g - S_{gr}}{1-S_{wr}-S_{orw}-S_{gr}} \tag{3.56}$$

Finally, the interfacial tension between water and the hydrocarbon phases is constant and should be provided as part of the user input. On the other side, for the interfaces between two hydrocarbon phases, the σ_{ij} is calculated by the Macleod-Sugden correlation, Macleod (1923) and Sugden (1924), as a function of molar fractions, phase mole densities and the component parachor (ψ_k).

$$\sigma_{ij}^{0.25} = 0.016018\sum_{k=1}^{n_c}\psi_k\left(\xi_i x_{ki} - \xi_j x_{kj}\right), \quad i=2,...,n_p, \quad j=2,...,n_p \tag{3.57}$$

3.4.5 Viscosity

Four evaluation methods are implemented on UTCOMP for viscosity: the Lohrenz correlation, look-up tables and both linear and quarter-power mixing rules. Only the first approach

is applied on this work. We begin the procedure evaluating the low-pressure, pure-component viscosity according to the Stiel e Thodos (1961) correlation.

$$\tilde{\mu}_i = \frac{3.4\text{x}10^{-4} T_{r,i}^{0.94}}{\zeta_i} \quad for \quad T_{r,i} \leq 0.15, \quad i = 1,...,n_c \tag{3.58}$$

or

$$\tilde{\mu}_i = \frac{1.776\text{x}10^{-4}(4.58T_{r,i} - 1.67)^{5/8}}{\zeta_i}, \quad for \quad T_{r,i} > 0.15, \quad i = 1,...,n_c \tag{3.59}$$

where $T_{r,i}$ denotes the reduced temperature and ζ_i is a parameter computed as

$$\zeta_i = \frac{5.44T_{c,i}^{1/6}}{MW_i^{1/2} P_c^{2/3}}, \quad i = 1,...,n_c \tag{3.60}$$

The subsequent step is to apply the $\tilde{\mu}_i$ in computing the low-pressure mixture viscosity as proposed by Herning e Zipperer (1936).

$$\mu_j^* = \sum_{i=1}^{n_c} x_{ij}\tilde{\mu}_i\sqrt{MW_i} / \sum_{i=1}^{n_c} x_{ij}\sqrt{MW_i}, \quad j = 1,...,n_p \tag{3.61}$$

Following, the phase viscosities are evaluated using the (Jossi) correlation:

$$\mu_j = \mu_j^* + 2.5\text{x}10^{-4}\frac{\xi_{jr}}{\eta_j} \quad for \quad \xi_{jr} \leq 0.18, \quad j = 1,...,n_p \tag{3.62}$$

or

$$\mu_j = \frac{\mu_j^* + \left(\chi_j^4 - 1\right)}{10^4\eta_j} \quad for \quad \xi_{jr} > 0.18, \quad j = 1,...,n_p \tag{3.63}$$

where ξ_{jr} is the reduced phase molar density, η_j and χ_j are equation parameters. These three terms are calculated as follows:

$$\xi_{jr} = \xi_j \sum_{i=1}^{n_c} x_{ij} v_{c,i} \tag{3.64}$$

$$\eta_j = 5.44\left(\sum_{i=1}^{n_c} x_{ij}T_{c,i}\right)^{1/6} / \left[\left(\sum_{i=1}^{n_c} x_{ij}W_i\right)^{1/2}\left(\sum_{i=1}^{n_c} x_{ij}P_{c,i}\right)^{2/3}\right], \quad j = 1,...,n_p \tag{3.65}$$

$$\chi_j = 1.023 + 0.23364\xi_{jr} + 0.58533\xi_{jr}^2 - 0.40758\xi_{jr}^3 + 0.093324\xi_{jr}^4, \quad j = 1,...,n_p \tag{3.66}$$

3.5 Source Term

The well fluxes described in Eqs. (3.5) and (3.6) require a deeper evaluation. In this work, the Well Index (WI) approach is applied. Although several models are implemented, we only take advantage of the Peaceman (1978) and Peaceman (1983) method for WI calculation, adapting it to EbFVM meshes as reported by Fung *et al.* (1992). Additionally, from the supported operation conditions in UTCOMP, the constant surface volumetric rate for injection wells and the constant bottom hole pressure (BHP) for both injection and producer wells are taken into account. We now discuss the source term form for each one of these conditions. Before, however, it is important to properly define the Well Index.

$$WI_j = \frac{\dot{q}_j}{P_w - P_j}, \quad j = 1, ..., n_p \tag{3.67}$$

where P_w denotes the well pressure at the point of evaluation. The Peaceman (1978) model, for vertical wells, computes the well index as below:

$$WI_j = \frac{\sqrt{k_x k_y}\Delta z \lambda_{rj}}{25.14872 ln\left(\frac{r_0}{r_w}\right)}, \quad j = 1, ..., n_p \tag{3.68}$$

In Eq. (3.68), the r_0 denotes the equivalent well radius, evaluate as follows:

$$r_0 = 0.28 \frac{\left[\left(\frac{k_y}{k_x}\right)^{\frac{1}{2}} \Delta x^2 + \left(\frac{k_x}{k_y}\right)^{\frac{1}{2}} \Delta y^2\right]^{\frac{1}{2}}}{\left(\frac{k_y}{k_x}\right)^{\frac{1}{4}} + \left(\frac{k_x}{k_y}\right)^{\frac{1}{4}}} \tag{3.69}$$

Concerning the operational conditions, for a constant surface volume injection regime the component mole flow rates are calculated at surface conditions. These rates must then be distributed among the well segments, as described below:

$$\dot{q}_{k,s} = \left[WI_s \sum_{j=1}^{n_p} \lambda_{j,s} / \left(\sum_{l=1}^{n_s} WI_l \sum_{j=1}^{n_p} \lambda_{j,l} \right) \right] \dot{q}_{k,T}, \quad s = 1, ..., n_s, \quad k = 1, ..., n_p \tag{3.70}$$

where the subscript s denotes the evaluation at each segment, n_s is the total number of segments and $\dot{q}_{k,T}$ the total mole flux for well. At the same time, we are able to compute the phase volumetric flow rates $\dot{Q}_{j,s}$ as follows:

$$\dot{Q}_{j,s} = \lambda_{j,s} WI_s \left(P_{j,s} - P_{w,s}\right), \quad s = 1, ..., n_s, \quad j = 1, ..., n_p \tag{3.71}$$

Still treating injection wells, the constant BHP condition leads to the following expressions for the hydrocarbon and water molar rates respectively:

$$\dot{q}_{k,s} = z_{k,inj}\frac{1-W_F}{v_{T,inj}}\sum_{j=1}^{n_p}\dot{Q}_{j,s}, \quad s = 1,...,n_s, \quad k = 1,...,n_c \tag{3.72}$$

$$\dot{q}_{w,s} = z_{w,inj}\frac{W_F}{v_{T,inj}}\sum_{j=1}^{n_p}\dot{Q}_{j,s}, \quad s = 1,...,n_s \tag{3.73}$$

where W_F is the water fraction, $z_{k,inj}$ stands for the $k-th$ component overall mole fraction, and $v_{T,inj}$ is the total molar volume, all evaluated for the injection fluid.

As mentioned before, only the constant BHP regime is considered for producer wells. In this case, Eqs. (3.74) and (3.75) describe the molar flow rates for both hydrocarbon components and water.

$$\dot{q}_{k,s} = \sum_{j=2}^{n_p} x_{kj,s}\xi_{j,s}\dot{Q}_{j,s}, \quad s = 1,...,n_s, \quad k = 1,...,n_c \tag{3.74}$$

$$\dot{q}_{w,s} = \xi_{w,s}\dot{Q}_{w,s} \tag{3.75}$$

4 NUMERICAL MODEL

It is known the set of equations developed in the previous chapter, even though fully describing the main aspects of multiphase fluid flow in porous media, cannot be inserted into a reservoir simulator before a discretization procedure. The Element-based Finite Volume Method (EbFVM), our choice in this work, is described in detail for two and three-dimensional meshes on the next section. Following, the discretized version of the model equations are shown, as well as the advection terms treatment.

4.1 EbFVM Approach

Different from the Cartesian discretization, meshes are first divide in elements on the EbFVM approach. These entities can assume triangular and quadrilateral shapes for two-dimensional grids. For 3D meshes four elements are possible: hexahedron, tetrahedron, prism and pyramid. Figure (1) presents an example 2D grid with both element types.

Figure 1 – EbFVM mesh sample.

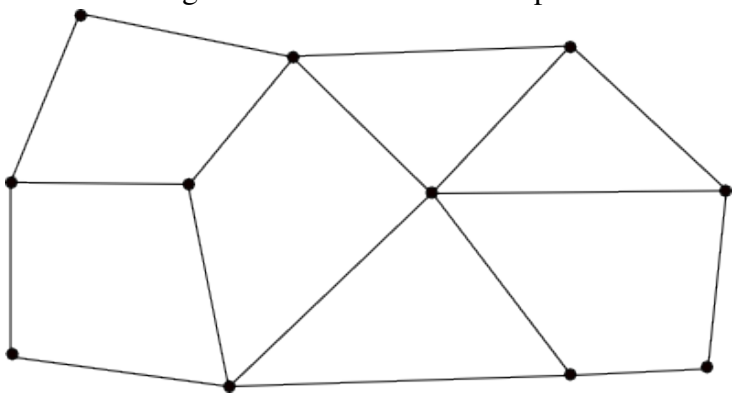

As the approach name suggests, the elements are not entities over which the material constraint is enforced. First, each element is split into sub-elements according to their number of nodes. For example, triangle elements have three sub-elements, and the quadrilateral ones present four. These entities are also called sub-control volumes (SCV) for the material balances and pressure equation are integrated over them. Finally, a single grid block is assembled by all SCV sharing the same node. A representation of this procedure for the mesh in Fig. (1) follows:

Notice the control volume we focused on Fig. (2) is put together with parts of both triangular and quadrilateral elements. This presents a huge difference from the cell-centered Finite Volume Method based on structured grids, where combining different types of cells is an

Figure 2 – Grid volume assembling in EbFVM mesh.

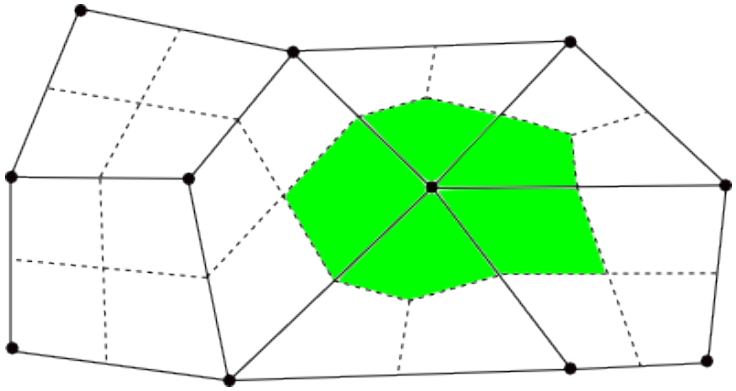

unusual and challenging practice.

Two main aspects need to be highlighted if we are to truly understand the EbFVM capabilities. First, this dual-mesh, cell-vertex approach accounts all equations at the element level, conferring the desired geometric flexibility. Second, all the grid elements we have seen so far are in the physical plane. No matter how distorted the element might look, all of them assume the same form when transported into the computational plane. This is shown for two-dimensional elements below.

Figure 3 – Quadrilateral element transformation.

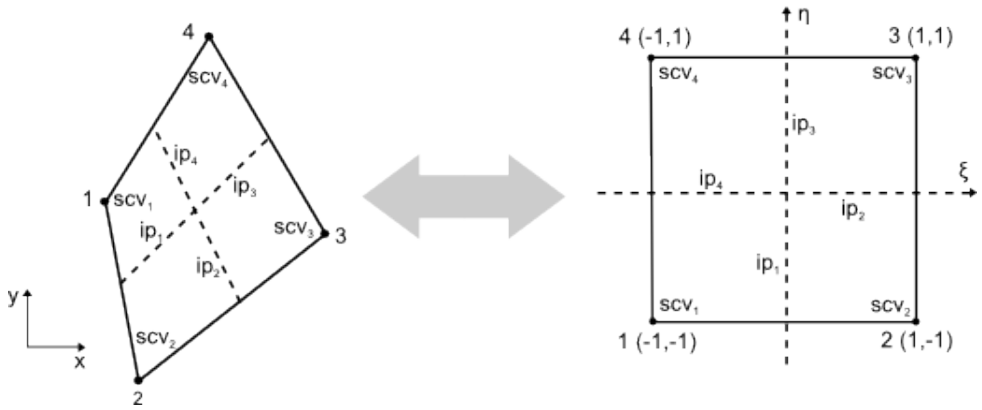

Figure 4 – Triangular element transformation.

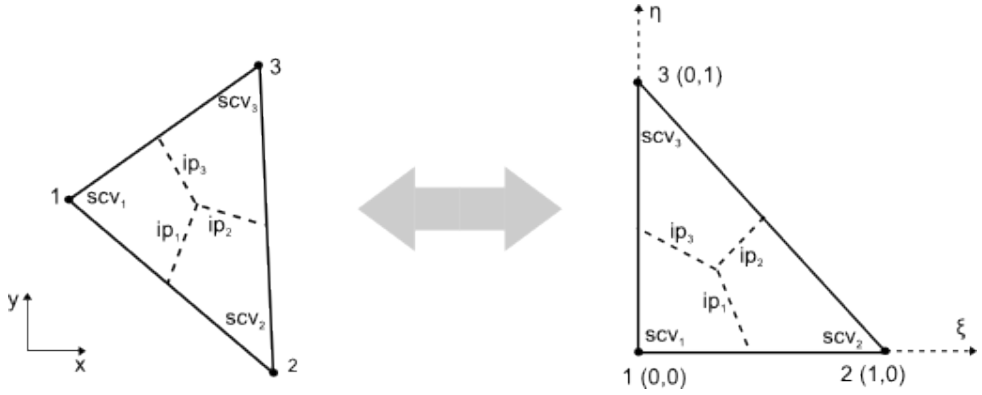

A practical note is in order at this moment. There is no theoretical maximum to the level of distortion a element can reach. Experience, however, shows certain limits should be imposed when handling crooked elements if numerical complications are to be avoided. These limits are not clear and must be evaluated when describing irregular geometries, specially around critical regions such as sharp edges. The relationship between the actual elements and their computational plane version are established by the $\tilde{N}_i$ shape functions, which can be applied not only for the spacial coordinates, but also for any required property. Equation (4.1) shows how to evaluate an arbitrary ϕ parameter at any position inside an element.

$$\phi(\xi,\eta,\gamma) = \sum_{i=1}^{n_v} \tilde{N}_i(\xi,\eta,\gamma)\,\Phi_i \tag{4.1}$$

where ξ, η and γ are numerical plane coordinates, n_v is the element total number of vertices and Φ_i denotes the parameter value at the element nodes. This expression applies for 2D and 3D grids, demanding only the specific shape functions in each case. For triangle and quadrilateral the $\tilde{N}_i$ are respectively presented as follows:

$$\tilde{N}_1(\xi,\eta) = 1-\xi-\eta; \quad \tilde{N}_2(\xi,\eta) = \xi; \quad \tilde{N}_3(\xi,\eta) = \eta \tag{4.2}$$

$$\begin{aligned} \tilde{N}_1(\xi,\eta) &= \frac{1}{4}(1-\xi)(1-\eta); \quad \tilde{N}_2(\xi,\eta) = \frac{1}{4}(1+\xi)(1-\eta) \\ \tilde{N}_3(\xi,\eta) &= \frac{1}{4}(1+\xi)(1+\eta); \quad \tilde{N}_4(\xi,\eta) = \frac{1}{4}(1-\xi)(1+\eta) \end{aligned} \tag{4.3}$$

Using the shape functions we can also evaluate the gradients for two and three-dimensional elements as below:

$$\frac{\partial\phi}{\partial x_j} = \sum_{i=1}^{n_v} \frac{\partial\tilde{N}_i}{\partial x_j}\Phi_i, \quad x_j = x,y,z \tag{4.4}$$

Equation (4.4) requires us to compute the shape functions derivatives with respect to x_j. The expression for two-dimensional grids is written as follows:

$$\frac{\partial\tilde{N}_i}{\partial x} = \frac{1}{det(J_t)}\left(\frac{\partial y}{\partial\eta}\frac{\partial\tilde{N}_i}{\partial\xi} - \frac{\partial y}{\partial\xi}\frac{\partial\tilde{N}_i}{\partial\eta}\right); \quad \frac{\partial\tilde{N}_i}{\partial y} = \frac{1}{det(J_t)}\left(\frac{\partial x}{\partial\xi}\frac{\partial\tilde{N}_i}{\partial\eta} - \frac{\partial x}{\partial\eta}\frac{\partial\tilde{N}_i}{\partial\xi}\right) \tag{4.5}$$

where the $det(J_t)$ is computed by the following expression:

$$det(J_t) = \frac{\partial x}{\partial\xi}\frac{\partial y}{\partial\eta} - \frac{\partial x}{\partial\eta}\frac{\partial y}{\partial\xi} \tag{4.6}$$

Finally, Figs. (4) and (3) present the integration points (ip), located at the sub-control volumes interfaces within an element. These regions, represented by the dashed lines, also denote

the many surfaces between a grid volume and its neighbors. Therefore, the material balance flux terms are integrated over each integration point, located at the center of these interfaces, as a part of the calculations for each control volume. Evaluating the flux, also requires us to know surface area. For 2D elements, even though the integration points are given by straight lines, the area designation still applies once the reservoir thickness h is defined.

$$d\vec{A} = h\left(dy\hat{i} - dx\hat{j}\right) \tag{4.7}$$

This ends the key EbFVM features and calculations for 2D meshes. The definitions for three-dimension grids are analogous. Nevertheless, there are important specifics worth of investigation. First, the already mentioned element types are presented as follows.

Figure 5 – Three-dimensional grid elements: a)Hexahedron, b)Tetrahedron, c)Prism, and d)Pyramid.

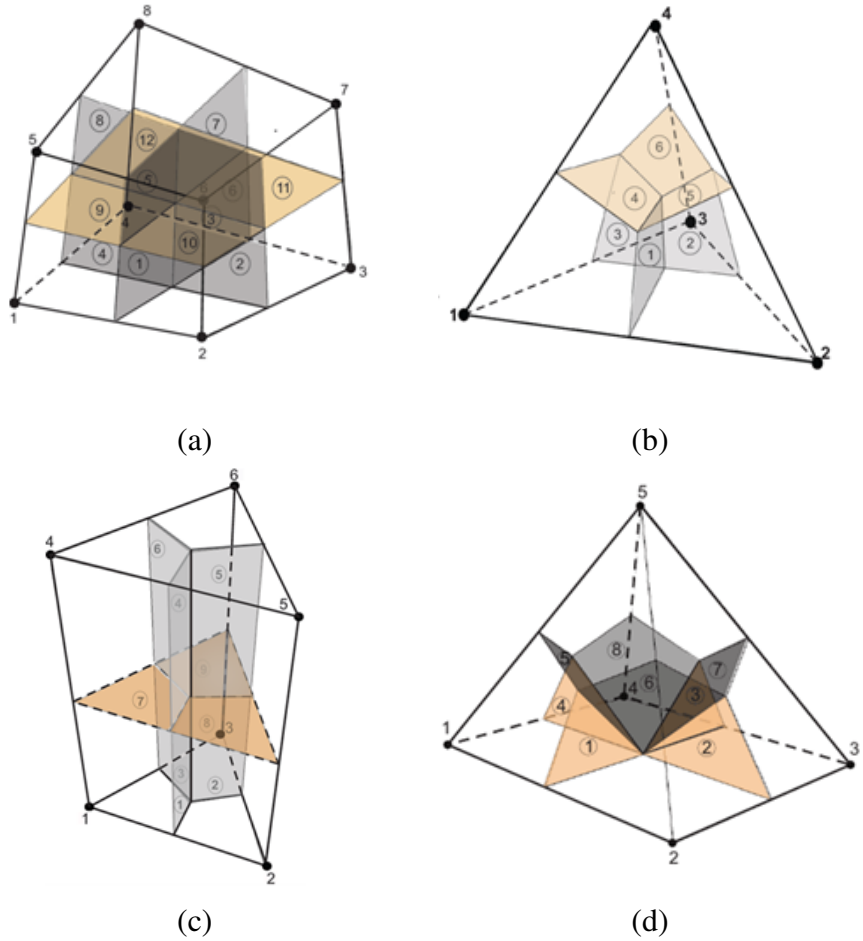

(a) (b)

(c) (d)

For simplicity, only the computational plane versions of these elements are shown. Some practical issues must be discussed before we advance further. Initially, it is possible to generate 3D grids using only one of the elements shown in Fig. (5). However, most actual grids

are composed mainly of hexahedrons and tetrahedrons. This happens because the former has the largest number of nodes per element. The latter is specially useful for local grid refinement. Following, it is not possible to generate mixed meshes of only two element types. There lies the importance of prisms and pyramids, usually applied as intermediates between hexahedron and tetrahedron elements.

After this discussion we can finally present the shape functions for hexahedron, tetrahedron, prism and pyramid elements in that order:

$$\begin{aligned}
\tilde{N}_1(\xi,\eta,\gamma) &= \frac{1}{8}(1+\xi)(1-\eta)(1+\gamma); \quad \tilde{N}_2(\xi,\eta,\gamma) = \frac{1}{8}(1+\xi)(1-\eta)(1-\gamma) \\
\tilde{N}_3(\xi,\eta,\gamma) &= \frac{1}{8}(1-\xi)(1-\eta)(1-\gamma); \quad \tilde{N}_4(\xi,\eta,\gamma) = \frac{1}{8}(1-\xi)(1-\eta)(1+\gamma) \\
\tilde{N}_5(\xi,\eta,\gamma) &= \frac{1}{8}(1+\xi)(1+\eta)(1+\gamma); \quad \tilde{N}_6(\xi,\eta,\gamma) = \frac{1}{8}(1+\xi)(1+\eta)(1-\gamma) \\
\tilde{N}_7(\xi,\eta,\gamma) &= \frac{1}{8}(1-\xi)(1+\eta)(1-\gamma); \quad \tilde{N}_8(\xi,\eta,\gamma) = \frac{1}{8}(1-\xi)(1+\eta)(1+\gamma)
\end{aligned} \tag{4.8}$$

$$\begin{aligned}
\tilde{N}_1(\xi,\eta,\gamma) &= 1-\xi-\eta-\gamma; \quad \tilde{N}_2(\xi,\eta,\gamma) = \xi; \\
\tilde{N}_3(\xi,\eta,\gamma) &= \eta; \quad \tilde{N}_4(\xi,\eta,\gamma) = \gamma
\end{aligned} \tag{4.9}$$

$$\begin{aligned}
\tilde{N}_1(\xi,\eta,\gamma) &= (1-\xi-\eta)(1-\gamma); \quad \tilde{N}_2(\xi,\eta,\gamma) = \xi(1-\gamma); \\
\tilde{N}_3(\xi,\eta,\gamma) &= \eta(1-\gamma); \quad \tilde{N}_4(\xi,\eta,\gamma) = \gamma(1-\xi-\eta); \\
\tilde{N}_5(\xi,\eta,\gamma) &= \xi\gamma; \quad \tilde{N}_6(\xi,\eta,\gamma) = \eta\gamma
\end{aligned} \tag{4.10}$$

$$\begin{aligned}
\tilde{N}_1(\xi,\eta,\gamma) &= \frac{1}{4}\left[(1-\xi)(1-\eta)-\gamma+\frac{\xi\eta\gamma}{1-\gamma}\right]; \\
\tilde{N}_2(\xi,\eta,\gamma) &= \frac{1}{4}\left[(1+\xi)(1-\eta)-\gamma-\frac{\xi\eta\gamma}{1-\gamma}\right]; \\
\tilde{N}_3(\xi,\eta,\gamma) &= \frac{1}{4}\left[(1+\xi)(1+\eta)-\gamma-\frac{\xi\eta\gamma}{1-\gamma}\right]; \\
\tilde{N}_4(\xi,\eta,\gamma) &= \frac{1}{4}\left[(1-\xi)(1+\eta)-\gamma-\frac{\xi\eta\gamma}{1-\gamma}\right]; \\
\tilde{N}_5(\xi,\eta,\gamma) &= \gamma
\end{aligned} \tag{4.11}$$

Now the shape functions derivatives are computed by the following equations:

$$\begin{aligned}
\frac{\partial\tilde{N}_i}{\partial x} = \frac{1}{det(J_t)}\Bigg[&\left(\frac{\partial y}{\partial\eta}\frac{\partial z}{\partial\gamma}-\frac{\partial y}{\partial\gamma}\frac{\partial z}{\partial\eta}\right)\frac{\partial\tilde{N}_i}{\partial\xi}-\left(\frac{\partial y}{\partial\xi}\frac{\partial z}{\partial\gamma}-\frac{\partial y}{\partial\gamma}\frac{\partial z}{\partial\xi}\right)\frac{\partial\tilde{N}_i}{\partial\eta}+ \\
&\left(\frac{\partial y}{\partial\xi}\frac{\partial z}{\partial\eta}-\frac{\partial y}{\partial\eta}\frac{\partial z}{\partial\xi}\right)\frac{\partial\tilde{N}_i}{\partial\gamma}\Bigg]
\end{aligned} \tag{4.12}$$

$$\frac{\partial \tilde{N}_i}{\partial y} = \frac{1}{det\,(J_t)}\left[\left(\frac{\partial x}{\partial \eta}\frac{\partial z}{\partial \gamma} - \frac{\partial x}{\partial \gamma}\frac{\partial z}{\partial \eta}\right)\frac{\partial \tilde{N}_i}{\partial \xi} + \left(\frac{\partial x}{\partial \xi}\frac{\partial z}{\partial \gamma} - \frac{\partial x}{\partial \gamma}\frac{\partial z}{\partial \xi}\right)\frac{\partial \tilde{N}_i}{\partial \eta} - \left(\frac{\partial x}{\partial \xi}\frac{\partial z}{\partial \eta} - \frac{\partial x}{\partial \eta}\frac{\partial z}{\partial \xi}\right)\frac{\partial \tilde{N}_i}{\partial \gamma}\right] \quad (4.13)$$

$$\frac{\partial \tilde{N}_i}{\partial z} = \frac{1}{det\,(J_t)}\left[\left(\frac{\partial x}{\partial \eta}\frac{\partial y}{\partial \gamma} - \frac{\partial x}{\partial \gamma}\frac{\partial y}{\partial \eta}\right)\frac{\partial \tilde{N}_i}{\partial \xi} - \left(\frac{\partial x}{\partial \xi}\frac{\partial y}{\partial \gamma} - \frac{\partial x}{\partial \gamma}\frac{\partial y}{\partial \xi}\right)\frac{\partial \tilde{N}_i}{\partial \eta} + \left(\frac{\partial x}{\partial \xi}\frac{\partial y}{\partial \eta} - \frac{\partial x}{\partial \eta}\frac{\partial y}{\partial \xi}\right)\frac{\partial \tilde{N}_i}{\partial \gamma}\right] \quad (4.14)$$

where

$$det\,(J_t) = \frac{\partial x}{\partial \xi}\left(\frac{\partial y}{\partial \eta}\frac{\partial z}{\partial \gamma} - \frac{\partial y}{\partial \gamma}\frac{\partial z}{\partial \eta}\right) - \frac{\partial x}{\partial \eta}\left(\frac{\partial y}{\partial \xi}\frac{\partial z}{\partial \gamma} - \frac{\partial y}{\partial \gamma}\frac{\partial z}{\partial \xi}\right) + \frac{\partial x}{\partial \gamma}\left(\frac{\partial y}{\partial \xi}\frac{\partial z}{\partial \eta} - \frac{\partial y}{\partial \eta}\frac{\partial z}{\partial \xi}\right) \quad (4.15)$$

Finally, the interface areas for the three-dimensional elements are calculated as below:

$$d\vec{A} = \left(\frac{\partial y}{\partial m}\frac{\partial z}{\partial n} - \frac{\partial y}{\partial n}\frac{\partial z}{\partial m}\right)dmdn\hat{i} - \left(\frac{\partial x}{\partial n}\frac{\partial z}{\partial m} - \frac{\partial x}{\partial m}\frac{\partial z}{\partial n}\right)dmdn\hat{j} + \left(\frac{\partial x}{\partial m}\frac{\partial y}{\partial n} - \frac{\partial x}{\partial n}\frac{\partial y}{\partial m}\right)dmdn\hat{k} \quad (4.16)$$

This concludes our discussion on the basic aspects of EbFVM. These principles, we must note, are applicable to any sort of problem, not only flow simulations.

4.2 Discretized Equations

In order to obtain the discretized model requires the integration of the material balance equations over each sub-control volume and time. First, we integrate Eq. (3.5) over time and volume, yielding the following expression:

$$\int_{scv,t}\frac{1}{V_b}\frac{\partial N_i}{\partial t}dVdt + \int_{scv,t}\vec{\nabla}\cdot\left(\sum_{j=2}^{n_p}\xi_j x_{ij}\vec{u}_j\right)dVdt + \int_{scv,t}\frac{\dot{q}_i}{V_b}dVdt = 0, \quad i = 1,...,n_c \quad (4.17)$$

The three integral terms are present isolated because each one of them is evaluated in a particular way. First of all, the second term on Eq. (4.17) can be rewritten applying the Gauss theorem. The result is shown below:

$$\int_{scv,t}\frac{1}{V_b}\frac{\partial N_i}{\partial t}dVdt + \int_A\sum_{j=2}^{n_p}\xi_j x_{ij}\vec{u}_j d\vec{A}dt + \int_{scv,t}\frac{\dot{q}_i}{V_b}dVdt = 0, \quad i = 1,...,n_c \quad (4.18)$$

This is a very important step, for it allows the fluxes to be evaluated at SCV interfaces, the integration points. Further, the integrations in time and volume are performed. Replacing the Darcy law definition, Eq. (3.7), into Eq. (4.18) and after some manipulation we arrive at the following result:

$$Acc_{i,k} - F_{i,k} + S_{i,k} = 0, \quad i = 1,...,n_c, \quad k = 1,...,n_v \tag{4.19}$$

Equation (4.19) is the mole balance condensed form. The $Acc_{i,k}$ denotes the accumulation term, $F_{i,k}$ accounts for the net advective flux, and $S_{i,k}$ is the well term. Their full expressions are given below:

$$Acc_{i,k} = \frac{V_{scv_k}}{V_{b,k}} \left(N_{i,k}^{n+1} - N_{i,k}^{n} \right), \quad i = 1,...,n_c, \quad k = 1,...,n_v \tag{4.20}$$

$$F_{i,k} = \Delta t \int_A \sum_{j=2}^{n_p} \xi_j^m x_{ij}^m \frac{k_{rj}^m}{\mu_j^m} \overrightarrow{\overrightarrow{K}} \cdot \vec{\nabla} \Phi_j^m \cdot d\vec{A}_k, \quad i = 1,...,n_c, \quad k = 1,...,n_v \tag{4.21}$$

$$S_{i,k} = \Delta t \frac{V_{scv_k}}{V_{b,k}} \dot{q}_{i,k}, \quad i = 1,...,n_c, \quad k = 1,...,n_v \tag{4.22}$$

where $n+1$ and n denote the current and previous time steps respectively. There is still some work remaining for $F_{i,m}$, since Eq. (4.21) is not yet ready for implementation. An accurate approximation is to evaluate the surface integral as a sum of the advection terms in all integration points. We should remember the *ips* are positioned at the center of each interface, hence the flux properties are also computed at this point.

$$F_{i,k} = \Delta t \sum_{l}^{n_{ip}} \sum_{j=2}^{n_p} \left[\xi_j^m x_{ij}^m \frac{k_{rj}^m}{\mu_j^m} \overrightarrow{\overrightarrow{K}} \cdot \vec{\nabla} \Phi_j^m \cdot d\vec{A} \right]_l, \quad i = 1,...,n_c, \quad k = 1,...,n_v \tag{4.23}$$

where n_{ip} is the total number of integration points in the $i-th$ SCV. Here it is possible to see the shape functions relevance. The gradient term in Eq. (4.23) is rewritten using Eq. (4.4) yielding the expression as follows:

$$F_{i,k} = \Delta t \sum_{l}^{n_{ip}} \sum_{j=2}^{n_p} \left[\xi_j^m x_{ij}^m \frac{k_{rj}^m}{\mu_j^m} \overrightarrow{\overrightarrow{K}} \cdot \sum_{h}^{n_v} \vec{\nabla} \tilde{N}_h \Phi_{j,h}^m \cdot d\vec{A} \right]_l, \quad i = 1,...,n_c, \quad k = 1,...,n_v \tag{4.24}$$

We finally obtained $F_{m,i}$ in terms of known expressions, as well as fluid and formation properties. Still, some considerations regarding Eq. (4.24) are in order. The evaluation of

simulation parameters in EbFVM is peculiar and not intuitive. This assertion is better explained showing the discretized hydraulic potential equation at an arbitrary l integration point.

$$\Phi^m_{j,l} = P^{n+1}_l + P^m_{cjr,l} - \rho^m_{j,elem} g D_l, \quad j = 1,...,n_p \tag{4.25}$$

Most terms in Eq. (4.25) are evaluated at the ip through an interpolation from the mesh vertices, where these properties are stored. The phase mass density, however, has the *elem* subscript. This means all SCV inside a single element use the same property value when computing the flux term. The same happens for absolute permeability and formation porosity. No harm comes from this dual-mesh approach because, as we mentioned, all calculations are performed first at the sub-control volumes.

In analogous way, Eqs. (3.6) and (3.19), respectively the water balance and pressure expressions, are submitted to discretization. Following the same structure as in Eq. (4.19), the results are presented for water:

$$Acc_{w,k} = \frac{V_{scv_k}}{V_{b,k}} \left(N^{n+1}_{w,k} - N^n_{w,k} \right), \quad k = 1,...,n_v \tag{4.26}$$

$$F_{w,k} = \Delta t \sum_l^{n_{ip}} \left[\xi^m_w \frac{k^m_{rw}}{\mu^m_w} \overrightarrow{\overrightarrow{K}} \cdot \sum_h^{n_v} \vec{\nabla} \tilde{N}_h \Phi^m_{w,h} \cdot d\vec{A} \right]_l, \quad k = 1,...,n_v \tag{4.27}$$

$$S_{w,m} = \Delta t \frac{V_{scv_k}}{V_{b,k}} \dot{q}_{w,k}, \quad k = 1,...,n_v \tag{4.28}$$

In turn, for the pressure equation we have:

$$Acc^P_k = \left[V_{scv_k} \phi^0_{elem} C_f - \frac{V_{scv_k}}{V_{b,k}} \frac{\partial V^n_{T,k}}{\partial P} \right] \left(P^{n+1}_k - P^n_k \right) - \frac{V_{scv_k}}{V_{b,k}} \left(V^n_{T,k} - V^n_{p,k} \right), \quad k = 1,...,n_v \tag{4.29}$$

$$F^P_k = \Delta t \overline{V}^n_{Tw,k} \sum_l^{n_{ip}} \left[\xi^m_w \frac{k^m_{rw}}{\mu^m_w} \overrightarrow{\overrightarrow{K}} \cdot \sum_h^{n_v} \vec{\nabla} \tilde{N}_h \Phi^m_{w,h} \cdot d\vec{A} \right]_l + \Delta t \sum_{i=1}^{n_c} \overline{V}^n_{Ti,k} \sum_l^{n_{ip}} \sum_{j=2}^{n_p} \left[\xi^m_j x^m_{ij} \frac{k^m_{rj}}{\mu^m_j} \overrightarrow{\overrightarrow{K}} \cdot \sum_h^{n_v} \vec{\nabla} \tilde{N}_h \Phi^m_{j,h} \cdot d\vec{A} \right]_l, \quad k = 1,...,n_v \tag{4.30}$$

$$S^P_k = \Delta t \sum_{i=1}^{n_c+1} \overline{V}^n_{Ti,k} \frac{V_{scv_k}}{V_{b,k}} \dot{q}_{i,k}, \quad k = 1,...,n_v \tag{4.31}$$

So far, all presented development can be applied into both IMPEC and FI models. Exactly for this reason, a key aspect regarding the time level evaluation has been ignored. Several parameters on the previously shown equations are accompanied by the m superscript, which basically states both n and $n+1$ time levels are applicable. The IMPEC approach is achieved setting all undefined properties evaluation at the previous time step. The FI method, on the other hand, would require m to always be replaced by $n+1$. In an Adaptive Implicit Method the reservoir is split on IMPEC, or explicit, and FI, or implicit, regions. Once the implicitness degree in every grid node is set, its properties are computed accordingly. This concept is expanded in the next section and further detailed on the next chapter.

4.3 Interpolation Function

The flux terms as in Eqs. (4.24), (4.27) and (4.30) require properties to be computed at the integration points. A first logical approach would be approximate their values by the shape functions, as in Eq. (4.1). We are dealing, however, with advective fluxes. This sort of interpolation, an unstructured version of a central differences scheme, causes severe numerical oscillation, as noted by Maliska (2004). UTCOMP contains several more suitable interpolation functions. In the present work, our choice is the upwind scheme. Let us take the ip_1 interface in Fig. (3) as an example. For an arbitrary phase related fluid property ϕ_j, the interpolation function follows:

$$\phi_{j,ip_1} = \begin{cases} \phi_{j,1} & if \quad \left(\overrightarrow{\overrightarrow{K}} \cdot \vec{\nabla}\Phi_j^m \cdot d\vec{A}\right)_{ip_1} > 0 \\ \phi_{j,2} & if \quad \left(\overrightarrow{\overrightarrow{K}} \cdot \vec{\nabla}\Phi_j^m \cdot d\vec{A}\right)_{ip_1} \leq 0 \end{cases} \quad , \quad j = 1, ..., n_p \tag{4.32}$$

The expression basically means an interface is interpolated on the upstream position of the two surrounding nodes.

5 THE ADAPTIVE IMPLICIT METHOD

As discussed earlier, UTCOMP has IMPEC and FI formulations already implemented. These methods are also developed around the same physical modeling and discretization method presented in the previous chapters. The main goal of the AIM is to combine the advantages of both approaches while mitigating their shortcomings. In order to achieve this task, we need a better understanding of the formulations advantages and issues.

As implemented by Chang (1990), the Acs *et al.* (1985) Implicit Pressure Explicit Composition formulation presents a single implicit primary variable, yielding the smallest possible linear system for a reservoir simulation, hence the lowest computational effort per time step. Choosing to compute most primary unknowns explicitly is also the cause for the key issue with the method: time step size related numerical instability. For various simpler case studies this stability issue is not relevant, but, as noted by Collins *et al.* (1992) and Quandalle e Savary (1989), the time step limitation makes IMPEC models frequently unsuitable for real field applications, and enhanced recovery processes, such as coning studies. Fully Implicit methodologies, on the other hand, are the most stable class of formulations. This is achieved solving all primary unknowns implicitly, which eliminates the time step related instability. Coupling all unknowns into the Jacobian matrix also generates much larger numerical requirements, which are not always properly balanced by larger time steps. In the present work, we use the Fully Implicit model proposed by Fernandes (2014). Applying this FI formulation facilitates the code integration, once it is also based on the Acs *et al.* (1985) choice of primary equations and variables.

The advent of Adaptive Implicit Methods comes from the realization only a small fraction of grid volumes require an implicit evaluation at any given time step ((FUNG *et al.*, 1989)). Usually the neighborhood of wells and the moving fluid front, where high phase velocities occur, are the sources of instability in IMPEC models. Therefore, only these regions should be calculated FI, while most of the reservoir can remain computed explicitly without any stability loss. The Jacobian matrix then assumes an intermediate size, generally much smaller than a Fully Implicit linear system, greatly reducing the computation demand for a simulation. At the same time, once the sources of instability are set implicit, larger time steps are feasible. Note the AIM addresses directly the main flaws of both IMPEC and FI, while taking advantage of their most desirable features.

There are still some lingering practical issues. First, we should note the high flux front moves with time, rendering the selection of implicit blocks dynamic. Another matter is

how to identify, for any given time, which blocks to compute implicit without producing any overkill or leave possible sources of instability unchecked. Finally, the Jacobian matrix is not directly obtained in its final form. The reduction procedure has to be performed every time the FI blocks distribution changes. All these points are discussed in the following sections.

5.1 Jacobian Evaluation

At any given point during an AIM run, there will be at least a single FI vertex, since the wells, perennial sources of instability, should be treated implicitly along the entire run. Hence, our system of equations is necessarily non-linear. A Newton-Raphson iterative procedure is required in order to linearize our set of equations. Additionally, all primary expressions need to be rewritten in residual form, which can be simply exemplified by modifying the hydrocarbon material balance as presented in Eq. (3.5).

$$RN_i = \frac{1}{V_b}\frac{\partial N_i}{\partial t} + \vec{\nabla}\cdot\left(\sum_{j=2}^{n_p}\xi_j x_{ij}\vec{u}_j\right) + \frac{\dot{q}_i}{V_b}, \quad i = 1,...,n_c \tag{5.1}$$

The same can be done for the water and pressure equations:

$$RN_w = \frac{1}{V_b}\frac{\partial N_w}{\partial t} + \vec{\nabla}\cdot(\xi_w\vec{u}_w) + \frac{\dot{q}_w}{V_b} \tag{5.2}$$

$$RP = \left[\phi^0 C_f - \frac{1}{V_b}\left(\frac{\partial V_t}{\partial P}\right)_{N_i}\right]\frac{\partial P}{\partial t} + \overline{V}_{tw}\vec{\nabla}\cdot(\xi_w\vec{u}_w) + \sum_{i=1}^{n_c}\overline{V}_{ti}\sum_{j=2}^{n_p}\vec{\nabla}\cdot\left(\xi_j x_{ij}\vec{u}_j\right) + \sum_{i=1}^{n_c+1}\overline{V}_{ti}\frac{q_i}{V_b} \tag{5.3}$$

The linearized equations for mole and pressure equations then assume the following form, respectively:

$$\sum_{j=1}^{nnb_i}\left[\frac{\partial RN_{i,k}}{\partial P_j}\delta P_j + \sum_{l=1}^{n_c+1}\frac{\partial RN_{i,k}}{\partial N_{l,j}}\delta N_{i,j}\right] = RN_{i,k}, \quad i = 1,...,n_b, \quad k = 1,...,n_c+1 \tag{5.4}$$

$$\sum_{j=1}^{nnb_i}\left[\frac{\partial RP_i}{\partial P_j}\delta P_j + \sum_{l=1}^{n_c+1}\frac{\partial RP_i}{\partial N_{l,j}}\delta N_{i,j}\right] = RP_i, \quad i = 1,...,n_b \tag{5.5}$$

where *nnb* denotes the number of neighboring vertices, including the i node itself, and δ stands for the primary unknowns changes over an iterative step. This can also be presented in matrix

form:

$$\begin{bmatrix} j_{1,1} & \cdots & j_{1,n_b} \\ \vdots & \ddots & \vdots \\ j_{n_b,1} & \cdots & j_{n_b,n_b} \end{bmatrix} \begin{bmatrix} x_1 \\ \vdots \\ x_{n_b} \end{bmatrix} = \begin{bmatrix} b_1 \\ \vdots \\ b_{n_b} \end{bmatrix} \tag{5.6}$$

In Eq. (5.6) each term represents a sub-matrix as shown below:

$$j_{i,k} = \begin{bmatrix} \frac{\partial RP_i}{\partial P_k} & \frac{\partial RP_i}{\partial N_{1,k}} & \cdots & \frac{\partial RP_i}{\partial N_{n_c,k}} & \frac{\partial RP_i}{\partial N_{w,k}} \\ \frac{\partial RN_{1,i}}{\partial P_k} & \frac{\partial RN_{1,i}}{\partial N_{1,k}} & \cdots & \frac{\partial RN_{1,i}}{\partial N_{n_c,k}} & \frac{\partial RN_{1,i}}{\partial N_{w,k}} \\ \vdots & \vdots & \ddots & \vdots & \vdots \\ \frac{\partial RN_{n_c,1}}{\partial P_k} & \frac{\partial RN_{n_c,1}}{\partial N_{1,k}} & \cdots & \frac{\partial RN_{n_c,1}}{\partial N_{n_c,k}} & \frac{\partial RN_{n_c,1}}{\partial N_{w,k}} \\ \frac{\partial RN_{w,i}}{\partial P_k} & \frac{\partial RN_{w,i}}{\partial N_{1,k}} & \cdots & \frac{\partial RN_{w,i}}{\partial N_{n_c,k}} & \frac{\partial RN_{w,i}}{\partial N_{w,k}} \end{bmatrix} \tag{5.7}$$

$$x_i = \begin{bmatrix} \delta P_i \\ \delta N_{1,i} \\ \vdots \\ \delta N_{n_c,1} \\ \delta N_{w,1} \end{bmatrix} \tag{5.8}$$

$$b_i = \begin{bmatrix} -RP_i \\ -RN_{1,i} \\ \vdots \\ -RN_{n_c,1} \\ -RN_{w,1} \end{bmatrix} \tag{5.9}$$

Notice all balance equations, as well as the pressure equation are included in the linear system, independently of each unknown status. The linear system in Eq. (5.6) first need reducing before being actually solved. This procedure is described for a simple EbFVM mesh. Figure (6) shows the referred grid. From the mesh, only the first and last vertices are computed implicit. In the previous chapter we highlighted the superscript m meant the time step level in which a given property should be evaluated depended on whether each volume was IMPEC or FI. For example, the primary equations written for vertex (1) account not only for its own influence, but also of its neighbors impact through the advection term. However, blocks (2), (3) and (4) are all IMPEC. This leads to the mole balance and pressure equations

Figure 6 – EbFVM mesh with 9 volumes.

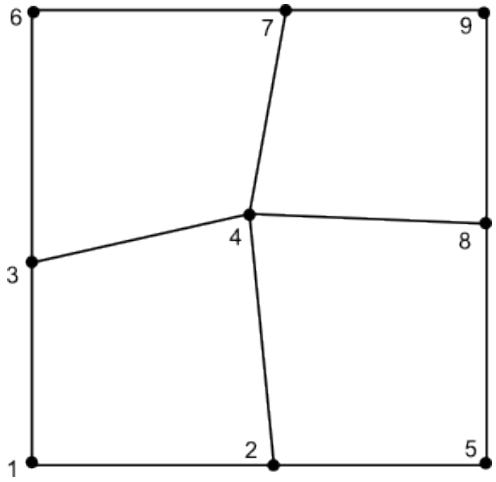

assuming a form where m is $n+1$ to all volume (1) related properties, and n for the remaining parameters. Notice the final shape of these expressions is dictated by the implicitness level of the own volume and all the neighboring blocks. The appendix presents more details on this matter. Applying the same logic to the entire mesh yields the Jacobian matrix different from Eq. (5.6). For a 3 hydrocarbon pseudo-components reservoir fluid the resulting linear system is shown in the following illustration. In Fig. (7), the x indicate the non-zero values. Notice

Figure 7 – Full Jacobian Matrix.

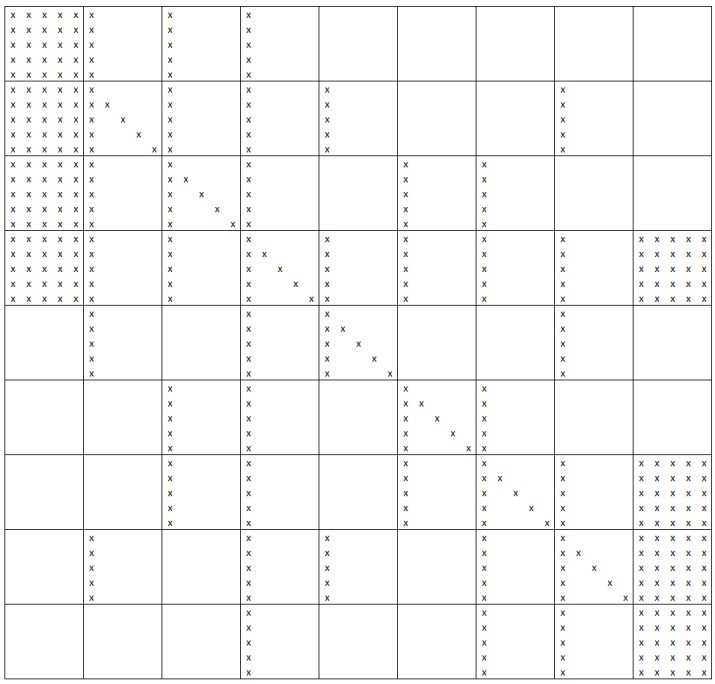

each element in the Jacobian is a (n_c+2)x(n_c+2) sub-matrix and all primary variables are present. The reduction procedure takes place by removing the explicit unknowns equations and rearranging the remaining coefficients. This leads to the linear system as shown in Fig. (8),

where the deformed sub-matrices evidence the performed changes. The Jacobian shown above

Figure 8 – Reduced Jacobian Matrix.

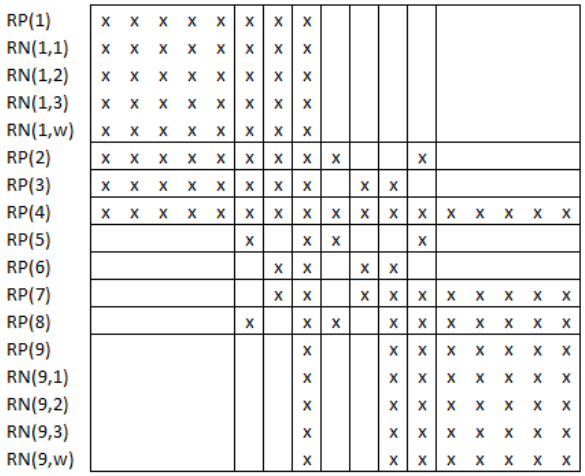

is considerably smaller than Fig. (7), yielding a much smaller numerical effort. Following the linear system calculations, the implicit variables are updated. The removed equations are now used to compute the explicit primary unknowns independently. This approach, very similar to the one presented by Thomas e Thurnal (1983), has little implementation requirements and can also be used on methods with fixed degrees of implicitness, as in Drumond-Filho *et al.* (2015).

5.2 Switching Criteria

Until this point, this chapter has elucidated just how to mingle IMPEC and FI volumes together in such a way to produce stable and accurate results. There is still the serious matter of deciding which blocks to set implicit or explicit at every time step during a run. In reality, even an efficient AIM framework is rendered useless if the simulator is not able to precisely identifying whether or not each grid volume is unstable and act accordingly.

Several studies have been done in order to optimize the switching procedure, from simple threshold methods, as in Forsyth e Sammon (1986), to complex based models based on the Courant-Friedrichs-Lewy (CFL) condition, as exemplified by Russel (1989), Grabenstetter *et al.* (1991) and Fung *et al.* (1989). For the purposes of this work, two switching criteria were implemented. The first one is a threshold criterion suggested by Thomas e Thurnal (1983). The second method comes from the CFL-based condition proposed by Coats (2001). Both are presented in following sub-sections.

5.2.1 Threshold Criterion

The threshold method implemented on this work differs from Thomas e Thurnal (1983), called original threshold method (OTM) for the remaining of this study, in two main ways. First, the OTM compare all primary variables (oil phase pressure and phase saturations) changes over the previous time step against its respective thresholds. The proposed method compares only the phase saturations against a variation limit regardless of being primary variables, which is not the case in UTCOMP. This choice comes from the assumption saturation changes are fairly accurate on identifying large throughputs and easier to compare, given their normalized nature. Additionally, the implemented threshold criterion admits only two implicitness levels: IMPEC or FI. This means whenever a single phase presents a large saturation variance, all the primary variables are set implicit. The OTM, on the other hand, allows any implicitness level, for if any given unknown change surpasses its threshold, only this variable turns implicit.

Evaluating thresholds requires nearly no computational effort, and there lies the greatest advantage of this technique. On the other hand, there is no physical basis for defining the threshold values, as stated by Thomas e Thurnal (1983). This leads to a series of trial-and-error runs in order to verify an optimal values for each case study. The figure below illustrates the procedure for the threshold criterion implemented for a single time step. In Fig. (9), IMPEC volumes where the test returns $TRUE$ are switched, as well as FI blocks where test is $FALSE$.

5.2.2 CFL-based Criterion

Here the implementation follows the criterion developed by Coats (2001), in which selected blocks are submitted to a stability test as shown in Eq. (5.10).

$$\frac{F_i \Delta t}{V_{p,i}} < 1, \quad i = 1, ..., n_b \tag{5.10}$$

The parameter F_i is a function of flow rates, reservoir and fluid properties. Two functions are derived, each one addressing specific instability issues. The first one relates to the explicit treatment of relative permeabilities and capillary pressures, both saturation-dependent parameters. Its complete development is shown in detail on "(Appendix A)". The final equation is shown below for a multidimensional three-phase flow:

$$F_i = \frac{1}{2} \left| f11_i + f22_i + \sqrt{\left(f11_i + f22_i\right)^2 - 4det\left(F_i\right)} \right|, \quad i = 1, ..., n_b \tag{5.11}$$

Figure 9 – Threshold criterion flow chart.

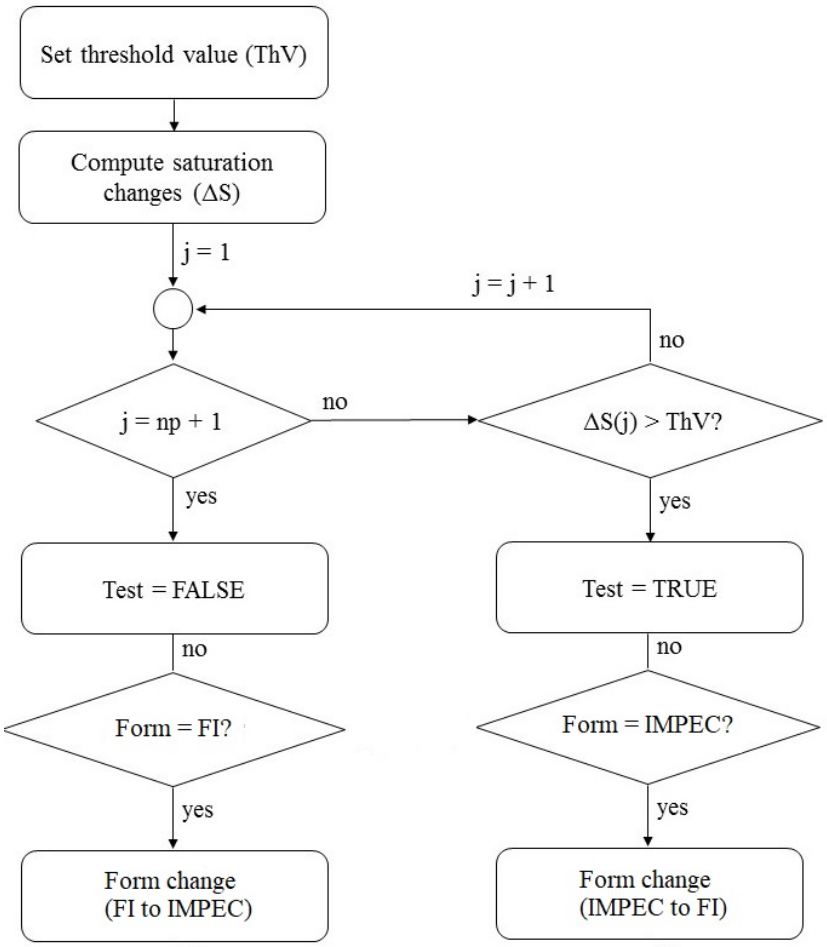

where the frs_i parameters for a given volume are a sum of terms over its neighboring vertices. For example, $f11_i$ is computed as

$$f11_i = \sum_{j=1}^{J_i} f11_{ij}, \quad i = 1, ..., n_b \tag{5.12}$$

In Eq. (5.12), J_i is the total number of neighbors for a block, and the $f11_{ij}$ are the terms on the i/j interfaces. The same logic applies for the remaining parameters. Computing F_i then requires evaluating the interface terms as follows:

$$f11_{ij} = \frac{T_{ij}}{\lambda_t}\left[(\lambda_o + \lambda_g)\,\lambda'_{ww}\,|\Delta\Phi_w| - \lambda_w\lambda'_{ow}\,|\Delta\Phi_o| - \lambda_w\,(\lambda_o + \lambda_g)\left(P'_{cwo,i} + P'_{cwo,j}\right)\right] \tag{5.13}$$

$$f12_{ij} = -\frac{T_{ij}}{\lambda_t}\left[\lambda_w\lambda'_{og}\,|\Delta\Phi_o| + \lambda_w\lambda'_{gg}\,|\Delta\Phi_g| - (\lambda_o + \lambda_g)\,\lambda'_{wg}\,|\Delta\Phi_w| + \lambda_w\lambda_g\left(P'_{cgo,i} + P'_{cgo,j}\right)\right] \tag{5.14}$$

$$f21_{ij} = -\frac{T_{ij}}{\lambda_t}\left[\lambda_g\lambda'_{ww}\,|\Delta\Phi_w| + \lambda_g\lambda'_{ow}\,|\Delta\Phi_o| - \lambda_g\lambda_w\left(P'_{cgo,i} + P'_{cgo,j}\right)\right] \tag{5.15}$$

$$f22_{ij} = \frac{T_{ij}}{\lambda_t}\left[-\lambda_g \lambda_{og}^{'} \left|\Delta\Phi_o\right| + \left(\lambda_w + \lambda_o\right)\lambda_{gg}^{'}\left|\Delta\Phi_g\right| - \lambda_g \lambda_{wg}^{'}\left|\Delta\Phi_w\right| + \lambda_g\left(\lambda_o + \lambda_w\right)\left(P_{cgo,i}^{'} + P_{cgo,j}^{'}\right)\right] \tag{5.16}$$

Additionally, the last term in Eq. (5.11) is calculated by the following expression:

$$det\left(F_i\right) = f11_i f22_i - f12_i f21_i \tag{5.17}$$

Two classes of terms are still left unknown at this point. They are the phase mobility and capillary pressure derivatives with respect to phase saturations, $\lambda_{jk}^{'}$ and $P_{cjk,i}^{'}$, respectively computed as

$$\lambda_{jk}^{'} = \frac{\partial \lambda_j}{\partial S_k}, \tag{5.18}$$

$$P_{cjk,i}^{'} = \frac{\partial P_{cjr,i}}{\partial S_{k,i}}. \tag{5.19}$$

We should note Eq. (5.18) is applied at the interfaces and Eq. (5.19) at the vertices. Finally, the frs_{ij} are stored at the gas phase upstream vertex should λ_g be greater than zero. If this is not the case, the terms are stored at the water phase upstream block position. Notice most properties and derivatives present in this approach are already evaluated on UTCOMP. This means there is actually little additional computational effort, despite any previous assumptions. The second F_i function deals with the compositions explicit treatment, and assumes the form described in Eq. (5.20) for a three-phase flow.

$$F_i = Max\left(k\right)\frac{Q_o \rho_o x_{ok} + Q_g \rho_g x_{gk}}{S_o \rho_o x_{ok} + S_g \rho_g x_{gk}}, \quad k = 1, ..., n_c \tag{5.20}$$

where Q_o and Q_g are the total flow rates through all interfaces for the oil and gas phases respectively.

The CLF condition is evaluated computing F_i by both methods and applying the larger value in Eq. (5.10). Should the criterion be met, the vertex is set IMPEC. Otherwise, the FI approach is advisable. Coats (2001) has also tested CFL conditions for values up to 2.0, obtaining stable runs for some case studies. Such analysis was not performed on this work.

The remaining matter concerning the AIM on UTCOMP is deciding which blocks to test for possible formulation switching and when to perform it. The initial assumption would be

all vertices should be checked. This approach, however, proves to be highly demanding, specially for the CFL-based criterion. Besides, at a given time level, it is known most volumes will not be changed. Collins *et al.* (1992) proposes all implicit blocks, explicit blocks neighboring implicit ones, and blocks where a mobile phase first appears should be the only ones tested. A comparison of both approaches is conducted in the next chapter.

As for the moment to perform the checking, test vertices every time step can also prove to be cumbersome. From time levels n to $n+1$, few vertices are expect to undergo a switching, even though a large amount for volumes are tested. Usually performing the checking procedure every few time steps. This is specially true for recently turned implicit blocks (FUNG *et al.*, 1989). Regarding the Newton-Raphson iterative procedure within a time step, Grabenstetter *et al.* (1991) has observed checking the stability condition at every iterative level highly increases the computational effort demand and the amount of iterations required for convergence. Hence, our approach is to check the selected blocks only at the beginning of the time step.

6 RESULTS AND DISCUSSION

In this chapter, we evaluate the AIM for both switching criteria methods discussed in the previously. The proposed model is compared with the IMPEC and FI formulations already present in UTCOMP and validated in previous studies. This comparison is performed in terms of oil and gas production rate curves, degree of implicitness, and overall computation time for two and three-dimensional grids. Before presenting these results, we dedicate the first two sections to investigate some aspects of the Adaptive method. First, the choice of grid nodes to be tested for formulation switching is the focus of our analysis. Two approaches to this matter are compared. Following, inspired by similar works in the literature, we verify the actual CFL value stable limits for two case studies.

6.1 Choice of Tested Grids Nodes

As mentioned in the previous chapter, there are two ways of selecting which blocks will undertake the formulation check procedure. We summarize them below:

- All grid blocks are tested (TestAll)
- All implicit nodes, explicit nodes on the neighborhood of implicit volumes and nodes where a new mobile phase first appears (TestSome)

The first approach, *TestAll*, is obvious choice at first. The *TestSome* way, on the other hand, is proposed by Collins *et al.* (1992). The comparison between these methods is undertaken for a single 7,021 nodes two-dimensional mesh composed of quadrilateral elements with two case studies. The problem follows a quarter of five-spot configuration. Figure (10) shows the applied grid and each case study is detailed in the following sub-sections. The blue and red dots on the grid represent the injector and producer wells, respectively.

6.1.1 Case study 1

The first case investigated in this section is a gas flooding problem. The reservoir fluid is a light oil composed of three pseudo-components. Initially, only oil and water phases are present. The latter is immobile throughout the run. The injection fluid is responsible for the appearance of the gas phase. We are going to designate this case as QOFS-3comp from now on. More details on the reservoir, fluids and operational conditions are given in the following tables.

Additionally, the binary interaction coefficients and relative permeability data are

Figure 10 – Two-dimensional quadrilateral grid composed of 7,021 nodes.

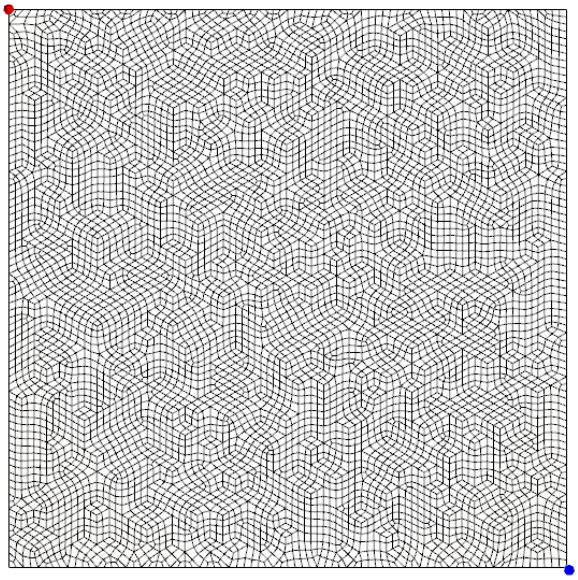

Table 1 – Reservoir data for case QOFS-3comp.

Property	**Value**
Length, width and thickness	170.68 m, 170.68 m, 30.49 m
Porosity	0.30
Initial water saturation	0.25
Initial pressure	20.68 MPa
Permeability in x, y and z directions	$9.86\text{x}10^{-14}$ m^2, $9.86\text{x}10^{-14}$ m^2, $9.86\text{x}10^{-15}$ m^2
Formation temperature	299.82 K

Table 2 – Fluid composition data for case QOFS-3comp.

Component	**Initial Reservoir Composition**	**Injection Fluid Composition**
CO_2	0.01	0.95
C_1	0.19	0.05
nC_{16}	0.80	0.00

Table 3 – Component data for case QOFS-3comp.

Component	**P_c (MPa)**	**T_c (K)**	**v_c (m^3/kmol)**	**MW (kg/kmol)**	**Ac. Factor**
CO_2	7.39	304.21	$9.40\text{x}10^{-2}$	44.01	0.225
C_1	4.60	190.60	$9.99\text{x}10^{-2}$	16.04	0.022
nC_{16}	1.74	734.68	$8.17\text{x}10^{-1}$	222.00	0.684

presented in order to better describe the problem.

First we compare the oil and gas production curves in Figs. (11) and (12) using the CFL and threshold criteria. The results show great agreement between all the curves, regardless

Table 4 – Operational conditions for case QOFS-3comp.

Operational condition	Value
Fixed gas rate injection	5.66×10^5 m^3/d
Producer's bottom hole pressure	20.68 MPa

Table 5 – Binary interaction coefficient data for case QOFS-3comp.

Component	CO_2	C_1	nC_{16}
CO_2	-	0.12	0.12
C_1	0.12	-	-
nC_{16}	0.12	-	-

Table 6 – Relative permeability data for case QOFS-3comp.

Parameter	Value
Model	Modified Stone II
End point rel. permeabilities (k^0_{rw}, k^0_{row}, k^0_{rog}, k^0_{rg})	1.00, 1.00, 1.00, 1.00
Residual saturations (S_{wr}, S_{orw}, S_{org}, S_{gr})	0.25, 1×10^{-6}, 1×10^{-6}, 0.00
Exponents (e_w, e_{ow}, e_{og}, e_g)	1.00, 1.00, 1.00, 1.00

of the switching criterion or testing approach. Following, Tab. (7) shows the comparison for the CPU time, degree of implicitness and other run parameters. Herein it can be observed the effects of testing all grid volumes are insignificant for the Threshold criterion, while producing an important increase of implicit blocks, and CPU time as a consequence, for the CFL criterion. This behavior was already expected, since testing more nodes will most likely generate some overkill. The Threshold method behavior, although desirable, is unexpected. The following case study data should be verified before drawing any conclusions. We also note all threshold values presented in this work have already undergone the preliminary runs phase, meaning we are comparing runs with optimal thresholds.

Table 7 – Simulation data for case QOFS-3comp.

Formulation	Avg. DT (d)	Step	FI%	CPU time (s)
AIM CFL (TestSome)	0.018	800	2.117	5024.454
AIM CFL (TestAll)	0.017	800	16.418	7000.965
AIM Threshold (TestSome)*	0.019	800	0.028	4867.840
AIM Threshold (TestAll)*	0.019	800	0.028	4929.408

*The threshold is set to 0.01.

Figure 11 – Oil production rates for Case study 1 (QOFS-3comp).

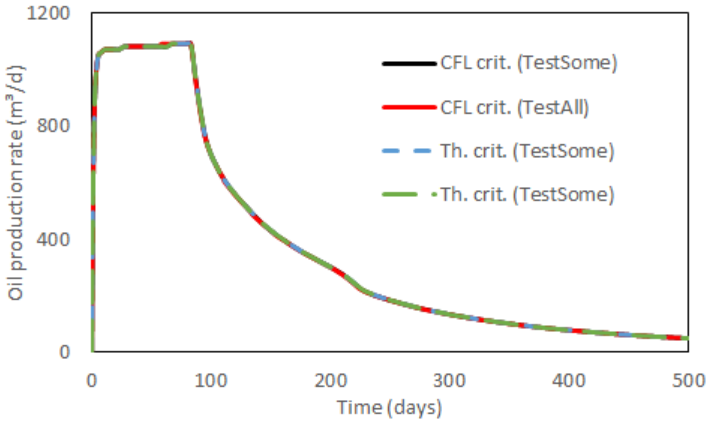

Figure 12 – Gas production rates for Case study 1 (QOFS-3comp).

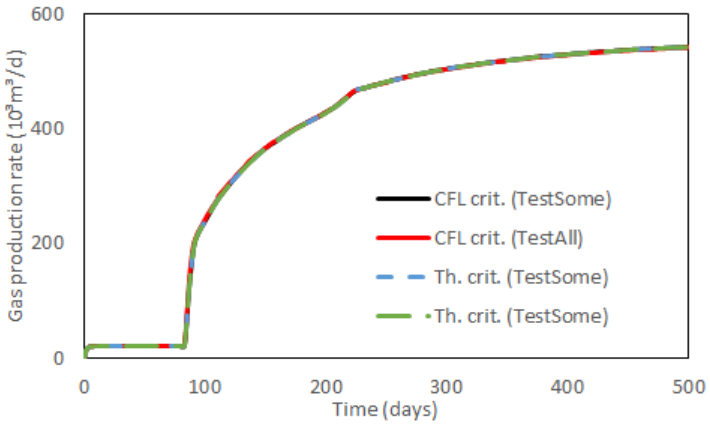

Before we proceed, an explanation is in order. The STEP parameter on Tab. (7) designates the number of time steps between two formulation checks. We choose to highlight it for its importance on the CPU time.

6.1.2 Case study 2

The second case study is similar to the first one. Again, we have a gas flooding problem in a quarter of five-spot reservoir configuration. The main difference lies on the reservoir fluid, lighter than the previous one, and the injection fluid, not rich in CO_2. Additionally, the three phases (oil, gas and water) are present in the reservoir at the simulation starting point. Once again water is immobile. We name this case QOFS-6comp. All case data is shown in the following tables:

The comparison study performed is analogous to the previous case. First, the plot for both oil and gas production rates is shown in Figs. (13) and (14). The curves are nearly overlapping, verifying no accuracy issue arises from neither switching criteria as a result of

Table 8 – Reservoir data for case QOFS-6comp.

Property	Value
Length, width and thickness	170.68 m, 170.68 m, 30.49 m
Porosity	0.35
Initial water saturation	0.17
Initial pressure	10.34 MPa
Permeability in x, y and z directions	$9.86\text{x}10^{-15}$ m^2, $9.86\text{x}10^{-15}$ m^2, $9.86\text{x}10^{-15}$ m^2
Formation temperature	344.26 K

Table 9 – Fluid composition data for case QOFS-6comp.

Component	Initial Reservoir Composition	Injection Fluid Composition
C_1	0.50	0.77
C_3	0.03	0.20
C_6	0.07	0.01
C_{10}	0.20	0.01
C_{15}	0.15	0.005
C_{20}	0.05	0.005

Table 10 – Component data for case QOFS-6comp.

Component	P_c (MPa)	T_c (K)	v_c (m^3/kmol)	MW (kg/kmol)	Ac. Factor
C_1	4.60	190.60	$9.99\text{x}10^{-2}$	16.04	0.022
C_3	4.25	369.83	$2.00\text{x}10^{-1}$	44.10	0.152
C_6	3.01	507.44	$3.70\text{x}10^{-1}$	86.20	0.301
C_{10}	2.10	617.67	$6.30\text{x}10^{-1}$	142.30	0.488
C_{15}	1.38	705.56	1.04	206.00	0.650
C_{20}	1.12	766.67	1.34	282.00	0.850

Table 11 – Operational conditions for case QOFS-6comp.

Operational condition	Value
Fixed gas rate injection	$2.83\text{x}10^4$ m^3/d
Producer's bottom hole pressure	8.96 MPa

the different implicitness levels. Second, the simulation data is compared. There we see a very different result from the previous case. Testing all grid volumes, as seen in Tab. (14), has generated a much higher degree of implicitness regardless of the switching criteria. The much larger amount of implicit nodes during the run causes a significant decrease in performance.

We conclude this analysis verifying the case studies present a tendency to increase

Table 12 – Binary interaction coefficient data for case QOFS-6comp.

Component	C_1	C_3	C_6	C_{10}	C_{15}	C_{20}
C_1	-	-	-	-	0.05	0.05
C_3	-	-	-	-	0.005	0.005
C_6	-	-	-	-	-	-
C_{10}	-	-	-	-	-	-
C_{15}	0.05	0.005	-	-	-	-
C_{20}	0.05	0.005	-	-	-	-

Table 13 – Relative permeability data for case QOFS-6comp.

Parameter	Value
Model	Modified Stone II
End point rel. permeabilities (k^0_{rw}, k^0_{row}, k^0_{rog}, k^0_{rg})	0.40, 0.90, 0.90, 1.00
Residual saturations (S_{wr}, S_{orw}, S_{org}, S_{gr})	0.30, 0.10, 0.10, 0.00
Exponents (e_w, e_{ow}, e_{og}, e_g)	3.00, 2.00, 2.00, 2.00

Figure 13 – Oil production rates for Case study 2 (QOFS-6comp).

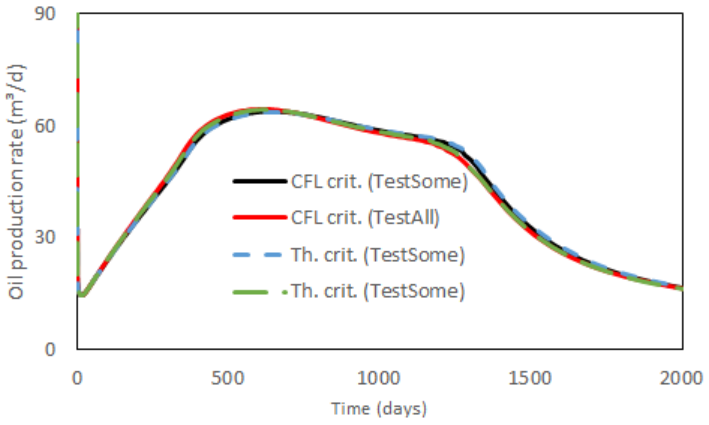

Figure 14 – Gas production rates for Case study 2 (QOFS-6comp).

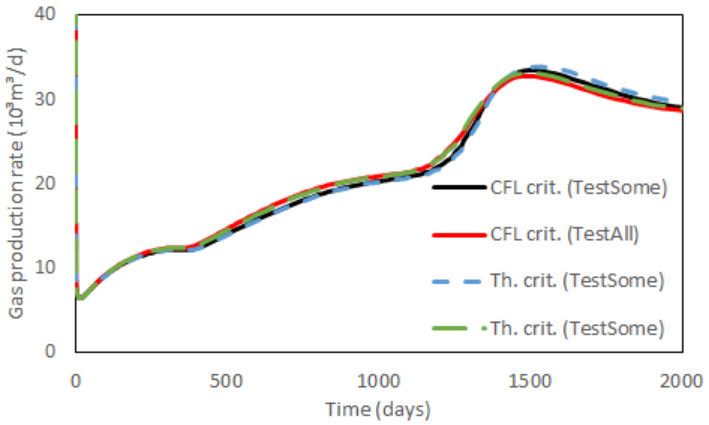

Table 14 – Simulation data for case QOFS-6comp.

Formulation	Avg. DT (d)	Step	FI%	CPU time (s)
AIM CFL (TestSome)	0.279	200	30.810	4272.871
AIM CFL (TestAll)	0.284	200	98.206	7134.949
AIM Threshold (TestSome)*	0.278	200	10.728	3741.849
AIM Threshold (TestAll)*	0.283	200	87.072	6464.071

*The threshold is set to 10^{-5}.

the number of implicit blocks if every checking procedure is performed in the entire grid. Whenever a node located far from the most stability critical regions is tested, there is a chance an unnecessary switch might take place, once both criteria are designed with some level of approximation. This way, it is most likely more FI volumes should appear. The choice of tested blocks has been implemented as an user input, however the author recommends the *TestSome* option generally.

6.2 Stable CFL Limit

In this section we investigate whether the CFL limit should be fixed at unity. This analysis is mainly based on Coats (2001) and Cao e Aziz (2002), whose works report stable runs for values higher than CFL=1. The case studies used employ the same data from the previous section. Several runs are conducted for different CFL values. They are compared in terms of conformity and performance.

6.2.1 Case study 1

Here we have the QOFS-3comp case. All data from Tab. (1) to (6) applies. The comparison for the oil and gas rates is given below. The results show overlapping curves and do not indicate any instabilities has occurred. The simulation data shown in Tab. (15) reveals a clear tendency. Higher CFL values, meaning looser stability limits, produce lower implicitness levels and faster runs, even though the total range of variation was not large for this case.

6.2.2 Case study 2

The same evaluation is conducted for the QOFS-6comp case. All parameters remain the same. The production curves are given in Fig. (17) and (18). Once more they show clear

Figure 15 – Oil production rates for various CFL values (QOFS-3comp).

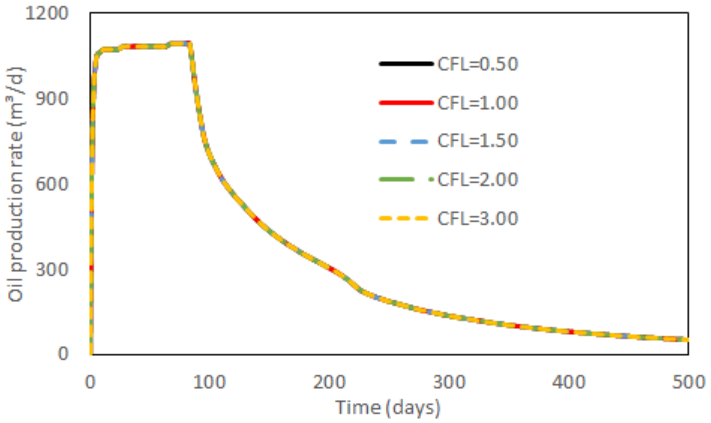

Figure 16 – Gas production rates for various CFL values (QOFS-3comp).

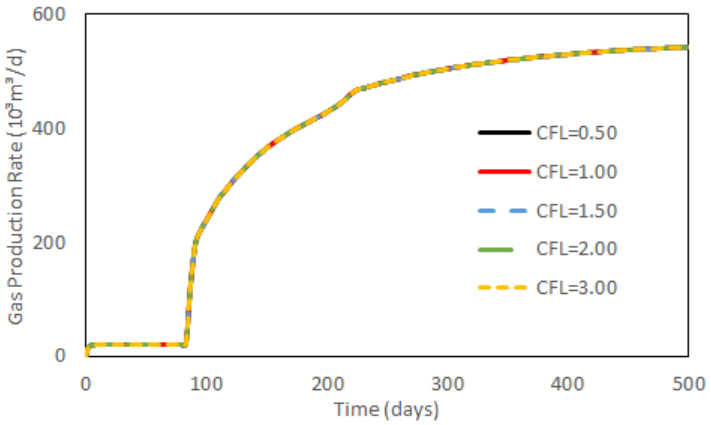

Table 15 – Simulation data for various CFL values (QOFS-3comp).

AIM	Avg. DT (d)	Step	FI%	CPU time (s)
CFL = 0.50	0.019	500	3.393	4984.567
CFL = 1.00	0.019	500	3.371	4978.475
CFL = 1.50	0.019	500	3.200	4973.866
CFL = 2.00	0.019	500	2.817	4915.875
CFL = 3.00	0.019	500	2.105	4870.132

agreement for the different CFL limits. The same trend is verified in terms of how the degree of implicitness affects CPU time, only now the influence seems stronger.

Neither of the cases has shown oscillatory instability for high CFL values. Simultaneously, we observe clear advantages to applying larger stability limits to the CFL criterion. Therefore, it was decided to turn the CFL condition to user input data. Note this is a brief study on stability limits for the CFL. Further conclusions require a deeper analysis.

Figure 17 – Oil production rates for various CFL values (QOFS-6comp).

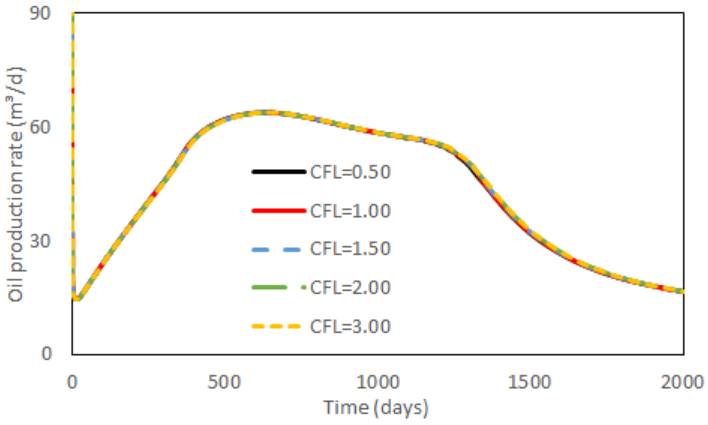

Figure 18 – Gas production rates for various CFL values (QOFS-6comp).

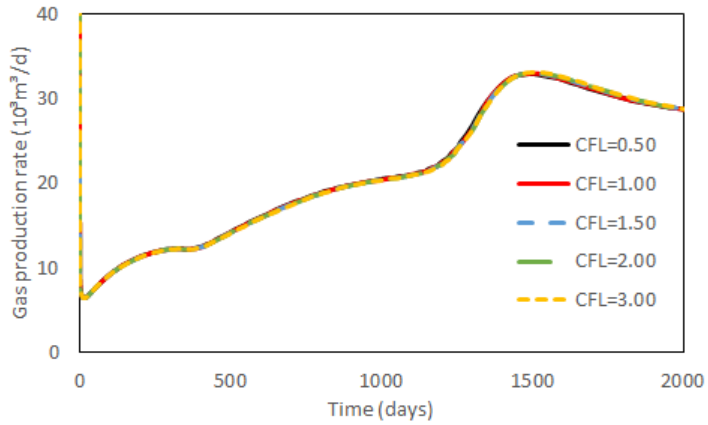

Table 16 – Simulation data for various CFL values (QOFS-6comp).

AIM	Avg. DT (d)	Step	FI%	CPU time (s)
CFL = 0.50	0.280	150	55.342	4986.659
CFL = 1.00	0.280	150	51.398	4874.960
CFL = 1.50	0.277	150	47.457	5057.100
CFL = 2.00	0.279	150	45.611	4677.064
CFL = 3.00	0.278	150	42.284	4582.134

6.3 Comparison Between AIM, IMPEC and FI

Up to this point, we have performed some studies on specific AIM features. In this section we aim at the main scope of the present work: verify how the Adaptive approach behaves in comparison with the IMPEC and FI formulations. Several case studies are evaluated for various 2D and 3D reservoirs. The results for the threshold criterion AIM are already optimized. The data on the preliminary trial runs is presented in Appendix B. As for the CFL stability test, all data below concerns the CFL=1 limit.

6.3.1 QOFS-3comp 2D

Here we compare all formulations for three meshes representing the same quarter of five-spot configuration. The first grid was already presented in Fig. (10). The other two are respectively a 7,449-nodes triangular mesh and a 7,942-nodes mesh composed of both triangular and quadrilateral elements. The figure below better describes them:

Figure 19 – Two-dimensional meshes: (a) 7,449 nodes with triangular elements and (b) 7,942 nodes with mixed elements.

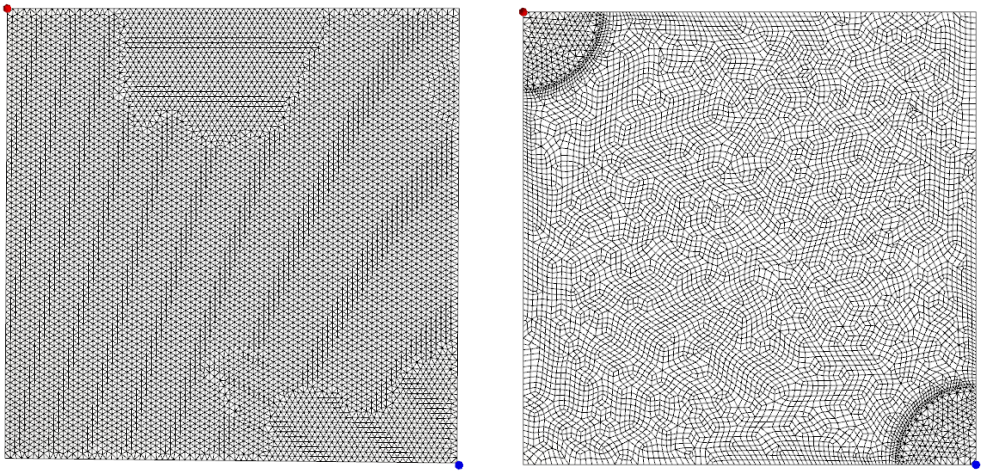

(a) (b)

First we present the results for the QOFS-3comp case. Figures (20) and (21) show the production curves for the quadrilateral grid overlap, testifying for the AIM accuracy. As for the performance, Tab. (17) highlights a significant enhancement when compared to both original methods. This is easily observed in the last column, where all CPU times are normalized using the IMPEC time as the reference. It is also important to note the IMPEC outperforms the Fully Implicit formulation. The phase behavior in this case does not allow for large time steps, which in turn affects the FI performance. Additionally, it is easy to see the average time steps for the case are small when compared with real field applications. As mentioned before, we are dealing with simple problems designed for this kind of comparison. The reservoirs shown in Fig. (10) and (19) have small dimensions, resulting in small grid volumes. In these conditions, larger time steps are not advisable even for FI runs.

Before we advance into the other two presented meshes, there should be an analysis on the production rates. As observed in Fig. (20) and (21), both curves are constant up to 100 days. Afterwards, the oil production sharply decreases, while the gas rate greatly increases,

Figure 20 – Oil production rates comparison for the 7,021 nodes quadrilateral mesh (QOFS-3comp case).

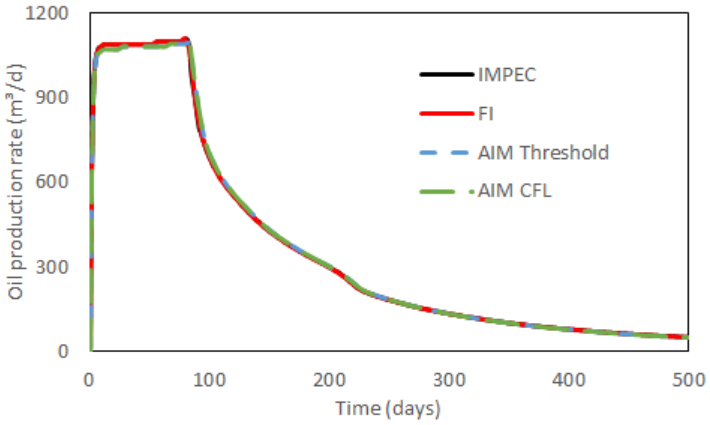

Figure 21 – Gas production rates comparison for the 7,021 nodes quadrilateral mesh (QOFS-3comp case).

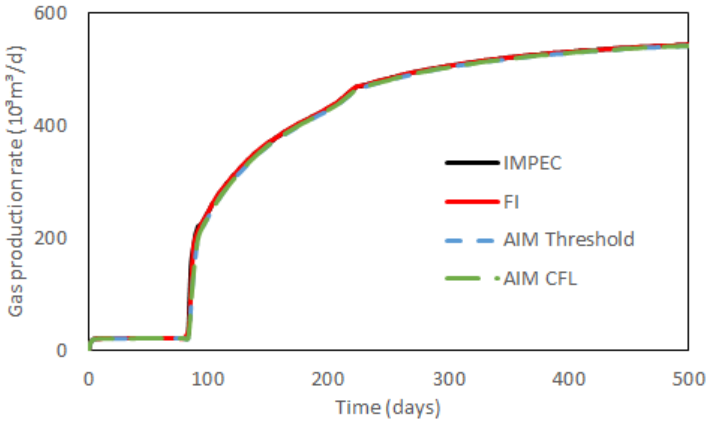

Table 17 – Simulation data comparison for 7,021 nodes quadrilateral mesh (QOFS-3comp).

Formulation	Avg. DT (d)	Step	FI%	CPU time (s)	Norm. time
IMPEC	0.004	-	0.00	11264.971	1.00
FI	0.019	-	100.0	16033.326	1.42
AIM Threshold*	0.019	800	0.028	4874.232	0.43
AIM CFL	0.019	800	2.117	5024.454	0.44

Note: The threshold is set to 0.1.

indicating the breakthrough is reached. A better description of this stage is presented below.

Following, the results for the 7,449 vertices triangular grid are displayed. Here, the IMPEC presents the worst performance mainly because a smaller average time step was required to maintain stability. Again, the adaptive formulation produces much faster runs while retaining stability and accuracy.

Closing this sub-section are the data for the 7,942 volumes mixed mesh. Similar results to the previous grids are encountered. We should also note the two switching criteria

Figure 22 – Gas saturation profile at 100 days for Case 1.

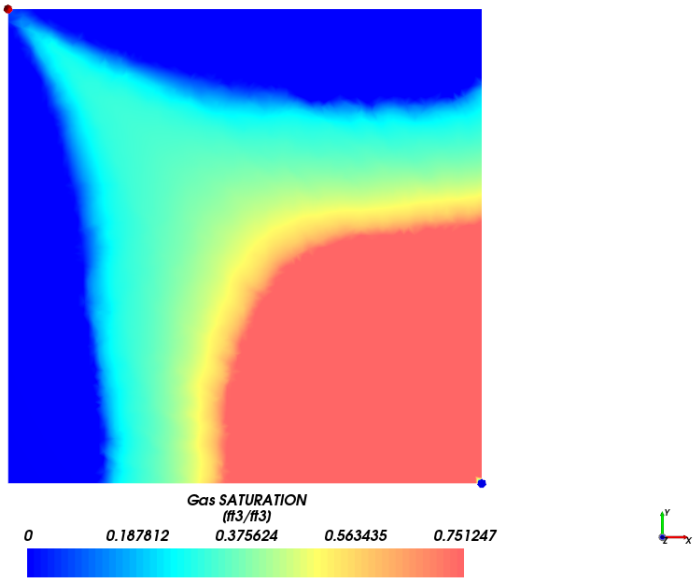

Figure 23 – Oil production rates comparison for the 7,449 nodes triangular mesh (QOFS-3comp case).

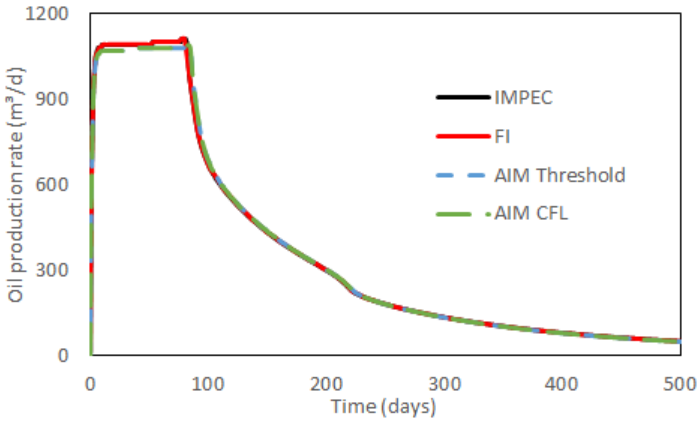

Figure 24 – Gas production rates comparison for the 7,449 nodes triangular mesh (QOFS-3comp case).

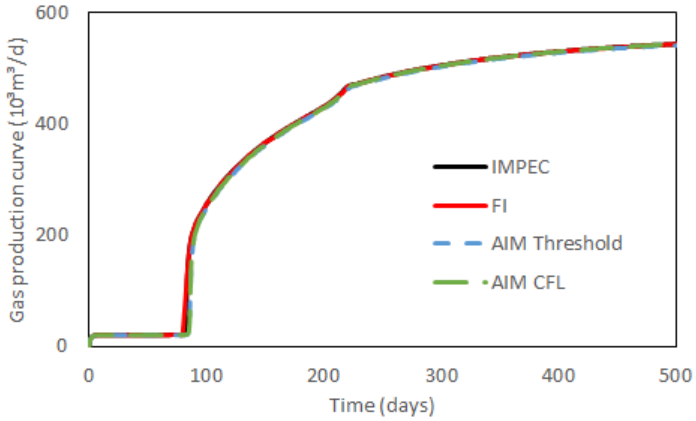

produce similar performances so far. Despite the theoretical and practical limitations highlighted for the threshold approach, the literature presents corroborating results such as in Fung *et al.*

Table 18 – Simulation data comparison for 7,449 nodes triangular mesh (QOFS-3comp).

Formulation	Avg. DT (d)	Step	FI%	CPU time (s)	Norm. time
IMPEC	0.002	-	0.00	24789.224	1.00
FI	0.013	-	100.0	18829.308	0.76
AIM Threshold	0.007	1000	0.028	14001.243	0.56
AIM CFL	0.007	1000	0.958	14164.964	0.57

Note: The threshold is set to 10^{-4}.

(1989) Grabenstetter *et al.* (1991).

Figure 25 – Oil production rates comparison for the 7,942 nodes mixed mesh (QOFS-3comp case).

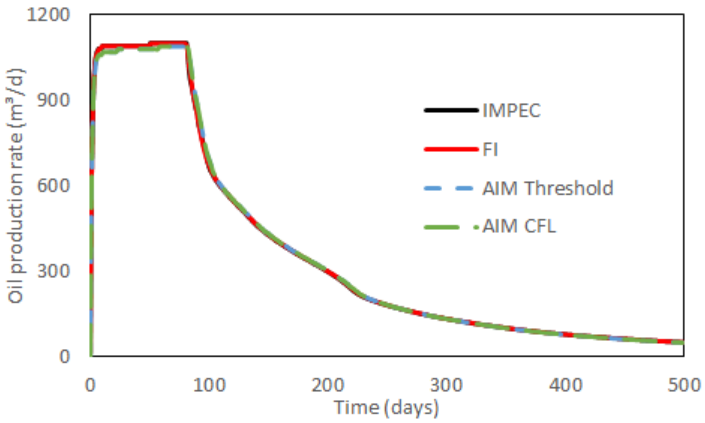

Figure 26 – Gas production rates comparison for the 7,942 nodes mixed mesh (QOFS-3comp case).

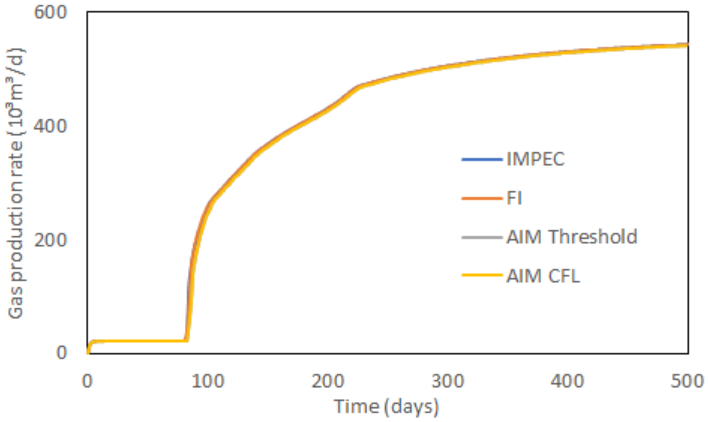

6.3.2 QOFS-6comp 2D

The same grids are now applied for the QOFS-6comp case. The problem is defined as in Tab. (8) to (13). For the mesh composed of quadrilateral elements, the production rates are

Table 19 – Simulation data comparison for 7,942 nodes mixed mesh (QOFS-3comp).

Formulation	Avg. DT (d)	Step	FI%	CPU time (s)	Norm. time
IMPEC	0.004	-	0.00	13328.208	1.00
FI	0.019	-	100.0	19647.748	1.47
AIM Threshold	0.019	900	0.025	5818.987	0.44
AIM CFL	0.019	900	1.105	5769.724	0.43

Note: The threshold is set to 0.1.

displayed in Figs. (27) and (28), showing great agreement between all formulations. As for the performance data, this time the FI is clearly better than IMPEC. Still, the adaptive formulation manages to be nearly twice as fast than the implicit approach. Once more, the time step size is limited by the reservoir dimensions. Now, however, the time step constantly increases along the runs. Even so, its maximum is only reached close to the end of simulation.

Figure 27 – Oil production rates comparison for the 7,021 nodes quadrilateral mesh (QOFS-6comp case).

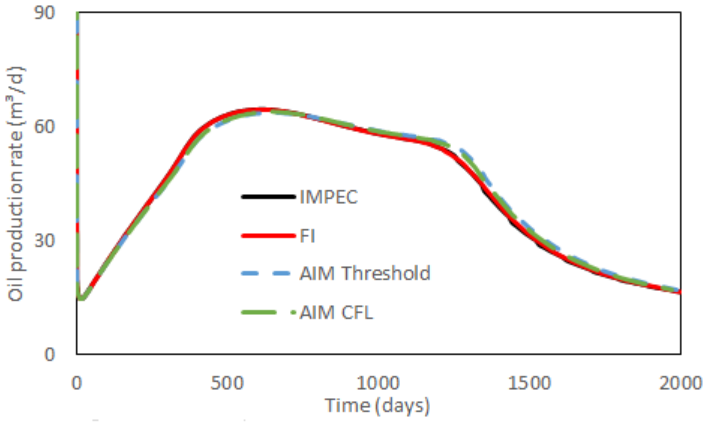

Figure 28 – Gas production rates comparison for the 7,021 nodes quadrilateral mesh (QOFS-6comp case).

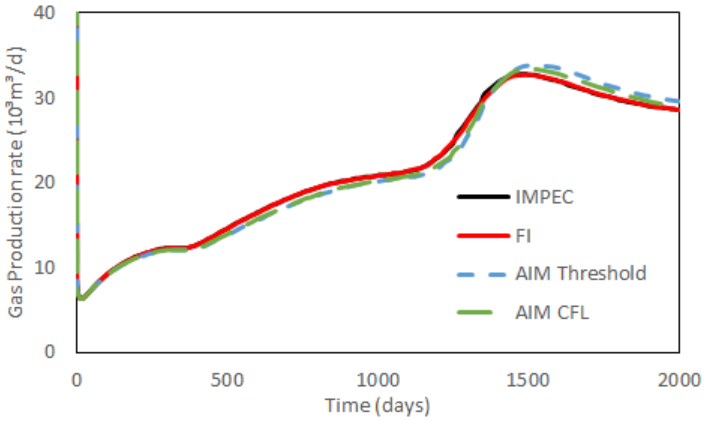

Table 20 – Simulation data comparison for 7,021 nodes quadrilateral mesh (QOFS-6comp).

Formulation	Avg. DT (d)	Step	FI%	CPU time (s)	Norm. time
IMPEC	0.029	-	0.00	11186.323	1.00
FI	0.284	-	100.0	7467.998	0.67
AIM Threshold	0.278	200	10.728	3741.849	0.33
AIM CFL	0.279	200	30.810	4272.871	0.38

Note: The threshold is set to 10^{-5}.

The productions curves show very different shapes when compared to Case 1. First, right at the beginning of the runs we see a quick decrease in both oil and gas rates. Revisiting Tab. (8) and (11), it is possible to identify a initial pressure gradient between the reservoir and the production well. Once the wells are opened, this gradient leads to some primary production. The gas influx, however, is not enough to maintain such pressure difference. Therefore, the production rates rapidly decrease. As for the change on the curves around 1300 days, the explanation, again, falls to moment of breakthrough. Figure (29) illustrates this better.

Figure 29 – Gas saturation profile at 1300 days for Case 2.

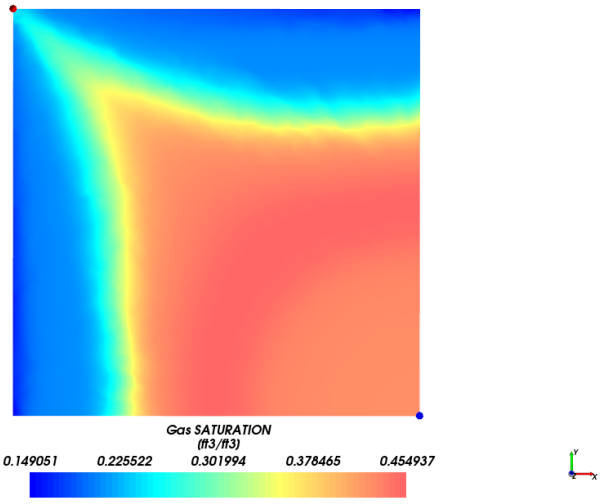

For the triangular mesh, similar results are obtained. The main difference is the FI and AIM formulations manage to be even faster compared to the IMPEC.

Table 21 – Simulation data comparison for 7,449 nodes triangular mesh (QOFS-6comp).

Formulation	Avg. DT (d)	Step	FI%	CPU time (s)	Norm. time
IMPEC	0.019	-	0.00	18959.361	1.00
FI	0.288	-	100.0	7205.306	0.38
AIM Threshold	0.282	200	3.550	4036.892	0.21
AIM CFL	0.282	200	15.742	4183.801	0.22

Note: The threshold is set to 10^{-5}.

Figure 30 – Oil production rates comparison for the 7,449 nodes triangular mesh (QOFS-6comp).

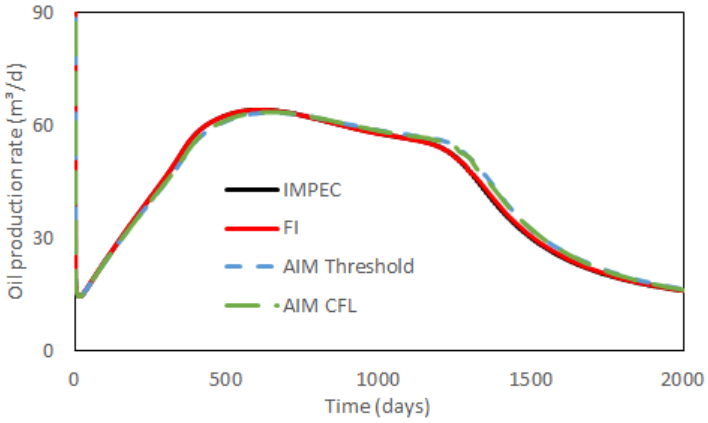

Figure 31 – Gas production rates comparison for the 7,449 nodes triangular mesh (QOFS-6comp case).

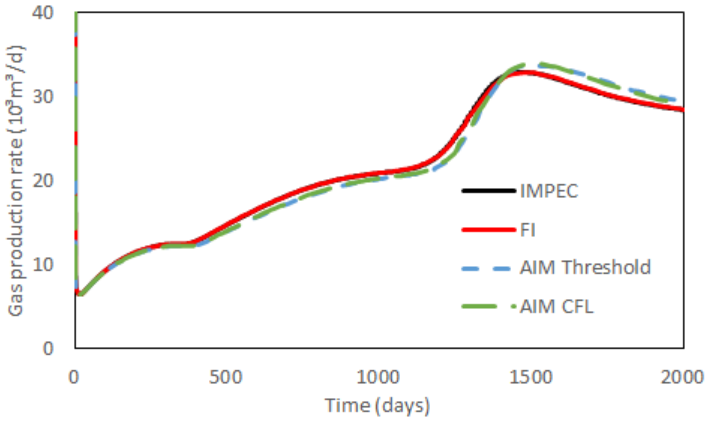

Closing this sub-section are the QOFS-6comp results for the 7,942 volumes mixed mesh. The same trends are also reported here. As shown in Figs. (32) and (33), the AIM is accurate when compared to the original methods. At the same time, the CPU time comparison testifies again for the new formulation efficiency. We should at this point also highlight the threshold criterion has consistently produced the best results, achieving not only faster runs, but also smaller implicitness levels when compared with the CFL switching technique. One of the main reasons behind this lies on the severely tight thresholds applied, achieved after several test runs.

Table 22 – Simulation data comparison for 7,942 nodes mixed mesh (QOFS-6comp).

Formulation	**Avg. DT (d)**	**Step**	**FI%**	**CPU time (s)**	**Norm. time**
IMPEC	0.019	-	0.00	19131.263	1.00
FI	0.282	-	100.0	9011.515	0.47
AIM Threshold	0.274	200	0.074	4053.413	0.21
AIM CFL	0.276	200	22.275	4623.373	0.24

Note: The threshold is set to 10^{-4}.

Figure 32 – Oil production rates comparison for 7,942 nodes mixed mesh (QOFS-6comp).

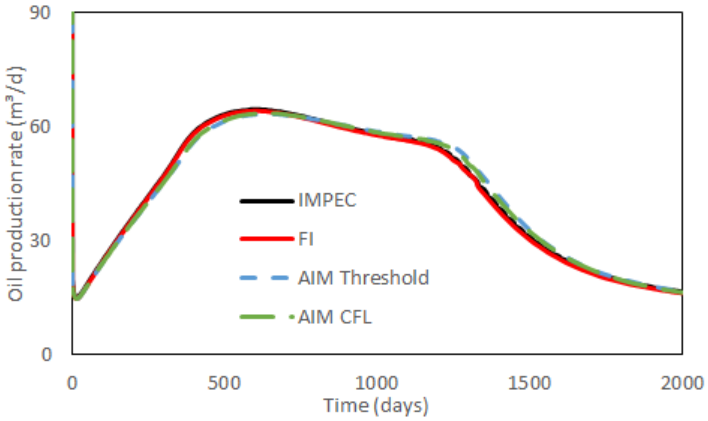

Figure 33 – Gas production rates comparison for 7,942 nodes mixed mesh (QOFS-6comp).

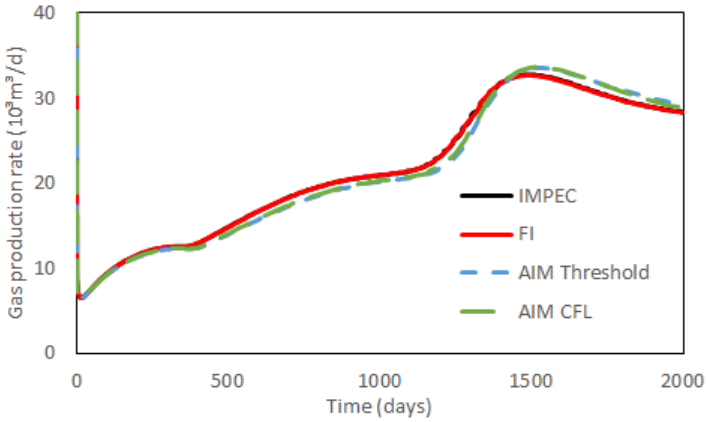

6.3.3 QOFS-6comp 3D

The next step is to compare the formulations for three-dimensional grids. The first one applied is a 19,004 nodes mesh composed solely of hexahedron elements. The reservoir and fluid data are the same of Tab. (8) to (13). Figure (34) illustrates the geometry and its dimensions. The configuration is a quarter of five-spot, with single producer and injector wells.

The data comparison, as before, is shown in Fig. (35) and (36). All curves nearly overlap, testifying for the AIM accuracy. It should be noted no IMPEC run attempt produced a reasonable performance. This run was then considered failed, hence its absence. In Tab. (23), the normalized time column, now with respect to the FI CPU time, show the adaptive approach is much faster. This time, we also present the average molar balance errors for the successful runs. This data shows, even thought the AIM produces larger errors than the FI formulation, they are still not significant.

Before we proceed, it is important to have a better understanding of the shape assumed by the production rate curves. Figure (37) presents the saturation profile around 150

Figure 34 – Three-dimensional 19,044 volumes grid composed of hexahedron elements.

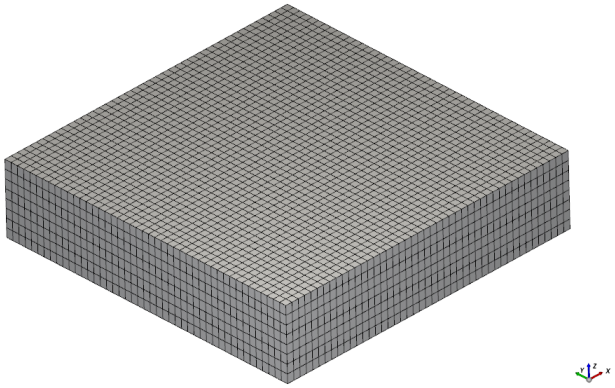

Figure 35 – Oil production rates comparison for the 19,044 nodes hexahedron elements mesh.

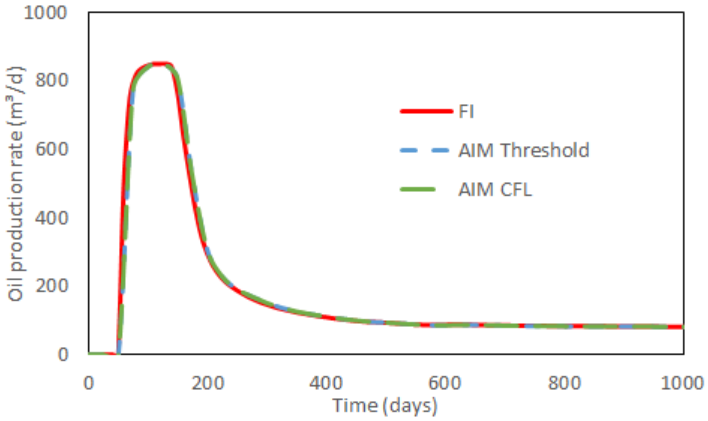

Figure 36 – Gas production rates comparison for the 19,044 nodes hexahedron elements mesh.

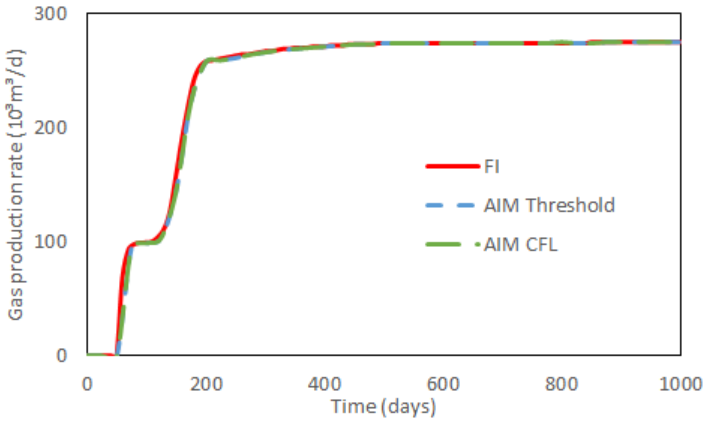

days, when the breakthrough is reached. This explain the rapid decrease of oil production and the surge on produced gas.

Table 23 – Simulation data comparison for 19,044 nodes hexahedron elements mesh.

Formulation	Avg. DT (d)	Step	FI%	CPU time (s)	Norm. time
IMPEC	-	-	0.00	FAILED	-
FI	0.049	-	100.0	237248.843	1.00
AIM Threshold*	0.049	300	0.095	135620.562	0.57
AIM CFL	0.049	300	45.07	149813.468	0.63

Note: The threshold is set to 0.01.

Table 24 – Molar balance error data for 19,044 nodes hexahedron elements mesh.

Formulation	Average percent molar balance error
IMPEC	FAILED
FI	$4.43x10^{-2}$
AIM Threshold	2.84x10
AIM CFL	2.91

Figure 37 – Gas saturation field at 150 days for the QOFS-6comp 3D case.

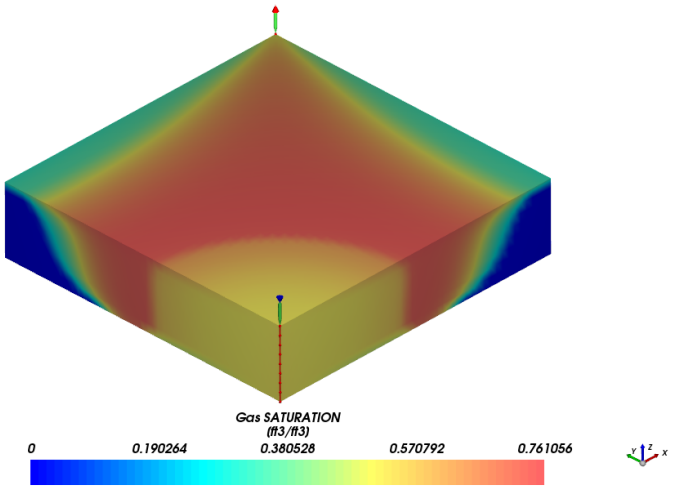

6.3.4 2D Irregular reservoir-6comp

So far, only very simple reservoir configurations have been applied. Verifying the AIM behavior requires more complex geometries to be evaluated in conditions closer to an actual production field. Hence, the mesh in Fig. (38), composed of triangular elements, is selected for this task. The recovery process is conducted by two production wells, positioned close to the east and west extremities, while a single well, close to the center of the geometry, injects CO_2 rich gas. Additionally, the reservoir contains heterogeneous porosity and permeability fields, as displayed in Fig. (39) and (40).

Besides porosity and permeability, all data fluid and reservoir data are in accordance with Tab. (8) to (13). The oil and gas production rates, as well as the performance data are

Figure 38 – Two-dimensional irregular reservoir grid composed of 27,271 nodes.

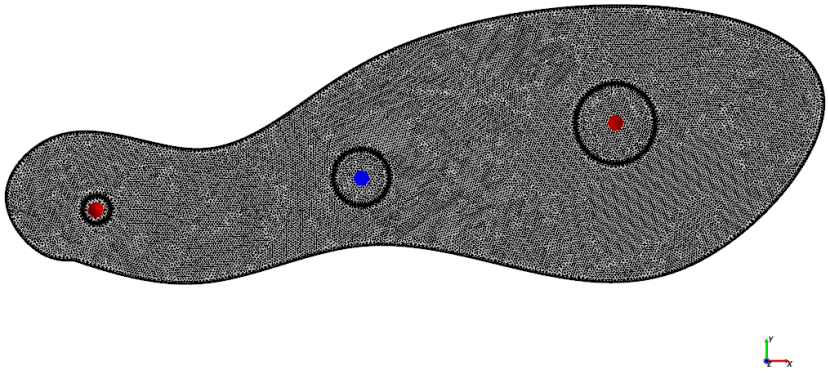

Figure 39 – Porosity field for two-dimensional irregular reservoir grid composed of 27,271 nodes.

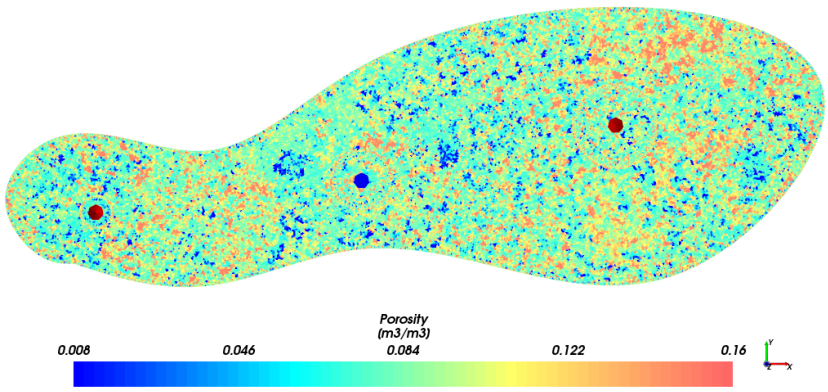

Figure 40 – X and Y permeability field for two-dimensional irregular reservoir grid composed of 27,271 nodes.

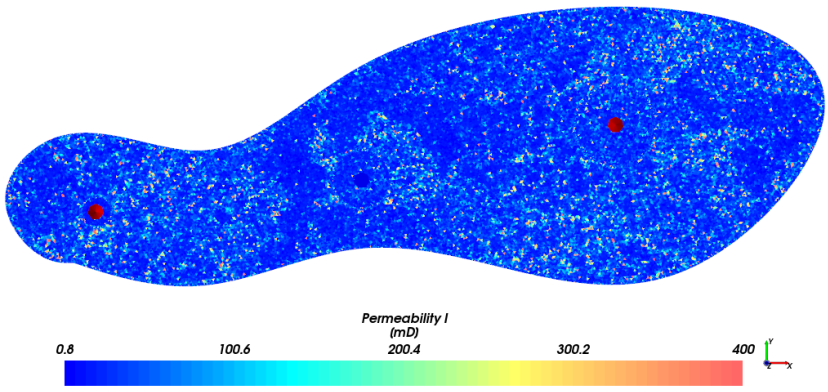

presented below. No IMPEC run attempt succeeded, despite several attempts to adjust time step control parameters, therefore no curve is shown in Fig. (41) and (42). The comparison with FI, however, still shows faster runs while displaying nearly overlapping curves. We should note there was no optimization process for the threshold value, given the large computation time required for each run. The chosen value was arbitrarily defined.

Figure 41 – Oil production rates comparison for the 27,271 nodes mixed elements mesh.

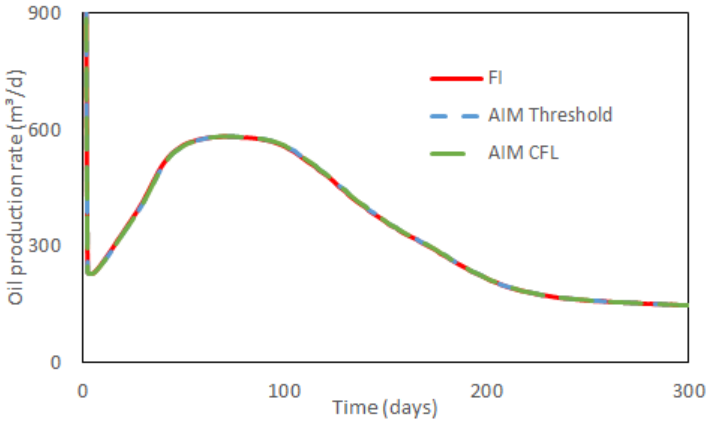

Figure 42 – Gas production rates comparison for the 27,271 nodes mixed elements mesh.

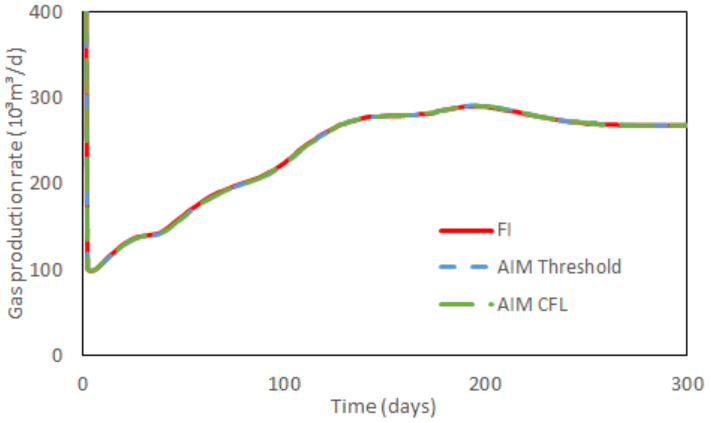

Table 25 – Simulation data comparison for 27,271 nodes mixed elements mesh.

Formulation	Avg. DT (d)	Step	FI%	CPU time (s)	Norm. time
IMPEC	-	-	0.00	FAILED	-
FI	0.005	-	100.0	274476.750	1.00
AIM Threshold*	0.005	1500	0.011	152444.312	0.55
AIM CFL	0.005	1500	11.32	163030.718	0.59

Note: The threshold is set to 0.01.

The production curves show a decrease on oil rates at the early stages of the run. An

Table 26 – Molar balance error data for 27,271 nodes mixed elements mesh.

Formulation	**Average percent molar balance error**
IMPEC	FAILED
FI	$1.72\text{x}10^{-6}$
AIM Threshold	$2.09\text{x}10^{-1}$
AIM CFL	$2.09\text{x}10^{-1}$

evaluation of the saturation profile is in order to understand this behavior. Figure (43) shows the gas saturation distribution at 150 days. It is possible to see the gas front has nearly reached both wells. As a consequence, the inclination of the curves changes.

Figure 43 – Gas saturation field at 150 days for two-dimensional irregular reservoir grid composed of 27,271 nodes.

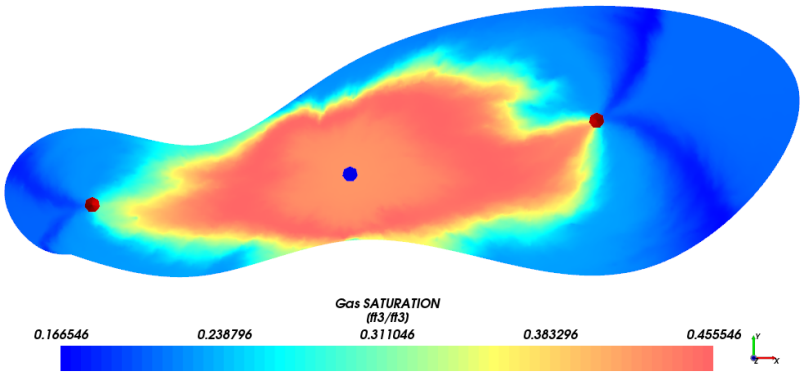

6.3.5 3D Irregular reservoir-6comp

The last case study evaluated in this work also concerns a three-dimensional reservoir. There are, however, two main differences from the previous case. First, we are not dealing with a quarter of five-spot configuration. This time the reservoir geometry presents an irregular shape and the production is performed by multiple wells, as shown in Fig. (44). Following, an evaluation on the effects of a full permeability tensor are investigated. So far, all problems contained only null off-diagonal terms. Now, a full tensor is applied as shown in Tab. (27).

We should also mention, even though most conditions are identical to the ones describe in the two-dimensional QOFS-6comp case, the wells operational situation is given by Tab. (28).

Figure 44 – Three-dimensional 19,928 volumes grid composed of hexahedron, tetrahedron and pyramid elements.

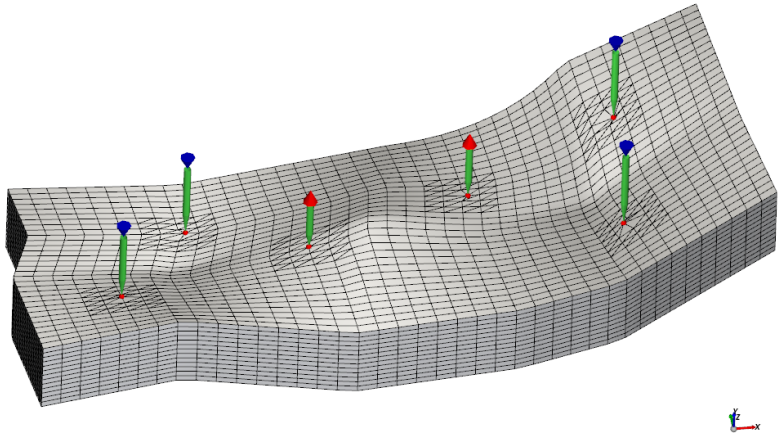

Table 27 – Permeability tensor for 3D irregular reservoir-6comp case.

	X	**Y**	**Z**
X	$9.87\text{x}10^{-14}$	$1.97\text{x}10^{-14}$	$1.97\text{x}10^{-14}$
Y	$1.97\text{x}10^{-14}$	$9.87\text{x}10^{-14}$	$1.97\text{x}10^{-14}$
Z	$1.97\text{x}10^{-14}$	$1.97\text{x}10^{-14}$	$9.87\text{x}10^{-15}$

Table 28 – Operational conditions for the Irregular grid-6comp case.

Operational condition	**Value**
Fixed gas rate injection	$1.69\text{x}10^{5}$ m^3/d
Producer's bottom hole pressure	8.96 MPa

The results are then displayed in Fig. (45) and (46). The curves show total agreement between the IMPEC, FI and AIM CFL runs, while the adaptive method using the threshold criterion produces a different result, specially for the oil production rates. Table (29) indicates the AIM Threshold simulation presented severe convergence issues, since its total CPU time was many times larger than the other formulations. Additionally, the AIM CFL was not able to attain a significant better performance than FI. This is likely due to the extremely high level of implicitness. The main point of discussion is, however, the inability of the more implicit formulations to surpass the IMPEC performance, even considering the much smaller average time step. Given previous similar case studies for 2D and 3D meshes did not report similar results, we can establish a relationship between the full permeability tensor and the inability for FI and AIM to produce stable and fast runs.

Before we further analyze this data and it connection with the use of a full permeabil-

Figure 45 – Oil production rates comparison for the 19,928 volumes mesh.

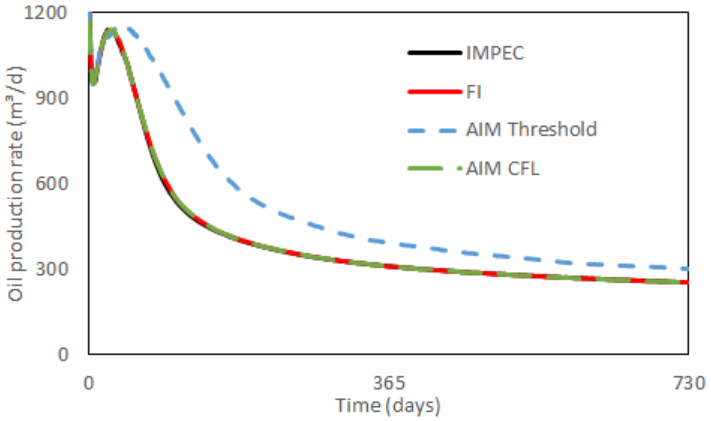

Figure 46 – Gas production rates comparison for the 19,928 nodes mesh.

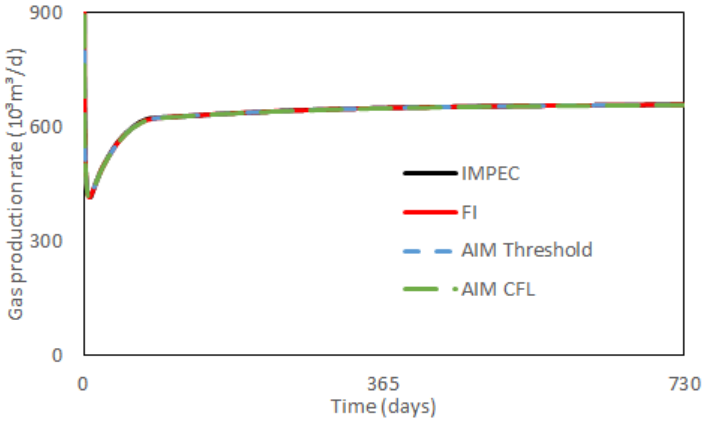

Table 29 – Simulation data comparison for 19,928 nodes mesh.

Formulation	Avg. DT (d)	Step	FI%	CPU time (s)	Norm. time
IMPEC	0.09	-	0.00	8370.930	1.00
FI	1.61	-	100.0	14465.112	1.73
AIM Threshold*	0.88	5	2.75	66527.476	7.95
AIM CFL	1.61	5	92.36	13793.797	1.65

Note: The threshold is set to 0.001.

ity tensor, let us investigate the production curves shape. Figure (47) displays the gas saturation profile at 700 days, close to end of the run. It basically shows there is a clear separation between the oil and gas phases. There is no indication of a gas front or achieved breakthrough. Even so, the steady gas production is in accordance with such behavior.

Figure 47 – Gas saturation field at 700 days for the 19,928 volumes mesh.

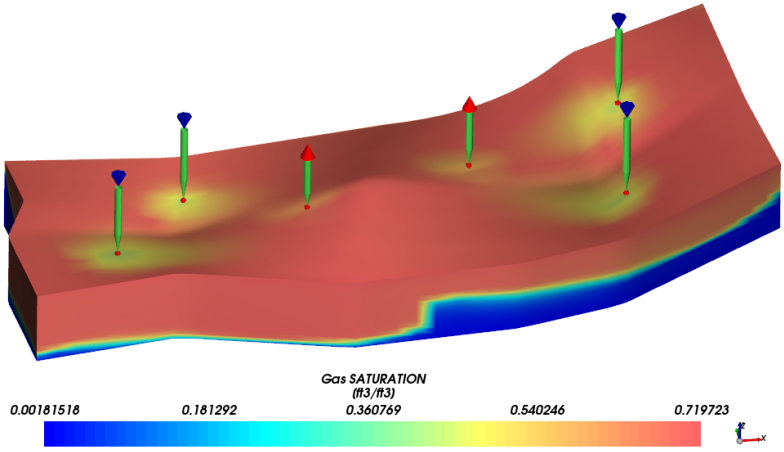

7 CONCLUSIONS

This work has implemented a Adaptive Implicit Formulation in a compositional simulator with EbFVM unstructured grids. The model is the product of a combination of the IMPEC ACS *et al.* (1985) and the FI FERNANDES (2014) models. Two criteria for formulation switching, based on the works of THOMAS; THURNAL (1982) and COATS (2001) are tested.

Primarily, some aspects of the AIM were investigated. Regarding the approaches for shifting between explicit and implicit evaluation, two test were conducted. The first one aimed at the which grid volumes required to undergo this procedure. The data shows verifying both criteria in all blocks produced higher levels of implicitness and slower runs for the two gas flooding problems investigated. Further, an analysis on CFL stable limits highlighted looser restriction can be applied without necessarily causing numerical instability. We should note these tests are not conclusive. They serve as a guide for future applications of the simulator.

The comparison with the IMPEC and FI formulations is then conducted in terms of accuracy and performance. First, the oil and gas production curves analysis for gas flooding problems in 2D and 3D meshes reveals great accuracy in comparison with IMPEC and FI. For all case studies, it is observed the curves nearly overlap. Next, the performance evaluation reveals the adaptive method repeatedly succeeded to obtain faster runs, even while coping with time step size limitations or high levels of implicitness. This data is obtained for different reservoir configurations, from simple homogeneous quarter of five-spots to irregular geometries combined with heterogeneous porosity and permeability fields. A single case study does not agree with this trend. The 3D irregular reservoir problem shows the adaptive method unable to outperform the explicit formulation.

An additional conclusion can be drawn from these cases regarding the switching criteria. For most problems, both CFL and Threshold approaches displayed very similar results in terms of CPU time. However, evaluating the average implicitness degree in each run shows the CFL criterion consistently produces more implicit volumes. These results partially contradict the literature on the matter, for the CFL switching method is widely regarded as more efficient. Part of the explanation lies with the already mentioned choice of threshold value. The runs for 2D meshes required several runs until the optimal limit was selected. For the 3D grids simulations, as well as the irregular geometry two-dimensional mesh, the large amount of CPU time required in each run made such procedure impracticable. Therefore, arbitrary values were chosen.

7.1 Future work

Several future steps and studies can be drawn from these conclusions. The first one concerns an investigation on the switching criteria and its performance for problems surrounded of different conditions, such as recovery by water injection. Evaluating the effects of a full permeability tensor on the AIM efficiency also presents a great opportunity at better understanding the adaptive approach. Finally, this study can be expanded to verify how some of the physical model assumptions, such as the neglected physical dispersion and water mass transfer, affect production curves and relative performance.

BIBLIOGRAPHY

ACS, G.; DOLESCHALL, S.; FARKAS, E. General purpose compositional model. **Society of Petroleum Engineers Journal**, v. 25, p. 543–553, 1985.

ARAUJO, A. L.; FERNANDES, B. R.; FILHO, E. P. D.; ARAUJO, R. M.; LIMA, I. C.; GONçALVES, A. D.; MARCONDES, F.; SEPEHRNOORI, K. 3d compositional reservoir simulation in conjuction with unstructured grids. **Brazilian Journal of Chemical Engineering**, v. 33, p. 347–360, 2016.

BALIGA, B. R.; PATANKAR, S. V. A new finite-element formulation for convection-diffusion problems. **Numerical Heat Transfer Journal**, v. 3, p. 393–409, 1980.

BERTIGER, W. I.; KELSEY, F. J. Inexact adaptive newton methods. **Proceedings of the SPE Reservoir Simulation Symposium, Dallas, USA, February 10-13**, 1985.

BRANCO, C. M.; RODRIGUEZ, F. A semi-implicit formulation for compositional reservoir simulation. **SPE Advanced Technology Series**, v. 4, p. 171–177, 1996.

BUCKLEY, S. E.; LEVERETT, M. C. Mechanism of fluid displacement in sands. **Proceedings of the AIME**, v. 146, 1942.

CAO, H.; AZIZ, K. Performance of impsat and impsat-aim models in compositional simulation. **Proceedings of the SPE Annual Technical Conference, San Antonio, USA, September 29-October 2**, 2002.

CHANG, Y. B. **Development and Application of an Equation of State Compositional Simulator**. Tese (Doutorado) — Department of Petroleum and Geosystems Engineering, The University of Texas at Austin, 1990.

CHIEN, M. C. H.; LEE, S. T.; CHEN, W. H. A new fully implicit compositional simulator. **Proceedings of the SPE Reservoir Simulation Symposium, Dallas, USA, February 10-13**, 1985.

CHU, W. H. Development of a general finite difference approximation for a general domain. **Journal of Computational Physics**, v. 8, p. 392–408, 1971.

COATS, K. H. An equation of state compositional model. **Society of Petroleum Engineers Journal**, v. 20, p. 363–376, 1980.

COATS, K. H. **"Reservoir Simulation", Petroleum Engineering Handbook**. [S.l.]: Society of Petroleum Engineers, 1982.

COATS, K. H. Impes stability: The stable step. **Paper SPE 69225, proceedings of the SPE Symposium on Reservoir Simulation, Houston, TX, February 11-14**, 2001.

COLLINS, D. A.; NGHIEM, L. X.; LI, Y. K.; GRABENSTETTER, J. E. An efficient approach to adaptive-implicit compositional simulation with an equation of state. **SPE Reservoir Engineering Journal**, v. 7, p. 259–264, 1992.

CORDAZZO, J. **Petroleum Reservoir Simulation Using the EbFVM Method and Algebric Multigrid (In Portuguese)**. Tese (Doutorado) — Department of Mechanical Engineering, Federal University of Santa Catarina, 2006.

COREY, A. T. **Mechanics of Immiscible Fluids in Porous Media**. [S.l.]: Water Resources Publications, 1986.

CUNHA, A. R.; MALISKA, C. R.; SILVA, A. F.; LIVRAMENTO, M. A. Two-dimensional two-phase petroleum reservoir simulation using boundary-fitted grids. **Journal of the Brazilian Society of Mechanical Sciences**, v. 16, p. 423–429, 1994.

DARWISH, M. S.; MOUKALLED, F. Tvd schemes for unstructured grids. **International Journal of Heat and Mass Transfer**, v. 46, p. 599–611, 2003.

DRUMOND-FILHO, E. P.; FERNANDES, B. R.; MARCONDES, F.; SEPEHRNOORI, K. Specified adaptive implicit method for unstructured grids in compositional reservoir simulation. **Proceedings of the 23rd ABCM International Congress of Mechanical Engineering, Rio de Janeiro, Brazil, December 6-11**, 2015.

ECONOMIA iG. Produção de petróleo sobe 0,75http://economia.ig.com.br/2017-01-11/producao-recorde.html. **Accessed on 07/06/2017 at 08:53**, 2017.

EDWARDS, M. G. Cross flow tensors and finite volume approximation with by deferred correction. **Computer Methods in Applied Mechanics and Engineering**, v. 151, p. 143–161, 1998.

FARKAS, E.; VALKO, P. A direct impes-type volume balance technique for adaptive implicit steam models. **SPE Reservoir Engineering Journal**, v. 2, p. 88–94, 1994.

FERNANDES, B. R. **Implicit and Semi-Implicit Techniques for the Compositional Petroleum Reservoir Simulation Based on Volume Balance**. Dissertação (Mestrado) — Department of Chemical Engineering, Federal University of Ceará, 2014.

FERNANDES, B. R.; MARCONDES, F.; SEPEHRNOORI, K. Investigation of several interpolation functions for unstructured meshes in conjunction with compositional reservoir simulation. **Numerical Heat Transfer, Part A: Applications**, v. 64, p. 974–993, 2003.

FORSYTH, P. A. Adaptive implicit criteria for two-phase flow with gravity and capillary pressure. **Journal of Scientific and Statistical Computing**, v. 10, p. 227–252, 1989.

FORSYTH, P. A. A control-volume, finite-element method for local mesh refinement in thermal reservoir simulation. **SPE Reservoir Engineering Journal**, v. 5, p. 561–566, 1990.

FORSYTH, P. A.; SAMMON, P. H. Practical considerations for adaptive implicit methods in reservoir simulation. **Journal of Computational Physics**, v. 62, p. 265–281, 1986.

FUNG, L. S.-K.; COLLINS, D. A.; NGHIEM, L. X. An adaptive-implicit switching criterion based on numerical stability analysis. **SPE Reservoir Engineering Journal**, v. 4, p. 45–51, 1989.

FUNG, L. S.-K.; HIEBERT, A. D.; NGHIEM, L. X. Reservoir simulation with a control-volume finite-element method. **SPE Reservoir Engineering Journal**, v. 7, p. 349–357, 1992.

FUSSEL, L. T.; FUSSEL, D. D. An iterative technique for compositional reservoir models. **Society of Petroleum Engineers Journal**, v. 19, p. 211–220, 1979.

GRABENSTETTER, J.; LI, Y. K.; COLLINS, D. A.; NGHIEM, L. X. Stability-based switching criterion for adaptive-implicit compositional reservoir simulation. **Paper SPE 21225, proceedings of the SPE Symposium on Reservoir Simulation, Anaheim, CA, February 17-20**, 1991.

GUARDIAN, T. The guardian. environment. energy. background: What caused the 1970s oil price shock? https://www.theguardian.com/environment/2011/mar/03/1970s-oil-price-shock. **Accessed on 01/04/2017 at 15:20**, 2011.

HEINEMANN, Z. E.; BRAND, C. Gridding techniques in reservoir simulation. **Proceedings of the 1st International Forum on Reservoir Simulation, Apbach, AUS**, 1988.

HEINEMANN, Z. E.; BRAND, C.; MUNKA, M.; CHEN, Y. M. Modeling reservoir geometry with irregular grids. **Proceedings of the SPE Symposium on Reservoir Simulation, Houston, USA, February 6-8**, 1989.

HERNING, F.; ZIPPERER, L. Calculation of viscosity of technical gas mixtures from the viscosity of individual gases. **Gas and Wasserfach**, v. 79, p. 49–54, 1936.

HIRASAKI, G. J.; O'DELL, P. M. Representation of reservoir geometry for numerical simulation. **Society of Petroleum Engineers Journal**, v. 10, 1970.

HURTADO, F. S.; MALISKA, C. R.; SILVA, A. F. da; CORDAZZO, J. A quadrilateral element-based finite volume method formulation for the simulation of complex reservoirs. **SPE Latin American and Caribbean Petroleum Engineering Conference, Buenos Aires, Arg, April 15-18**, 2007.

KAZEMI, H.; VESTAL, C. R.; SHANK, G. D. An efficient multicomponent numerical simulator. **Society of Petroleum Engineers Journal**, v. 18, p. 355–368, 1978.

KOREN, B. A robust upwind discretization method for advection, diffusion and source terms. **Numerical Methods for Advection-Diffusion Problems**, p. 117–138, 1993.

LEVENTHAL, S. H.; KLEIN, M. H.; CULHAM, W. E. Curvilinear coordinate systems for reservoir simulation. **Society of Petroleum Engineers Journal**, v. 25, p. 893–901, 1985.

LEVERETT, M. C. Capillary behavior in porous solids. **Transactions of the AIME**, v. 142, p. 152–169, 1941.

MACLEOD, D. B. On a relation between surface tension and density. **Transactions of the Faraday Society**, v. 19, p. 38–41, 1923.

MALISKA, C. R. **Computational Heat Transfer and Fluid Dynamics (In Portuguese)**. [S.l.: s.n.], 2004.

MALISKA, C. R.; CUNHA, A. R.; LIVRAMENTO, M. A.; SILVA, A. F. Tridimensional petroleum reservoir simulation using generalized curvilinear grids. **Proceedings of the ENCIT, São Paulo, Brazil**, p. 363–366, 1994.

MALISKA, C. R.; RAITHBY, G. D. A method for computing three dimensional flows using non-orthogonal boundary-fitted co-ordinates. **International Journal for Numerical Methods in Fluids**, v. 4, p. 519–537, 1984.

MALISKA, C. R.; SILVA, A. F.; CZESNAT, A. O.; LUCIANETTI, R. M.; JR., C. R. M. Three-dimensional multiphase flow simulation in petroleum reservoirs using the mass fractions as dependent variables. **Proceedings of the 5th Latin American and Caribbean Petroleum Engineering Conference, Rio de Janeiro, Brazil, August 30- September 3**, 1997.

MARCONDES, F.; HAN, C.; SEPEHRNOORI, K. Implementation of corner point mesh into parallel, fully implicit, equation of state compositional reservoir simulation. **Proceedings of the 18th International Congress of Mechanical Engineering, Ouro Petro, Brazil, November 6-11**, 2005.

MARCONDES, F.; HAN, C.; SEPEHRNOORI, K. Effect of cross derivatives in discretization schemes in structured non-orthogonal meshes for compositional reservoir simulation. **Journal of Petroleum Science and Engineering**, v. 63, p. 53–60, 2008.

MARCONDES, F.; SANTOS, L. S.; VARAVEI, A.; SEPEHRNOORI, K. A 3d hybrid element-based finite-volume method for heterogeneous and anisotropic compostional reservoir simulation. **Journal of Petroleum Science and Engineering**, v. 108, p. 342–351, 2013.

MARCONDES, F.; SEPEHRNOORI, K. An element-based finite-volume method approach for heterogeneous and anisotropic compositional reservoir simulation. **Journal of Petroleum Science and Engineering**, v. 73, p. 99–106, 2010.

MARCONDES, F.; VARAVEI, A.; SEPEHRNOORI, K. An eos-based numerical simulation of thermal recovery process using unstructured meshes. **Brazilian Journal of Chemical Engineering**, v. 32, p. 247–258, 2015.

MASSON, C.; SAABAS, H. J.; BALIGA, B. R. Co-located equal-order control-volume finite-element method for two-dimensional axisymmetric incompressible fluid flow. **International Journal for Numerical Methods in Fluids**, v. 18, p. 1–26, 1994.

MONCORGE, A.; TCHELEPI, H. Stability criteria for thermal adaptive implicit compositional flows. **Society of Petroleum Engineers Journal**, v. 14, p. 311–322, 1995.

NGHIEM, L. X.; FONG, D. K.; AZIZ, K. Compositional modeling with an equation of state. **Society of Petroleum Engineers Journal**, v. 21, p. 687–698, 1981.

PEACEMAN, D. W. A nonlinear stability analysis for difference equations using semi-implicit mobility. **Society of Petroleum Engineers Journal**, v. 17, p. 79–91, 1977.

PEACEMAN, D. W. Interpretation of well-block pressures in numerical reservoir simulation. **Society of Petroleum Engineers Journal**, v. 18, p. 183–194, 1978.

PEACEMAN, D. W. Interpratation of well-block pressure in numerical reservoir simulation with nonsquare grid blocks and anisiotropic permeability. **Society of Petroleum Engineers Journal**, v. 23, p. 531–543, 1983.

PEDROSA, O.; AZIZ, K. Use of a hybrid grid in reservoir simulation. **SPE Reservoir Engineering Journal**, v. 1, p. 611–621, 1986.

PENG, D. Y.; ROBINSON, D. B. A new two-constant equation of state. **Industrial Engineering Chemestry Fundamentals**, v. 15, p. 59–64, 1976.

PERSCHKE, D. **Equation of State Phase Behavior Modeling For Compositional Simulation**. Tese (Doutorado) — Department of Petroleum and Geosystems Engineering, The University of Texas at Austin, 1988.

QUANDALLE, P.; SAVARY, D. An implicit in pressure and saturations approach to fully compositional simulation. **Paper SPE 18423, Proceedings of the SPE Symposium on Reservoir Simulation, Houston, USA, February 6-8**, p. 197–206, 1989.

REDLICH, O.; KWONG, J. N. S. On the thermodynamics of solutions. v. an equation of state. fugacities of gaseous solutions. **Chemical Reviews**, v. 44, p. 233–244, 1949.

ROE, P. L. Some characteristic-based schemes for the euler equations. **Annual Review of Fluid Mechanics**, v. 18, p. 337–365, 1986.

ROZON, B. J. A generalized finite volume discretization method for reservoir simulation. **Proceedings of the SPE Symposium on Reservoir Simulation, Houston, USA, February 6-8**, 1989.

RUSSEL, T. F. Stability analysis and switching criteria for adaptive implicit methods based on the cfl condition. **Paper SPE 18416, proceedings of the SPE Symposium on Reservoir Simulation, Houston, TX, February 6-8**, 1989.

SAABAS, H. J.; BALIGA, B. R. Co-located equal-order control-volume finite-element method for multidimensional, incompressible, fluid flow - part 1: Formulation. **Numerical Heat Transfer - Part B: Fundamentals**, v. 26, p. 381–407, 1994.

SAABAS, H. J.; BALIGA, B. R. Co-located equal-order control-volume finite-element method for multidimensional, incompressible, fluid flow - part 2: Verification. **Numerical Heat Transfer - Part B: Fundamentals**, v. 26, p. 409–424, 1994.

SANTOS, L. O. S. **Development of a Multi-Formulation Compositional Simulator**. Tese (Doutorado) — Department of Petroleum and Geosystems Engineering, The University of Texas at Austin, 2013.

SHELDON, J. W.; DOUGHERTY, E. D. The approximation of secondary recovery projects using moving interfaces. **Proceedings of the 36th SPE Annual Fall Meeting, Dallas, USA**, 1961.

STATISTA. Statista. fossil fuels. oil production in barrels per day - top fifteen countries 2015. https://www.statista.com/statistics/237115/oil-production-in-the-top-fifteen-countries-in-barrels-per-day/. **Accessed on 05/06/2017 at 12:20**, 2017.

STIEL, L. I.; THODOS, G. The viscosity of nonpolar gases at normal pressure. **AIChE Journal**, v. 7, p. 611–615, 1961.

STONE, H. L. Estimation of three-phase permeability and residual oil data. **Journal of Canadian Petroleum Technology**, v. 12, p. 53–61, 1973.

SUGDEN, S. A relation between surface tension, density, and chemical composition. **Journal of Chemical Society**, v. 125, p. 1177–1189, 1924.

SWAMINATHAN, C. R.; VOLLER, V. R. Streamline upwind scheme for control-volume finite elements, part 1: Formulations. **Numerical Heat Transfer - Part B: Fundamentals**, v. 22, p. 95–107, 1992.

SWAMINATHAN, C. R.; VOLLER, V. R. Streamline upwind scheme for control-volume finite elements, part 1: Implementation and comparison with supg finite-element scheme. **Numerical Heat Transfer - Part B: Fundamentals**, v. 22, p. 109–124, 1992.

TAN, T. B. Implementation of an improved adaptive-implicit method in a thermal compositional simulator. **Society of Petroleum Engineers Journal**, v. 3, p. 1123–1128, 1988.

THOMAS, G. W.; THURNAL, D. H. The mathematical basis of the adaptive implicit method. **Proceedings of the 6th SPE Symposium on Reservoir Simulation, New Orleans, USA, January 31- February 3**, 1982.

THOMAS, G. W.; THURNAL, D. H. Reservoir simulation using an adaptive implicit method. **Society of Petroleum Engineers Journal**, v. 23, p. 759–768, 1983.

THOMPSON, J. F.; THAMES, F. C.; MASTIN, C. W. Automatic numerical generation of body-fitted curvilinear coordinate system for field containing any number of arbitrary two-dimensional bodies. **Journal of Computational Physics**, v. 15, p. 299–319, 1974.

WADSLEY, W. A. Modelling reservoir geometry with non-rectangular coordinate grids. **Proceedings of the 55th SPE Annual Fall Technical Conference, Dallas, USA, September 21-24**, 1980.

WANG, P.; YOTOV, I.; WHEELER, M.; ARBOGAST, T.; DAWSON, C.; PARASHAR, M.; SEPEHRNOORI, K. A new generation eos compositional reservoir simulator: Part i - formulation and discretization. **Proceedings of the SPE Reservoir Simulation Symposium, Dallas, USA, June 8-11**, 1997.

WATTS, J. W. A compositional formulation of the pressure and saturation equations. **SPE Reservoir Engineering Journal**, v. 1, p. 243–252, 1986.

WATTS, J. W.; MIFFLIN, R. T.; WEISER, A. A fully coupled, fully implicit reservoir simulation for thermal and other complex reservoir processes. **Proceedings of the SPE Symposium on Reservoir Simulation, Anaheim, USA, February 17-20**, 1991.

WONG, T. W.; FIROOZABADI, A.; AZIZ, K. Relationship of the volume-balance method of compositional simulation to the newton-raphson method. **SPE Reservoir Engineering Journal**, v. 5, p. 415–422, 1990.

WONG, T. W.; FIROOZABADI, A.; R.NUTAKKI; AZIZ, K. A comparison of two approaches to compositional and black oil simulation. **Proceedings of the SPE Symposium on Reservoir Simulation, San Antonio, USA, February 1-4**, 1987.

YOUNG, L. C.; RUSSEL, T. F. Implementation of an adaptive implicit method. **Proceedings of the 12th SPE Symposium on Reservoir Simulation, New Orleans, USA, February 28-March 3**, 1993.

YOUNG, L. C.; STEPHENSON, R. E. A generalized compositional approach for reservoir simulation. **Society of Petroleum Engineers Journal**, p. 727–742, 1983.

APPENDIX A – IMPLICITNESS LEVEL INFLUENCE ON JACOBIAN MATRIX EQUATIONS

Here we develop our discussion over the reduced Jacobian matrix equation, once more following Fig. (6). The focus now is set around the grid element composed by the (1), (2), (4) and (3) nodes, shown in detail below:

Figure 48 – Grid element formed by the (1), (2), (3) and (4) vertices.

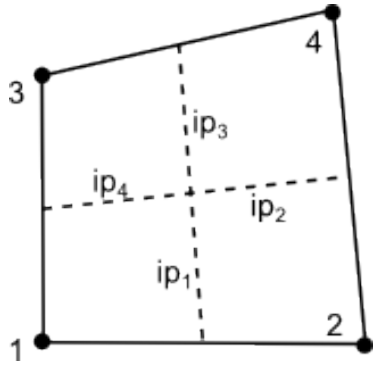

On chapter 5 it was stated vertex (1) was FI and the remaining nodes on Fig. (48) were IMPEC. Developing the complete discretized equations for each of theses volume would be to cumbersome. The analysis here is limited to the first node, which is conveniently formed by a single sub-control volume. Equation (4.19) can then be rewritten in residual form as follows:

$$RN_{i,1} = Acc_{i,1} - F_{i,1} + S_{i,1}, \quad i = 1,...,n_c \tag{A.1}$$

The accumulation and source terms do not require further consideration, for both are related solely to properties evaluated at the vertex. The advective portion of Eq. (A.1), on the other hand, is precisely where a relationship between neighboring blocks can be observed. In the current analysis, we have:

$$F_{i,1} = \Delta t \sum_{j=2}^{n_p} \left[\left(\xi_j^m x_{ij}^m \frac{k_{rj}^m}{\mu_j^m} \overrightarrow{\overrightarrow{K}} \cdot \sum_h^{n_v} \vec{\nabla} \tilde{N}_h \Phi_{j,h}^m \cdot d\vec{A} \right)_{ip_1} + \left(\xi_j^m x_{ij}^m \frac{k_{rj}^m}{\mu_j^m} \overrightarrow{\overrightarrow{K}} \cdot \sum_h^{n_v} \vec{\nabla} \tilde{N}_h \Phi_{j,h}^m \cdot d\vec{A} \right)_{ip_4} \right], \quad i = 1,...,n_c \tag{A.2}$$

Both terms in Eq. (A.2) are still evaluated at the integration points. Let us assume, for the sake of this discussion, vertex (1) is upwind only in respect to ip_1. This yields $F_i,1$ is

written below:

$$F_{i,1} = \Delta t \sum_{j=2}^{n_p} \left[\left(\xi_j^{n+1} x_{ij}^{n+1} \frac{k_{rj}^{n+1}}{\mu_j^{n+1}} \right)_1 \left(\overrightarrow{\overrightarrow{K}} \cdot \sum_h^{n_v} \vec{\nabla} \tilde{N}_h \Phi_{j,h}^m \cdot d\vec{A} \right)_{ip_1} + \left(\xi_j^n x_{ij}^n \frac{k_{rj}^n}{\mu_j^n} \right)_3 \left(\overrightarrow{\overrightarrow{K}} \cdot \sum_h^{n_v} \vec{\nabla} \tilde{N}_h \Phi_{j,h}^m \cdot d\vec{A} \right)_{ip_4} \right], \quad i = 1, ..., n_c \quad \text{(A.3)}$$

Notice the fluid properties, once defined the upstream vertices, assume the time step level accordingly. Now writing the summation over n_v for the element in study and after some manipulation yields:

$$F_{i,1} = \Delta t \sum_{j=2}^{n_p} \overrightarrow{\overrightarrow{K}} \cdot \vec{\nabla} \left(\tilde{N}_1 \Phi_{j,1}^{n+1} + \tilde{N}_2 \Phi_{j,2}^n + \tilde{N}_3 \Phi_{j,3}^n + \tilde{N}_4 \Phi_{j,4}^n \right) \cdot \left[\left(\xi_j^{n+1} x_{ij}^{n+1} \frac{k_{rj}^{n+1}}{\mu_j^{n+1}} \right)_1 d\vec{A}_{ip_1} + \left(\xi_j^n x_{ij}^n \frac{k_{rj}^n}{\mu_j^n} \right)_3 d\vec{A}_{ip_4} \right], \quad i = 1, ..., n_c \quad \text{(A.4)}$$

Finally, it becomes clear how each surrounding vertex affects node (1) hydrocarbon mole equation through their hydraulic potentials. This leads to a pressure dependence, regardless of the level of implicitness. Remembering Eq. (4.25) we see whenever a volume is evaluated implicit, its capillary pressure and phase mass density are computed at the current $n+1$ time level. An implicit relationship then arises with the neighbor amount of component moles. This does not occur in Eq. (A.4) because (2), (3) and (4) are all explicit. As a consequence, the derivatives with respect to these nodes amount of moles can be decoupled from the Jacobian matrix. For the same 3 hydrocarbon components reservoir fluid problem we have:

$$\frac{\partial RN_{i,1}}{\partial P_1} \delta P_1 + \sum_{j=1}^{n_c} \frac{\partial RN_{i,1}}{\partial N_{j,1}} \delta N_{j,1} + \frac{\partial RN_{i,1}}{\partial N_{w,1}} \delta N_{w,1} + \frac{\partial RN_{i,1}}{\partial P_2} \delta P_2 + \frac{\partial RN_{i,1}}{\partial P_3} \delta P_3 + \frac{\partial RN_{i,1}}{\partial P_4} \delta P_4 = -RN_{i,1}, \quad i = 1, ..., n_c \quad \text{(A.5)}$$

The expressions for water and pressure are developed in the same manner. We should note Eq. (A.5) describes a simple case. More complex meshes and inner domain vertices will produce much more complex equations.

APPENDIX B – THRESHOLD OPTIMIZATION PROCEDURE

Here are presented all trial runs used to obtain the optimized results shown in section 6.3. A comparison for the production curves as well as the data concerning the level of implicitness and CPU time.

B.1 QOFS-3comp 2D

The first data presented regards the 7021 volumes mesh composed of quadrilateral elements. Figures (49) and (50) show the three different threshold values do not produce variations on the production rates. This fact is verified analyzing the similar implicitness degrees and CPU times in Tab. (30). The three simulations basically yield the same results, leading to the choice of the largest threshold as optimal.

Figure 49 – Threshold AIM Oil production rates comparison for the 7,021 nodes quadrilateral elements mesh (QOFS-3comp case).

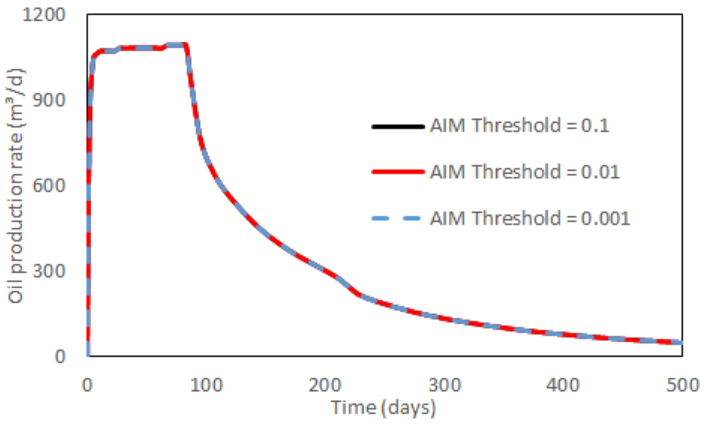

Figure 50 – Threshold AIM Gas production rates comparison for the 7,021 nodes quadrilateral elements mesh (QOFS-3comp case).

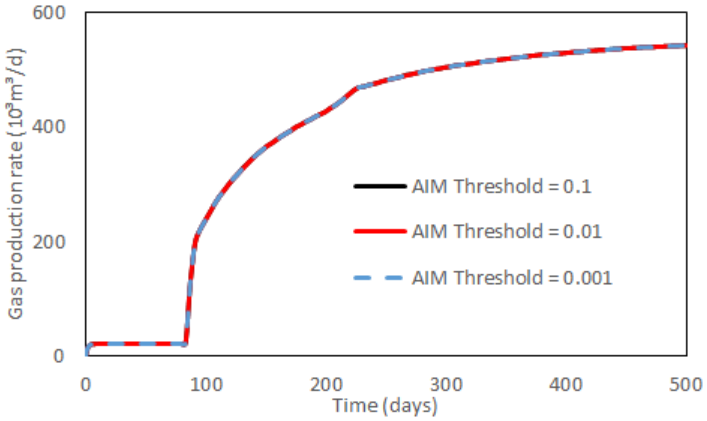

Table 30 – Threshold AIM simulation data comparison for 7,021 nodes quadrilateral elements mesh (QOFS-3comp)

Formulation	Avg. DT (d)	Step	FI%	CPU time (s)
AIM Thr.=0.1	0.019	800	0.028	4874.232
AIM Thr.=0.01	0.019	800	0.028	4867.840
AIM Thr.=0.001	0.019	800	0.028	4872.452

Next, the results for the 7449 volumes constituted of triangular elements are displayed in Fig. (51) and (52), as well as Tab. (31). Once more, the diverging threshold values lead to the same amount of implicit volumes along the runs. This, in turn, produces very similar computation times. The largest value, 0.1, is then chosen the ideal criterion.

Figure 51 – Threshold AIM Oil production rates comparison for the 7,449 nodes triangular elements mesh (QOFS-3comp case).

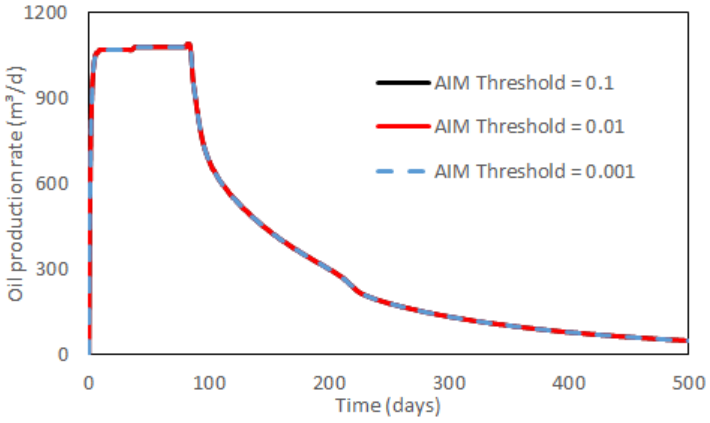

Figure 52 – Threshold AIM Gas production rates comparison for the 7,449 nodes triangular elements mesh (QOFS-3comp case).

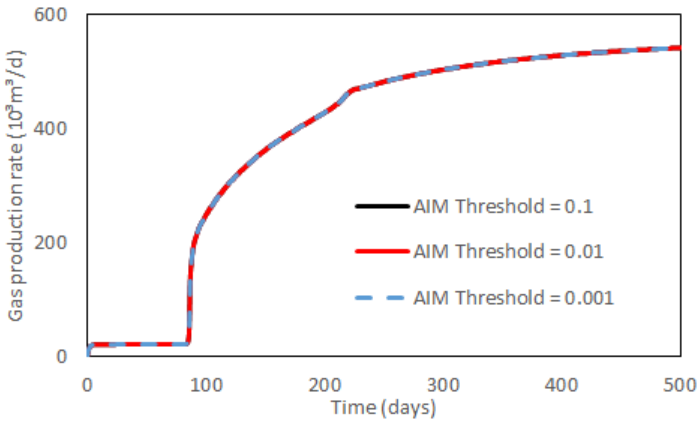

Table 31 – Threshold AIM Simulation data comparison for 7,449 nodes triangular elements mesh (QOFS-3comp).

Formulation	Avg. DT (d)	Step	FI%	CPU time (s)
AIM Thr.=0.1	0.007	1000	0.027	14001.243
AIM Thr.=0.01	0.007	1000	0.027	14194.767
AIM Thr.=0.001	0.007	1000	0.027	14011.559

Closing this section are the data of the runs using the 7942 volumes of mixed elements. As in the previous meshes, the implicitness level does not change for the tested thresholds, all runs behave equally and the CPU time is very similar. In this context, the largest threshold value is set to be compared with the remaining formulations.

Figure 53 – Threshold AIM Oil production rates comparison for the 7,942 nodes mixed elements mesh (QOFS-3comp case).

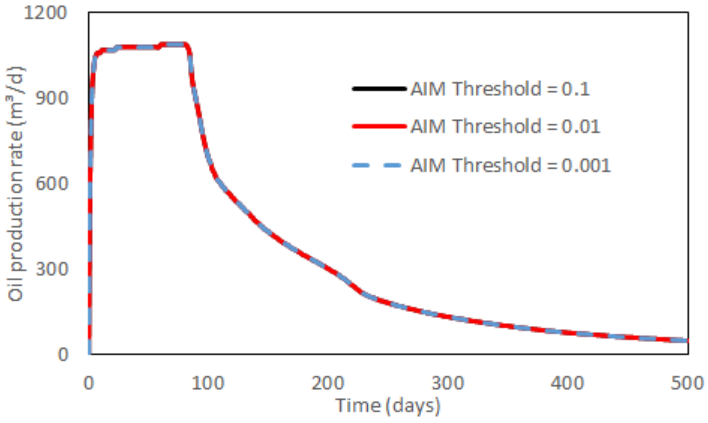

Figure 54 – Threshold AIM Gas production rates comparison for the 7,942 nodes mixed elements mesh (QOFS-3comp case).

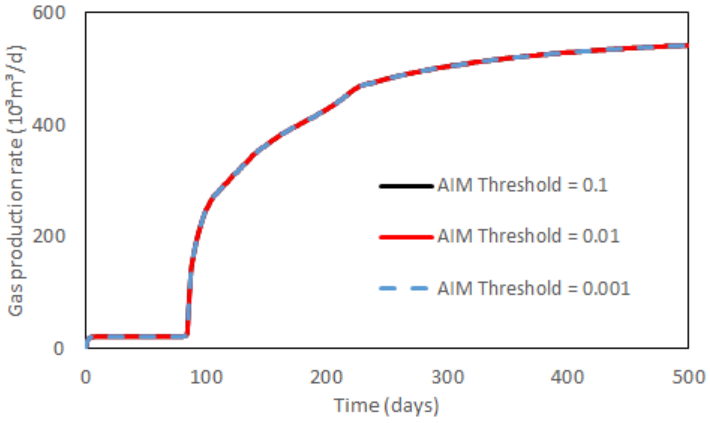

As concluding remarks for this case, we should highlight the QOFS-3comp problem

Table 32 – Threshold AIM Simulation data comparison for 7,942 nodes mixed elements mesh (QOFS-3comp).

Formulation	Avg. DT (d)	Step	FI%	CPU time (s)
AIM Thr.=0.1	0.019	900	0.025	5818.987
AIM Thr.=0.01	0.019	900	0.025	5792.901
AIM Thr.=0.001	0.019	900	0.025	5871.129

is able to achieve accurate results requiring very few implicit grid nodes without occurring on instabilities issues. Therefore, as observed, large threshold values are enough to obtain good performances.

B.2 QOFS-6comp 2D

Following, we analyze the effect of the threshold criterion on the AIM for the QOFS-6comp problem with 2D meshes. As before, the first evaluated mesh is the quadrilateral elements one. This time, the wide range of threshold values produces very different results. Figures (55) and (56) show increasingly disagreement between the production curves as the threshold criterion becomes larger. At the same time, Tab. (33) display a tendency for higher CPU times and lower levels of implicitness as the threshold limit increases. These results indicate looser switching criterion limits are allowing numerical instability to occur. This is specially easy to see for the AIM Thr.=0.01 production rates, as they display oscillatory behavior around 1500 days. Given these considerations, the optimized threshold is set to 10^{-5}.

Figure 55 – Threshold AIM Oil production rates comparison for the 7,021 nodes quadrilateral mesh (QOFS-6comp case).

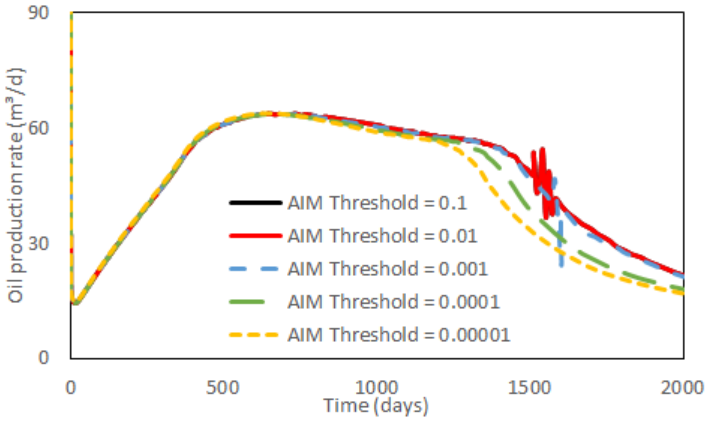

Proceeding, the 7449 volumes mesh results are displayed below. No major difference

Figure 56 – Threshold AIM Gas production rates comparison for the 7,021 nodes quadrilateral mesh (QOFS-6comp case).

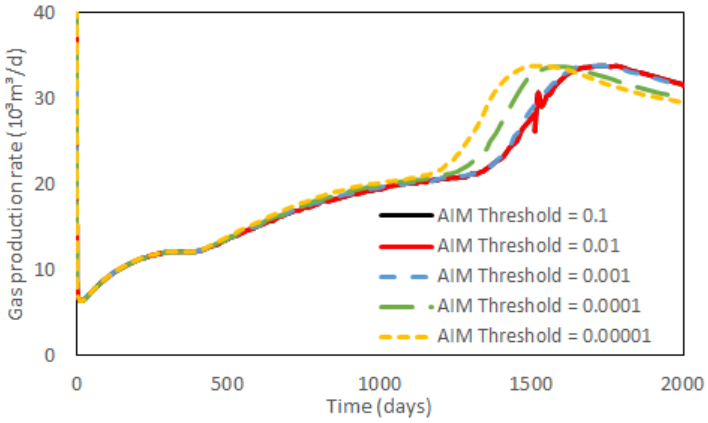

Table 33 – Threshold AIM Simulation data comparison for 7,021 nodes quadrilateral mesh (QOFS-6comp).

Formulation	**Avg. DT (d)**	**Step**	**FI%**	**CPU time (s)**
AIM Thr.=0.1	0.243	200	0.028	10927.447
AIM Thr.=0.01	0.243	200	0.028	10947.308
AIM Thr.=0.001	0.246	200	0.031	10348.358
AIM Thr.=10^{-4}	0.265	200	0.173	5905.665
AIM Thr.=10^{-5}	0.279	200	10.728	3741.849

between the curves is observed this time. The relationship between the threshold value and the amount of FI nodes, however, is the same. Looser criteria lead to fewer implicit blocks. The increasing computation time indicates, once again, a certain implicitness degree is required in order to enhance performance. This way, the final threshold is set to 10^{-5}.

Figure 57 – Threshold AIM Oil production rates comparison for the 7,449 nodes triangular elements mesh (QOFS-6comp case).

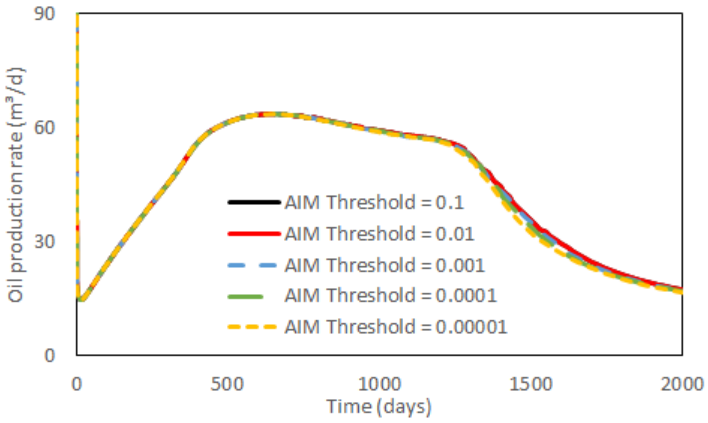

Figure 58 – Threshold AIM Gas production rates comparison for the 7,449 nodes triangular elements mesh (QOFS-6comp case).

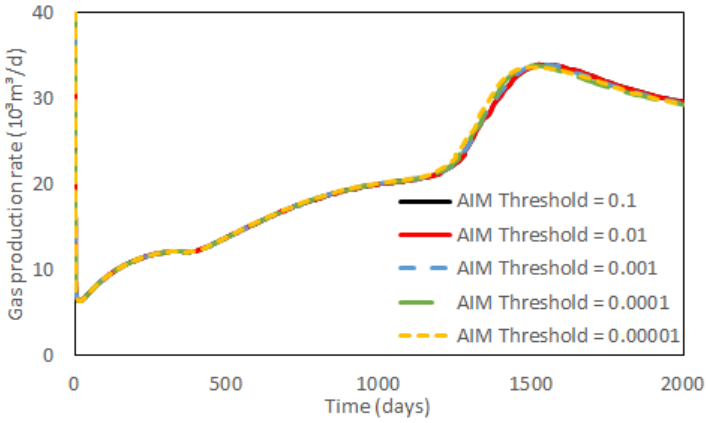

Table 34 – Threshold AIM Simulation data comparison for 7,449 nodes triangular elements mesh (QOFS-6comp).

Formulation	**Avg. DT (d)**	**Step**	**FI%**	**CPU time (s)**
AIM Thr.=0.1	0.276	200	0.027	5296.194
AIM Thr.=0.01	0.276	200	0.027	5234.471
AIM Thr.=0.001	0.277	200	0.029	4776.302
AIM Thr.=10^{-4}	0.279	200	0.079	4285.803
AIM Thr.=10^{-5}	0.282	200	3.550	4036.892

Finally, we show the 7942 volumes mesh results. Figures (59) and (60) testify for the agreement between all curves, pointing no major accuracy issues arrive from the very different criterion values. The same can not be said about performance. As in the previous meshes, the larger thresholds are associated with slower runs. This time, however, the optimal value, regarding both accuracy and performance, is 10^{-4}.

Figure 59 – Threshold AIM Oil production rates comparison for the 7,942 nodes mixed elements mesh (QOFS-6comp case).

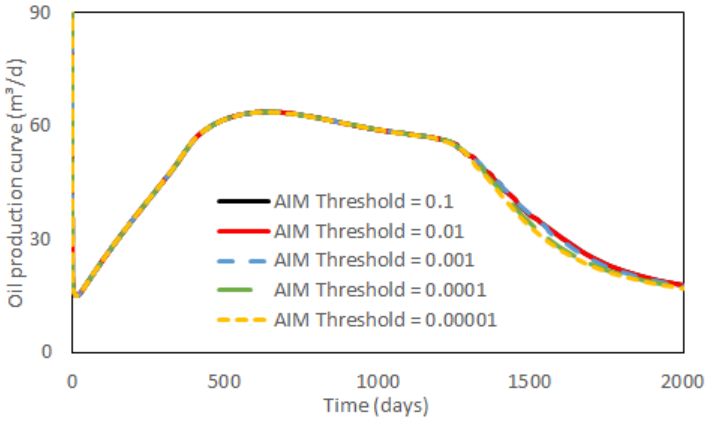

Figure 60 – Threshold AIM Gas production rates comparison for the 7,942 nodes mixed elements mesh (QOFS-6comp case).

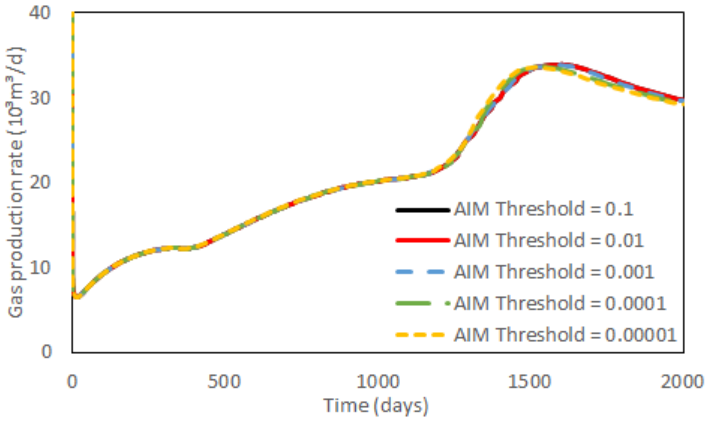

Table 35 – Threshold AIM Simulation data comparison for 7,942 nodes mixed elements mesh (QOFS-6comp).

Formulation	**Avg. DT (d)**	**Step**	**FI%**	**CPU time (s)**
AIM Thr.=0.1	0.271	200	0.025	4766.653
AIM Thr.=0.01	0.271	200	0.025	4761.381
AIM Thr.=0.001	0.272	200	0.027	4541.203
AIM Thr.=10^{-4}	0.274	200	0.074	4053.413
AIM Thr.=10^{-5}	0.275	200	4.294	4133.210

APPENDIX C – NEWTON-RAPHSON CONVERGENCE CRITERIA

This appendix is dedicated to present the Newton-Raphson convergence criteria applied in all case studies. Tables (36) and (37) show the same values were used for the FI and AIM formulations. It is important to highlight these are very restrictive tolerances chosen to guarantee accuracy and stability. These limits do not necessarily reproduce advisable values for real field application studies.

Table 36 – Fully Implicit (FI) convergence criteria for all case studies

Case study	**RP tol.**	**Pres. var. tol.**	**RN tol.**	**Mole var. tol.**
QOFS-3comp 2D	10^{-3}	10^{-3}	10^{-3}	10^{-3}
QOFS-6comp 2D	10^{-3}	10^{-3}	10^{-3}	10^{-3}
2D irr. 6comp	10^{-3}	10^{-3}	10^{-3}	10^{-3}
QOFS-6comp 3D	10^{-2}	10^{-2}	10^{-2}	10^{-2}
3D irr. 6comp	10^{-3}	10^{-3}	10^{-3}	10^{-3}

Table 37 – Adaptive Implicit Method (AIM) convergence criteria for all case studies

Case study	**RP tol.**	**Pres. var. tol.**	**RN tol.**	**Mole var. tol.**
QOFS-3comp 2D	10^{-3}	10^{-3}	10^{-3}	10^{-3}
QOFS-6comp 2D	10^{-3}	10^{-3}	10^{-3}	10^{-3}
2D irr. 6comp	10^{-3}	10^{-3}	10^{-3}	10^{-3}
QOFS-6comp 3D	10^{-2}	10^{-2}	10^{-2}	10^{-2}
3D irr. 6comp	10^{-3}	10^{-3}	10^{-3}	10^{-3}